Study of the hydrological cycle using satellite-borne isotopologue measurements and model results

Samuel Jonson Sutanto

Utrecht 2015

Institute for Marine and Atmospheric research Utrecht (IMAU)
Faculty of Science, Department of Physics
Utrecht University, the Netherlands

Promotor
Prof.dr. Thomas Röckmann

Examination committee
Prof.dr. Bart van den Hurk, Vrije Universiteit Amsterdam & KNMI
Prof.dr. Ilse Aben, SRON
Prof.dr. Maarten Krol, SRON, Wageningen & Utrecht University
Prof.dr. Jean Jouzel, Université de Versailles Saint Quentin, France
Dr. Martin Werner, Alfred Wegener Institute, Germany

Cover design: Hydrological cycle picture by Juliana Tan and layout by Monica Dewi Indrasari.

Printed in the Netherlands by Ridderprint.

Study of the hydrological cycle using satellite-borne isotopologue measurements and model results

Studie naar de hydrologische kringloop aan de hand van satelliet-isotoopmetingen en model resultaten

(met een samenvatting in het Nederlands)

Proefschrift

ter verkrijging van de graad van doctor aan de Universiteit Utrecht op gezag van de rector magnificus, prof.dr. G.J. van der Zwaan, ingevolge het besluit van het college voor promoties in het openbaar te verdedigen op maandag 22 juni 2015 des middags te 12.45 uur

door

Samuel Jonson Sutanto

geboren op 20 juli 1980 te Tegal, Indonesië

Promotor:
Prof.dr. T. Röckmann

Fretwell's Law: "Warning! Stable isotope data may cause severe and contagious stomach upset if taken alone. To prevent upsetting reviewers' stomach and your own, take stable isotope data with healthy dose of other hydrologic information. Then, you will find stable isotope data very beneficial."

Marvin O. Fretwell, pers. Comm. 1983, cited from Kendall and McDonnell, 1998.

Life is like global climate models in predicting the future warming. It is highly uncertain due to the clouds in between reality and expectation.

Contents

Summary

The circulation of water on Earth that describes the continuous movement of water from the land to the atmosphere and back again is called the hydrological cycle. The transport of water vapor through the hydrological cycle is crucial for life on Earth and for our climate. Water vapor provides rain water for the continental land masses, transports enormous amounts of energy in the form of latent heat from tropical to high latitudes, provides the substrate for clouds and ice sheets, which have a strong effect on the energy balance of the Earth, and is an important contributor to the atmospheric greenhouse effect. For these and other reasons, the hydrological cycle has been studied intensively.

In the atmosphere, water vapor is transported over large distances and undergoes often several phase changes, from evaporation to condensation, before returning to the ocean. These processes leave a characteristic imprint on the isotopic composition of atmospheric water vapor and the corresponding precipitation. Traditionally, most water isotopologue studies have investigated mainly the isotopic composition of precipitation because isotope measurements of water vapor are more complicated and sparse. Over the last-decade, global-scale measurements of atmospheric water vapor isotopologues (HDO/H_2O) have become available from different remote-sensing instruments that operate on satellites and overcome sampling difficulties of water vapor. **The main objective of this thesis, therefore, is to investigate how these measurements and related modeling of water vapor isotopologues can provide new insight into the hydrological cycle**.

This thesis uses mainly two satellite datasets, from the Tropospheric Emission Spectrometer (TES) and the SCanning Imaging Absorption spectroMeter for Atmospheric CHartographY (SCIAMACHY) and results from the isotope-enabled General Circulation Model (GCM) ECHAM4. Related datasets such as precipitation from the ERA-interim and Tropical Rainfall Measuring Mission (TRMM) observations, isotopic composition of precipitation from the Global Network of Isotopes in Precipitation (GNIP) network, the Niño-3 index to determine the strength of ENSO (El Niño-Southern Oscillation), and results from other GCMs equipped with water isotope modules from the Stable Water INtercomparison Group phase 2 (SWING2) database are also used. Analyses have been carried out using monthly averaged data both for the satellite HDO/H_2O measurements and the model results. Using these data, a number of interesting conclusions of the hydrological cycle have been obtained.

Continental evapo-transpiration is an important component of the continental water cycle since it transports as much as 60 % of the land precipitation back to the atmosphere and also consumes about half of the total energy from the sun absorbed by continental land masses. This thesis discusses several approaches that have been used to estimate the relative contribution of different evapo-transpiration fluxes and also their limitations and possible discrepancies between the methods. It is shown that transpiration is the largest contributor to the evaporation fluxes from continental area and the results from both isotope and non-isotope based methods are consistent (generally more than 70 % of transpiration fraction during summer). However, land-surface models tend to produce

lower transpiration fraction indicating that a reassessment of model parameterizations is needed.

Three different satellite datasets (TES version 4 and version 5, and SCIAMACHY) and the ECHAM model results are examined with focus on large global first order isotope effects. A number of established isotope effects on the global-scale as well as in the tropics, linked to the movement of InterTropical Convergence Zone (ITCZ), are observed in the TES version 5, SCIAMACHY and the ECHAM model. This analysis confirms the improvement of the new version of TES dataset (version 5) compared to version 4. A humidity bias correction and a posteriori analyses can be used to avoid complications arising from the mid troposphere humidity bias when the satellites averaging kernel is applied to the model results.

In Indonesia, prolonged dry and wet periods are mainly connected to ENSO variability, which cause drought and flooding events. In this study, two drought indices, Standardized Precipitation Index (SPI) and Standardized Precipitation Evaporation Index (SPEI), are calculated using the ECHAM model output and compared with the calculation from in-situ observations. The relationships of droughts and ENSO, and of the droughts and the isotopic composition of water are discussed in detail. The results indicate that isotopic composition of water vapor is a good climatic indicator for drought and flooding events and performs even better than the Niño-3 index.

Furthermore, the relations between ENSO, the tropical hydrological cycle, and the water isotopologues in the entire tropical Pacific are investigated. The focus here is in particular on the well-known changes of the tropical hydrological cycle at near-surface levels and higher altitudes and their link with ENSO. For the lower atmosphere, our results show that rainout processes, less rain re-evaporation of falling droplets, and increase of convective updrafts and diffusive exchange within the convective systems, play an important role in producing the "isotope amount effect". Simultaneously, convective updrafts control the water vapor at higher altitudes. Our findings contribute to a more complete understanding of the isotope amount effect.

The GCM simulations submitted to the Coupled Model Inter-comparison Project phase 5 (CMIP5) exhibit a wide range of equilibrium climate sensitivity (ECS; around 1.5-4.5 $^{\circ}\mathrm{C}$ warming for a doubling of the CO_2 concentration), leading to a wide range in future warming projections. The source of the discrepancy has recently been attributed to variations in lower tropospheric mixing, and it is investigated here whether differences in lower tropospheric mixing between models lead to characteristic vertical isotope gradients in the model, which could potentially be used to "calibrate" lower tropospheric mixing and thus narrow down the wide range in ECS estimates. The results confirm that regions with intense mixing and strong convection are marked by a flatter isotopic gradient. However, a model intercomparison does not show a similar relation: models simulating steeper or flatter isotopic gradients are not necessarily marked by weaker or stronger mixing (or smaller/larger ECS). A possible reason for the lack of a corresponding isotope signal might be that the different "isotope" GCMs vary considerably in the parameterization of important of hydrological processes and even in the parameterization of the water isotope fractionation processes themselves.

The results of this study show that the measurement of water isotopologues from satellite-borne instruments in conjunction with GCM models provide interesting new information when studying the land-surface-, and atmospheric hydrological cycle.

Samenvatting

De watercirculatie op aarde, waarin de constante beweging van water van het land naar de atmosfeer en weer terug wordt beschreven, wordt de hydrologische kringloop genoemd. Het transport van water in de hydrologische kringloop is cruciaal voor het leven op aarde en voor ons klimaat. Waterdamp zorgt voor regen op het land, transporteert grote hoeveelheden energie in de vorm van latente warmte van de tropen naar de hogere breedtegraden, vormt de basis voor wolken en ijsmassa's, wat weer een sterk effect heeft op de energiebalans van de aarde, en vormt een belangrijke factor in het (versterkte) atmosferische broeikaseffect. Hierom wordt de hydrologische kringloop intensief bestudeerd.

In de atmosfeer wordt waterdamp over grote afstanden getransporteerd en het ondergaat hierbij vaak verschillende faseveranderingen van verdamping tot condensatie, voordat het weer terugkeert naar de oceaan. Deze processen laten een karakteristieke afdruk achter op de isotopische compositie van atmosferische waterdamp en de bijbehorende neerslag. Van oudsher hebben de meeste waterdamp-isotopoloogstudies voornamelijk de isotopische compositie van neerslag bestudeerd, omdat isotoopmetingen van waterdamp gecompliceerder en zeldzamer zijn. In het laatste decennium zijn er echter metingen op wereldschaal van atmosferische waterdampisotopologen (HDO/H_2O) beschikbaar gekomen van verschillende remote sensing instrumenten die opereren op satellieten en waar de bemonstering van waterdamp geen probleem meer is. **De hoofddoelstelling van dit proefschrift is daarom om te onderzoeken hoe deze metingen in combinatie met het modeleren van waterdampisotopologen nieuw inzicht kunnen verschaffen in de hydrologische kringloop**.

In dit proefschrift worden voornamelijk twee satellietdatasets gebruikt: die van de Tropospheric Emission Spectrometer (TES) en die van de SCanning Imaging Absorption spectroMeter for Atmospheric CHartographY (SCIAMACHY). Daarnaast wordt er gekeken naar de modelresultaten van het voor isotoopberekeningen geschikte circulatiemodel (General Circulation Models, GCM) ECHAM4. Verder gerelateerde datasets, zoals voor neerslag de ERA-interim re-analysis data en de Tropical Rainfall Measuring Mission (TRMM) observaties, de isotopische compositie van neerslag van het Global Network of Isotopes in Precipitation (GNIP), de Niño-3 index om de sterke van de ENSO (El Niño-Southern Oscillation) vast te stellen en de resultaten van andere GCMs die uitgerust zijn met water-isotoopmodules van de Stable Water INtercomparison Group phase 2 (SWING2) dataset worden ook gebruikt. De analyses zijn uitgevoerd door gebruik te maken van maandgemiddelde data van zowel de satelliet-HDO/H_2O-metingen als de modelresultaten. Een aantal interessante conclusies over de hydrologische kringloop zijn verkregen door deze data te gebruiken.

Evapotranspiratie boven land is een belangrijke component van de continentale hydrologische kringloop, omdat het maar liefst 60 % van de neerslag op land terug naar de atmosfeer transporteert en ook ongeveer de helft van de totale energie van de zon gebruikt die geabsorbeerd wordt door continentale landmassas. Dit proefschrift bespreekt verschillende benaderingen, die gebruikt worden om de relatieve bijdrage van de verschillende

evapotranspiratie-fluxen in te schatten. Daarnaast worden ook de beperkingen en de mogelijke afwijkingen tussen de methoden beschreven. Er wordt aangetoond dat transpiratie de belangrijkste bijdrage levert aan de verdampingsfluxen van het land en dat de resultaten van zowel isotoop- als niet op isotoop gebaseerde methoden consistent zijn (doorgaans is de transpiratiefractie meer dan 70 % tijdens de zomer). Landoppervlakte modellen hebben echter de neiging om lagere transpiratiefracties te voorspellen, wat aangeeft dat een herbeoordeling van modelparameterisaties nodig is.

Drie verschillende satellietdatasets (TES versie 4 en versie 5 en SCHIAMACHY) en de modelresultaten van ECHAM zijn onderzocht met de focus op grootschalige globale eerste orde isotoopeffecten. Een aantal van de vastgestelde isotoopeffecten op zowel wereldschaal als in de tropen, gelinkt aan de beweging van InterTropical Convergence Zone (ITCZ), zijn waargenomen in de data van TES versie 5, SCHIAMACHY en het ECHAM model. Deze analyse bevestigd de verbetering van de nieuwe versie van de TES dataset (versie 5) vergeleken met versie 4. Een luchtvochtigheidsfout-correctie en een a posteriori analyse kunnen worden gebruikt om complicaties te voorkomen die ontstaan door de mid-troposferische luchtvochtigheidsfout, wanneer de "averaging kernel" van de satelliet wordt toegepast op de modelresultaten.

In Indonsië zijn aanhoudende droge en natte perioden voornamelijk verbonden aan de ENSO variabiliteit, die droogte en overstromingen veroorzaakt. In deze studie worden twee droogte-indices gebruikt: de Standardized Precipitation Index (SPI) en de Standardized Precipitation Evaporation Index (SPEI). Deze zijn berekend door gebruik te maken van de resultten van het ECHAM model en vergeleken met de berekening uit in-situ observaties. De relatie tussen droogte en ENSO, en tussen droogte en de isotopische compositie van water worden gedetailleerd besproken. De resultaten wijzen erop dat de isotopische waterdampsamenstelling een goede klimatologische indicator is voor droogte en overstroming en dat het zelfs betere resultaten laat zien dan de Niño-3 index.

Verder worden in deze studie de relaties tussen ENSO, de troposferische hydrologische kringloop en de waterisotopologen in de gehele tropische Stille Oceaan onderzocht. De focus ligt hierbij in het bijzonder op de bekende veranderingen in de hydrologische kringloop op niveaus dicht bij het oppervlak en op grotere hoogtes en hun relatie met de ENSO. Onze resultaten laten zien dat voor de onderste atmosfeer het proces van uitregenen, de lagere her-evaporatie van vallende waterdruppels en een toename van convectieve opwaartse luchtstromen en diffuse uitwisseling binnen het convectieve systeem een belangrijke rol spelen in het produceren van het "isotope amount effect". Tegelijkertijd beheersen convectieve opwaartse luchtstromen de hoeveelheden waterdamp op grotere hoogten. Onze bevindingen dragen bij aan een completer begrip van het "isotope amount effect".

De GCM simulaties ingediend bij het Coupled Model Inter-comparison Project phase 5 (CMIP5) belichten een wijde variabiliteit van equilibrium climate sensitivity (ECS) schattingen (ongeveer 1.5 C-4.5 $^{\circ}$C temperatuurstijging bij een verdubbeling van de CO_2 concentratie), wat leidt tot een wijde variabiliteit aan prognoses van toekomstige temperatuurstijgingen. De oorzaak van de afwijking is recentelijk toegeschreven aan variaties in de menging in de lagere troposfeer, en het wordt hier onderzocht of verschillen tussen de modellen in menging in de lagere troposfeer leiden tot karakteristieke verticale

14

isotoop-gradiënten in het model, wat mogelijk kan worden gebruikt om de lagere troposferische menging te "kalibreren" en dus de wijde variabiliteit in ECS schattingen iets kunnen verkleinen. De resultaten bevestigen dat regios met intensieve menging en sterke convectie worden gekenmerkt door een flauwere isotopische gradiënt. Uit de modelvergelijking blijkt echter geen soortgelijke relatie: modellen die sterkere of zwakkere gradinten simuleren worden niet noodzakelijk gekenmerkt door zwakkere of sterkere menging. Een mogelijke verklaring voor het gebrek aan corresponderende isotoop-signalen kan zijn dat de verschillende "isotopische" GCMs aanzienlijk verschillen in de parameterisatie van belangrijke hydrologische processen en zelfs in de paramerisatie van de waterisotoop-fractienatie processen zelf.

De resultaten van deze studie tonen aan dat de satellietmetingen van water-isotopen in combinatie met GCM-modellen interessante informatie kunnen verschaffen wanneer er wordt gekeken naar de land- en atmosferische hydrologische kringloop.

1   Introduction

"We forget that the water cycle and the life cycle are one"
Jacques Cousteau

1.1   The global hydrological cycle

The hydrological cycle or water cycle describes the continuous circulation of water on Earth through different reservoirs that are listed in Table 1.1. More than 97 % of all water on the planet resides in the global oceans, another 2 % in the polar ice sheets and glaciers. Less than 0.001 % of water is actually in the atmosphere. However, the turnover time of water in the atmosphere is only about 9 days, which is much faster than the one of most of the other reservoirs. This means that the atmosphere is a very active reservoir for the cycling of water on Earth.

The global hydrological cycle comprises a multitude of different components (Fig. 1.1), which together result in a continuous water cycling. Water is transferred from the surface to the atmosphere through evaporation from the oceans, open waters, or transpiration from the plants. When an air parcel rises up in the atmosphere, it cools down and water condenses from a gas to a liquid to form cloud droplets. The cloud droplets can grow and when they are heavy enough, they sink down, transporting water from the atmosphere back to the Earths surface as precipitation. At the surface, a fraction of the precipitated water returns back to the atmosphere via evaporation and transpiration, but water can also infiltrate into the ground as soil moisture and groundwater, or return as river runoff to the ocean or other water bodies where the cycle continues. This cycle involves a continuous exchange of moisture between the oceans, the atmosphere, and the land, including the land biosphere.

The global water cycle is a central element for life on Earth and one of the key elements of the climate system. Water vapor provides rain water for the continental land masses,

Table 1.1   Global water reservoirs and turnover times. Adopted from: Reeburgh (1997).

	10^3 km^3	%	Turnover time
Oceans	1,370,000	97.61	37,000 y
Polar ice, glaciers	29,000	2.08	16,000 y
Groundwater	4,000	0.29	300 y
Freshwater lakes	125	0.009	10-100 y
Saline lakes	104	0.008	10-10,000 y
Soil moisture	67	0.005	280 d
Atmosphere (water vapor)	14	0.0009	9 d
Rivers	1.32	0.00009	12-20 d
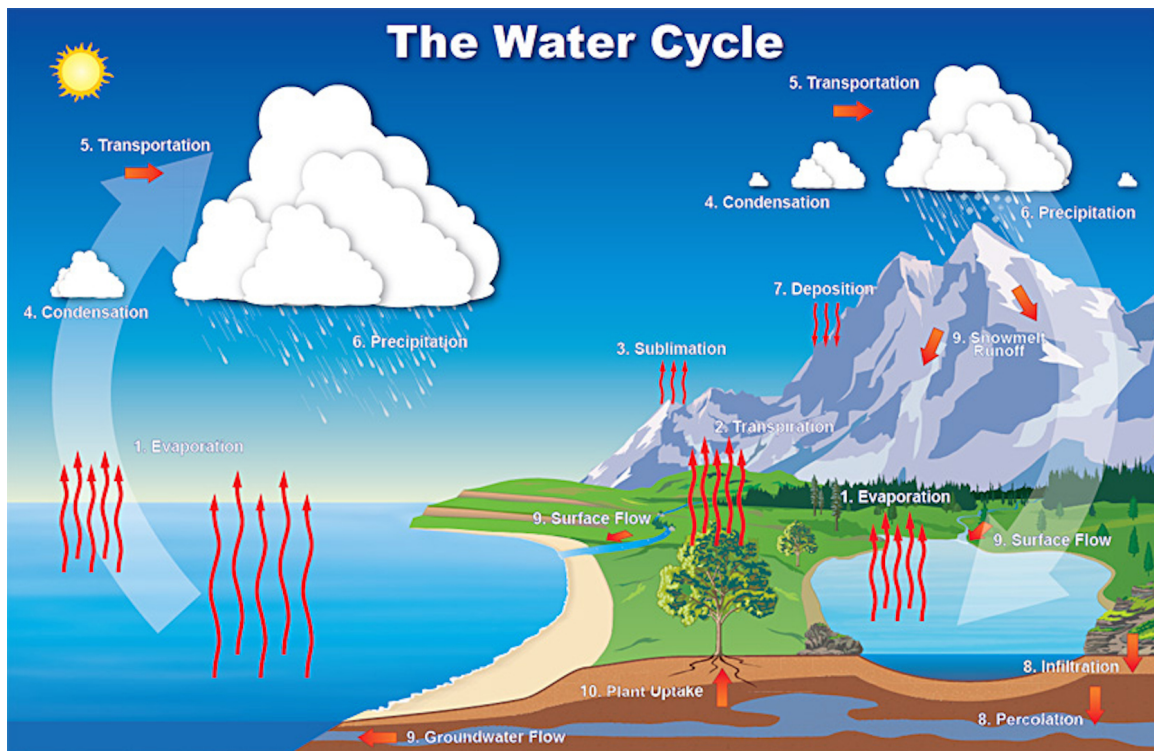
Figure 1.1 The hydrological cycle (water cycle) on Earth. Source: National Weather Service Jetstream project, National Oceanic and Atmospheric Administration (NOAA).

transports enormous amounts of energy in the form of latent heat from tropical to high latitudes, provides the substrate for clouds and ice sheets, which have a strong effect on the energy balance of the Earth, and is an important contributor to the atmospheric greenhouse gas effect. Liquid water is of utter importance for human agriculture and well-being and represents often a limited resource. For these and other reasons, the hydrological cycle has been studied intensively. In recent years, possible changes in the hydrological cycle associated with anthropogenic global warming have been in the focus of intensive research. Although important steps forward have been realized, large challenges remain in the understanding of ocean evaporation and land evapo-transpiration processes, as well as cloud formation and precipitation, in particular in tropical regions (IPCC, 2007; Stevens and Bony, 2013).

Land evapo-transpiration is an important component of the continental water cycle since it transports as much as 60 % of the land precipitation back to the atmosphere (Oki and Kanae, 2006) and also consumes about half of the total energy from the sun absorbed by continental land masses (Trenberth et al. 2009; Seneviratne et al. 2010; see Fig. 1.2). Figure 1.2 shows that almost half of the incoming solar radiation from the sun is absorbed by the surface (161 W m^{-2}) and half of that energy is transferred to the atmosphere as latent heat (80 W m^{-2}), which means by evapo-transpiration and re-condensation in the atmosphere. Within the evapo-transpiration fluxes, transpiration is the largest contributor to the total evapo-transpiration flux (Lawrence et al. 2007;
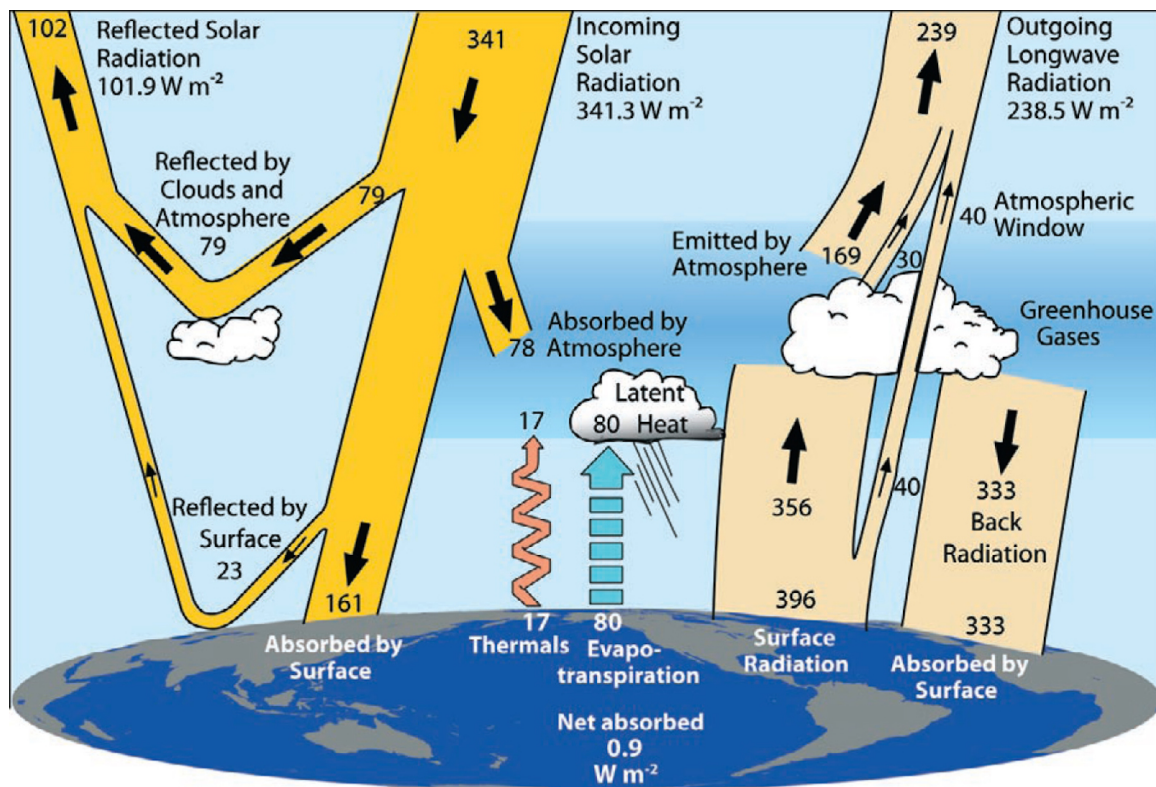
Figure 1.2 The global annual mean energy budget of Earth from March 2000 to May 2004 in W m^{-2}. The arrow size indicates the strength of the respective process. Source: Trenberth et al. (2009).

Blyth and Harding 2011) followed by canopy evaporation in the tropical rain forest and soil evaporation (Savenije 2004; Tsiko et al. 2012). Therefore, separation of different components in the evapo-transpiration flux is necessary for hydrological understanding and modeling purposes.

1.2 Atmospheric research using water isotopologues

1.2.1 Stable water isotopologues

Atoms are made up of a dense positively charged central nucleus surrounded by negatively charged electrons. The overall charge of an atom is neutral because the number of positive particles in the nucleus (protons) equals the number of electrons. Neutrons are uncharged particles with the same mass as a proton, and the sum of neutrons and protons is the atomic mass number. The number of protons in a nucleus is fixed for a given element and actually defines this element, but the number of neutrons can vary for elements. Isotopes are atoms of the same element that have the same numbers of protons and electrons but different numbers of neutrons, meaning that the various isotopes have different masses. We distinguish between stable and radioactive isotopes. Radioactive isotopes decay spontaneously with a very large range of lifetimes. In this

Table 1.2 Average natural abundances of hydrogen and oxygen isotopes on Earth. Source: Mook (2001).

Hydrogen		Oxygen	
Isotope	**Abundance (%)**	**Isotope**	**Abundance (%)**
^{1}H	99.985	^{16}O	99.76
^{2}H	0.015	^{17}O	0.038
^{3}H	$< 10^{-15}$	^{18}O	0.2

thesis we deal exclusively with stable isotopes. Stable isotopes are nuclides that do not decay to other isotopes on geological time scales although they may be produced by the decay of radioactive isotopes.

When different elements (atoms) combine to form certain molecules (e.g., two hydrogen atoms and one oxygen atom combine to form a water molecule) several isotopic varieties of the same chemical molecule can be made out of the different isotopes; these isotopically different molecules are called isotopologues. The most common isotopologue of water (HHO) consists of two hydrogen atoms with mass number one (^{1}H) and an oxygen atom with mass number 16 (^{16}O). When a light isotope of hydrogen or oxygen in water is replaced by a heavy isotope (e.g., ^{2}H, ^{17}O, ^{18}O), various heavy water isotopologues with one or more heavy isotopes can be formed. For atmospheric and hydrological cycle studies, the water isotopologues, ^{1}H$_2$^{18}O and ^{1}H^{2}H^{16}O or HDO (^{2}H = D, Deuterium), are commonly used. These water isotopologues are categorized as stable water isotopologues.

In terrestrial environments, the isotopic compositions of the same molecules in different reservoirs change because of isotope fractionation processes that often depend on mass. Different isotopologues behave chemically similar but due to the different masses the rates of different chemical and physical processes vary slightly. For example, different isotopologues have different zero point energy levels of the chemical bond, which lead to different chemical reaction rate coefficients, or different diffusion speed, which causes physical isotope separation during diffusion.

For the light elements, the heavy isotopes are considerably less abundant than the most common isotopes. For example, deuterium has a natural abundance in the ocean of approximately one atom in 6500 H atoms (0.015 %; Table 1.2). The stable isotopologues ^{17}O and the radioactive isotope ^{3}H are not used in this study, and are hence not considered further. Since water is made up of two hydrogen atoms and one oxygen atom, the isotopologue abundance is the same as the isotope abundance for ^{18}O (i.e., 0.2 %), but twice the isotope abundance for D (0.03 %)

1.2.2 Delta notation and fractionation constant

The isotopic composition of a sample is commonly expressed as a fractional difference of an isotope ratio R relative to a standard ratio and reported in delta (δ) notation:

$$\delta = \left(\frac{R_{\text{sample}}}{R_{\text{standard}}} \right) - 1 \tag{1.1}$$

where R is the heavy-to-light isotope ratio of a certain element in the sample or standard. In the case of water, $^2R = {^2}\text{H}/{^1}\text{H}$ is the deuterium-to-hydrogen ratio in the sample, and the international standard ratio is Vienna Standard Mean Ocean Water (VSMOW) with $^2R_{\text{VSMOW}} = 155.76 \pm 0.05 \times 10^{-6}$ and $^{18}R_{\text{VSMOW}} = 2005.2 \pm 0.45 \times 10^{-6}$ (Craig, 1961). As isotope variations are generally small, they are normally expressed as per mil (‰) difference from the standard being used. A higher or more positive δ values means that the heavy isotope content is higher than in the standard (also called "heavier"), and vice versa for lower or more negative δ values.

Numerous fractionation processes change the isotopic composition of water. Conceptually, two different types of fractionation processes are distinguished, equilibrium and kinetic fractionation. Equilibrium fractionation means that the two reservoirs that are connected via a chemical reaction or via a phase change remain in contact and can exchange isotopes to establish a chemical or thermodynamic equilibrium. An important example is the isotope equilibrium between the liquid/solid and the vapor phase in a closed system. In this case, the partial pressure of the respective water isotopologues over the liquid of the pure isotopologues controls the fractionation constant. Fractionation between two phases can be expressed by the isotopic fractionation factor α (alpha):

$$\alpha_{A-B} = R_A/R_B \tag{1.2}$$

Where R is the isotope ratio of the two phases A (e.g., water vapor) and B (e.g., liquid/solid water). In a closed system and in isotopic equilibrium, the heavy isotopologues of water are enriched in the condensed phase and depleted in the gas phase.

For kinetic fractionation, the fractionation constant is defined as the ratio of the rate coefficients of the heavy (index h) and light (index l) isotopologues, i.e.,

$$\alpha = k_h/k_l \tag{1.3}$$

Kinetic fractionation is associated with incomplete or unidirectional processes and can add an important contribution to the total fractionation for evaporation from water surfaces under windy condition or into dry air, evaporation of falling raindrops or formation of ice crystals in an oversaturated environment.

The enrichment factor ε_{A-B} (also called simply "fractionation" between A and B) is defined as:

$$\varepsilon_{A-B} = \left(\frac{R_A}{R_B} - 1 \right) = (\alpha_{A-B} - 1) \tag{1.4}$$

The equilibrium isotope fractionation factor (α) is nearly proportional to the inverse of temperature ($1/T$) at low temperatures in Kelvin (Majoube 1971b; Clark and Fritz 1997; Kendall and Caldwell 1998). Majoube (1971b) calculates the fractionation factor from liquid to vapor phase based on temperature as:
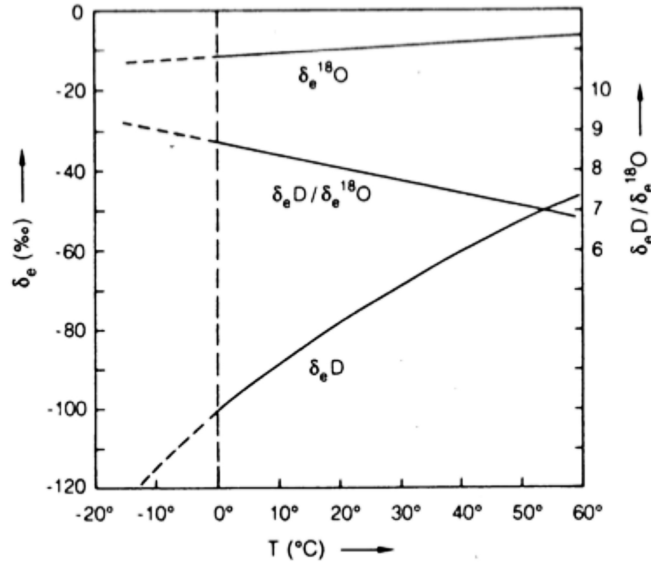
Figure 1.3 Relation between δD and δ^{18}O (left Y axis), and ratio δD/δ^{18}O (right Y axis) as a function of temperature. Source: Roedel (2000).

$$10^3 ln\alpha_{A-B} = \frac{10^6 a}{T^2} + \frac{10^3 b}{T} + c \qquad (1.5)$$

T is temperature in Kelvin, constants a, b, and c are a = 1.137, b = -0.4156, and c = -2.0667 for ^{18}O and a = 24.844, b = -76.248 and c = 52.612 for ^{2}H. Thus, under equilibrium condition, the isotopic enrichment of D and ^{18}O can be calculated as a function of temperature (Fig. 1.3).

A second order isotopic quantity, the deuterium excess (d-excess), provides an independent measure of the importance of kinetic effects. It was defined as the scaled difference between both water isotopologues (Dansgaard 1964):

$$d = \delta D - 8 \cdot \delta^{18}O(‰) \qquad (1.6)$$

The scaling factor 8 results from the approximate 1:8 relations between equilibrium fractionations for D and ^{18}O. Note that this ratio is temperature dependent and thus not fixed (Fig. 1.3). D then quantifies the difference from this relation, which is strongly influenced by the kinetic fractionation, arising from the different diffusivities of the different water isotopologues (HDO and $H_2{}^{18}$O). Therefore, the deuterium excess is often used to quantify not only the intensity of non-equilibrium processes in general but as specific proxy for hydrological processes such as lake or ocean surface evaporation conditions, vapor source regions identification, and moisture recycling.

For a fractionation process associated with a removal reaction, Dansgaard (1964) developed a simple model of isotopic fractionation. Such a Rayleigh distillation model describes the depletion of an air parcel from which water vapor is continuously removed,

e.g., via condensation, and the condensed phase cannot further exchange isotopes with the gas phase. The isotopic composition of the remaining vapor is then given by:

$$\delta D = (\delta D_0 + 1) \cdot f^{\alpha - 1} - 1 \tag{1.7}$$

Where f is the fraction of initial moisture remaining in the given air mass, α is the mean effective fractionation factor depending on temperature, and δD_0 is the initial δ value of the vapor.

1.3 The isotope effects

Since the first water isotopologue studies (Craig 1961; Dansgaard 1964) a number of empirical relationships between the isotopic composition of precipitation and several geographical or climatological parameters have been described. In the 1960s isotope ratio mass spectrometry had advanced sufficiently to allow many hundreds of isotope measurements within a reasonably short time span. The IAEA, a United Nation organization situated in Vienna, and World Meteorological Organization (WMO) built a worldwide precipitation sampling network and carried out isotope measurements on a monthly basis (Fig. 1.4). Since 1961, monthly precipitation samples over hundreds meteorological stations in more than 125 countries and territories have been collected as a part of the Global Network of Isotopes in Precipitation (GNIP). When analyzing the isotope data of the IAEA and relating them to various parameters (local temperatures, latitude, etc.) a number of relationships, so called "isotope effects", such as the temperature effect, the altitude effect, the latitudinal effect and the amount effect were discovered. In the following, the principal isotope effects will introduced, which repeatedly will be used in the subsequent chapters.

1.3.1 The temperature effect

The temperature effect denotes the spatial relationship between annual (or monthly or seasonal) mean temperatures and δ values of the respective precipitation (i.e., annual or monthly or seasonal mean). Such spatial relationships can be found on a regional (e.g., Greenland, Antarctica) or even on a global-scale. A linear relationship holds over a wide temperature range (-55 °C up to 15 °C) at globally distributed stations (Fig. 1.5). The heavy isotopologues of water become enriched in the precipitation when temperature increases. A simplified Rayleigh model allows explaining at least qualitatively the observed temperature effect. Dansgaard (1964) (Eq. 1.8) and Yurtsever (1975) (Eq. 1.9) derived the relation between monthly temperature (T) and isotopic composition of precipitation as:

$$^{18}\delta = 0.695T - 13.6\,‰ \tag{1.8}$$

$$^{18}\delta = (0.521 \pm 0.014)\,T - (14.96 \pm 0.21)\,‰ \tag{1.9}$$
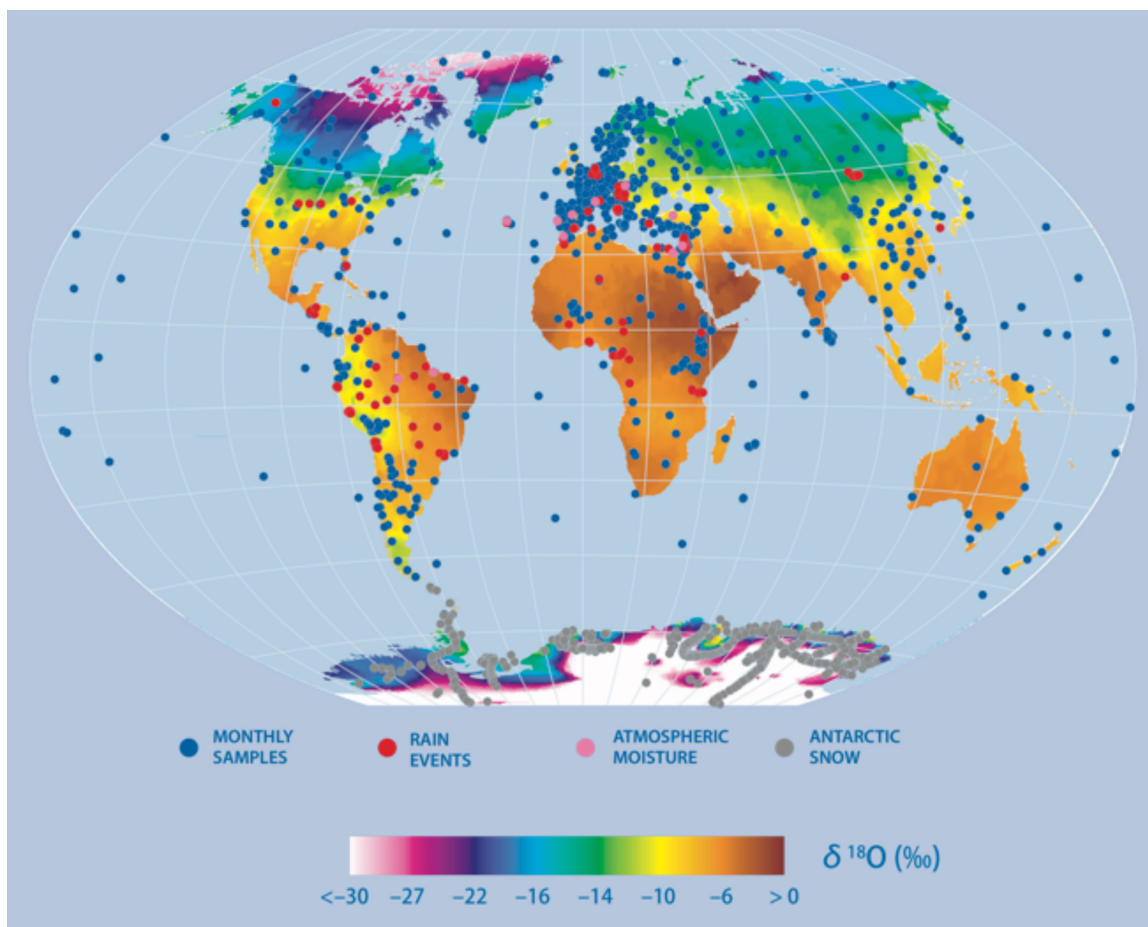
Figure 1.4 Global distribution of annual mean δ^{18}O (‰) in precipitation produced by interpolation of around 700 GNIP stations. Source: GNIP Brochure, IAEA.

Though the calculation of δ values using observed temperatures is in agreement with the observed isotopic composition of precipitation from worldwide GNIP stations, the results are not always valid for any given amount of precipitation. The isotopic composition of individual raindrops is a function of several parameters, e.g., the thermodynamic conditions during the cooling and the initial composition of the vapor (Dansgaard 1964).

1.3.2 The latitude and altitude effect

The latitude effect and the altitude effect denote linear relationships between δ values and these geographical quantities. Since both latitude and altitude correlate strongly with temperature, these effects are partly a direct consequence of the spatial temperature effect. There are some additional mechanisms involved that are independent of the temperature effect. For instance, the triggering of strong convective activity next to orographic obstacles and the associated strong rainout of the lifted air masses contributes to the altitude effect.
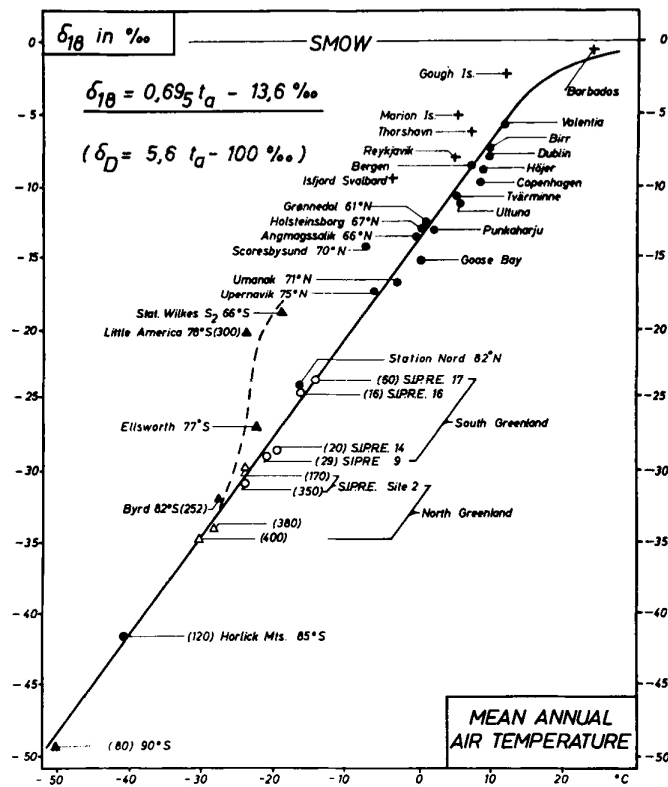
Figure 1.5 The annual mean $\delta^{18}O$ of precipitation as a function of the annual mean air temperature at the surface. Source: Dansgaard (1964).

The poleward transport of vapor from warmer regions to colder regions is the main cause for the latitudinal effect. During their transport from the tropics/sub-tropics to high-latitudes, air masses successively rainout. This rainout process is the main driver for the shown relationship between the isotopic composition of samples and the respective latitude (see Fig. 1.6). Though the principal mechanism behind this rainout is the decreasing temperatures at higher latitudes, the distribution of landmasses on earth contributes to the latitude effect as well. The main landmasses are situated between $30\,^{\circ}$N and $70\,^{\circ}$N. Air masses travelling over land are cut off from additional vapor sources from subjacent ocean surfaces. Therefore the δ-latitudes relation seems particularly steep from $30\,^{\circ}$N polewards (Fig 1.6). Simplifying one can say that the latitudinal effect is a combination between temperature and continental effect.

A strong, though slightly non-linear relation between the isotopic composition of water and altitude is demonstrated using data from the GNIP stations (Fig. 1.7). Again as expected from the temperature effect, the isotopic composition of precipitation becomes more negative at higher elevations. Based on Rayleigh model, Siegenthaler and Oeschger (1980) convoluted the temperature effect and the altitude effect using data from stations situated on mountain slopes at different altitudes. They found that the $\delta^{18}O$ and δD in precipitation are more depleted by -0.2 ‰ and -1.5 ‰ per 100 m altitude increase, respectively.
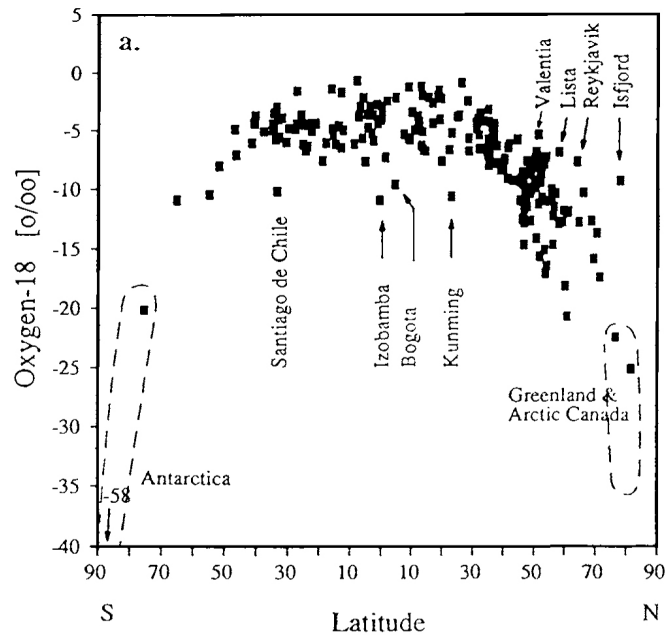
Figure 1.6 Long term annual mean $\delta^{18}O$ in precipitation from GNIP stations plotted as a function of latitude. Source: Rozanski et al. (1993).
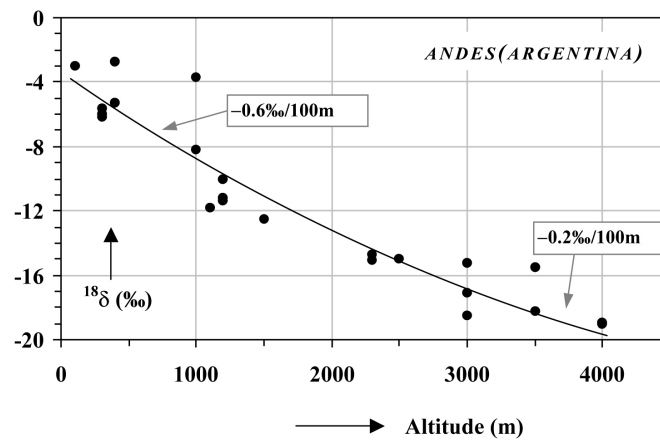
Figure 1.7 The altitude effect as evident in precipitation samples from the eastern slopes of the Andes Mountains. The magnitude of the effect is increasing from -0.2 to -0.6 ‰ / 100 m. Source: Gat et al. (2001).

1.3.3 The continental effect

Another geographical isotope effect is the continental effect, which is basically linked to the distance-from-coast of the respective precipitation sampling site. Along their trajectory across large continental land, air is disconnected from further oceanic water supply to compensate for the successive rain events. This leads to an additional distillation or rainout effect, depleting the travelling air masses on their way to the continental interior.

The farther the sampling site is from the oceanic vapor source, the more it is altered by rainout and, thus, the more intense the isotopic depletion. The isotope continental effect is therefore related to the temperature effect by the classical continentality of climate. However it adds an additional mechanism to the purely temperature controlled rainout processes. The strength of the respective continental effect in different parts of the world depends on the type of the continental surface and its respective vegetation coverage controlling thereby evapo-transpiration and moisture re-evaporation (Gat and Matsui 1991).

The water isotopologue map (isoscape) in Figure 1.8 illustrates the distribution of $\delta^{18}O$ in precipitation over the North American continent. The distribution of $\delta^{18}O$ was computed using a multi-linear regression of many climate and geographic parameters (not the distance to the coast) on the comparably dense network of sampling stations. It clearly illustrates the above-discussed isotope effects. Mountain chains are marked by more negative $\delta^{18}O$ values as a result of the altitude effect (the Rocky Mountains). The isoscape map gives also a nice illustration of the continental effect. The principal vapor source of the Central (Great Plaines) and Southern USA is the Gulf of Mexico with its warm ocean surface temperatures. Along the principal vapor trajectory from the gulf into the continental interior one observes a spatial isotopic gradient from -4 ‰ to -8 ‰. Further clear examples of the continental effect are discussed in the literature for many regions such as Europe, South America, and less pronounced in Africa due to data scarcity (Gat and Matsui 1991; Rozanski et al. 1993). The strength of the continental effect varies, as mentioned above, as a function of the recycling intensity and the associated vegetation coverage. It varies however also seasonally with typically much steeper isotopic gradients during winter when recycling is strongly reduced.

1.3.4   The amount effect

In regions with temperatures above $\pm$ 15 $^\circ$C, the linear relation between surface temperature and water isotopologues disappears nearly entirely. Besides of some mountain regions there is basically no temperature effect in the tropics and large parts of the sub-tropics. Instead, a relation between the amount of precipitation and its isotopic composition, the so-called amount effect, appears in the data (Fig. 1.9). This effect is well established on different spatial and time scales and was first described by Dansgaard (1964). He studied the amount effect on a large spatial scale comparing the annual mean precipitation and associated isotopic signals measured at a number of tropical islands and computed a linear regression slope for $\delta^{18}O$/precipitation of -1.6 ‰ per 100 mm rain (averaged over Canton, Christmas, Guam, Johnston, Seychelles and Wake islands). However, the effect shows up even more clearly on a seasonal scale in tropical/sub-tropical regions with a marked seasonality in precipitation. But even on a synoptical scale the amount effect is clearly apparent.

Figure 1.9 demonstrates that the isotopic composition of precipitation is progressively depleted in heavy isotopologues with increasing precipitation rate over a time span of a couple of hours. Although the data show an inverse correlation between precipitation amount and its isotopic composition, the causes and mechanisms leading to the isotope
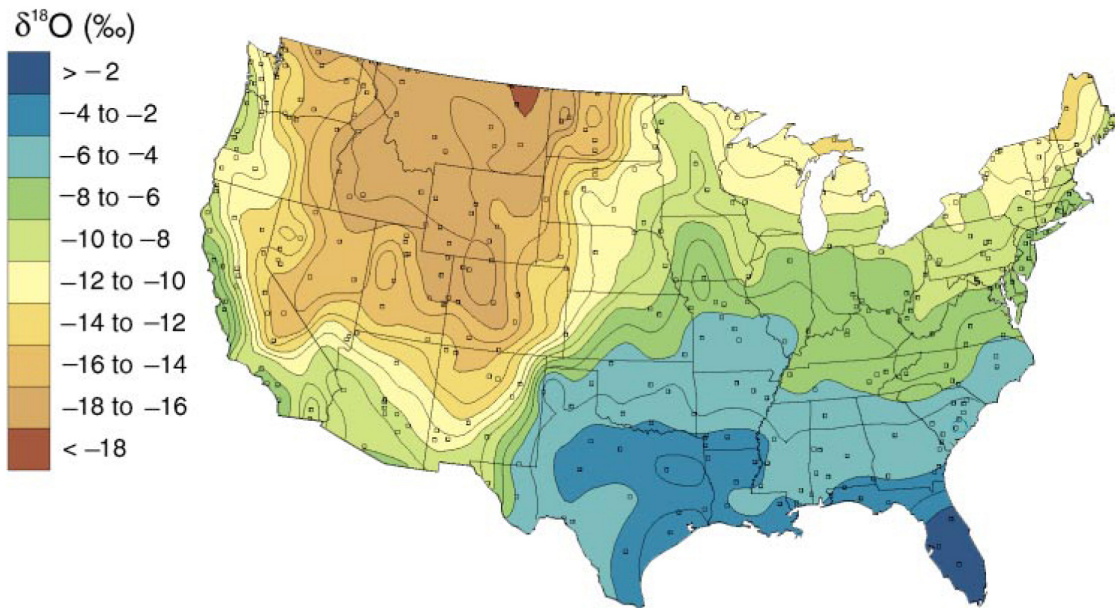
Figure 1.8 Continental effect observed in the USA from discharge-weighted mean δ^{18}O values. Source: Kendall and Coplen (2001).
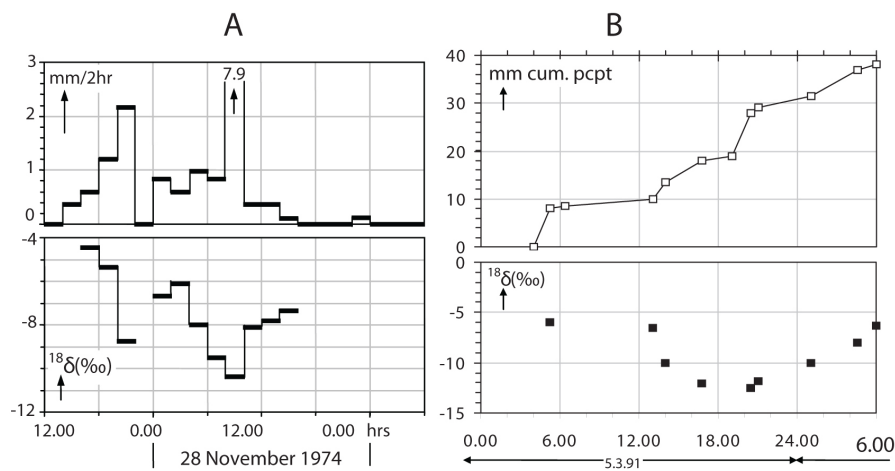
Figure 1.9 Precipitation rate (in mm / 2 hours) and its isotopic composition (a), and cumulative rain over some periods and its isotopic composition (b). Source: Gat et al. (2001).

amount effect are still under debate (Dansgaard 1964; Aggarwal et al. 2007; Risi et al. 2008).

Dansgaard (1964) already mentioned a number of possible processes, which may influence the isotope amount effect such as diffusive exchanges with the surrounding vapor, convection, and re-evaporation of the falling rain. A study from Risi et al. (2008) investigates the amount effect in more detail and shows that it is predominantly affected by two

main atmospheric processes, 1) re-evaporation of falling rain and diffusive exchange with surrounding vapor, and 2) recycling of the sub-cloud layer vapor feeding the convective system. Our study in chapter 5 supports the interpretation of Risi et al. (2008).

1.4 The role of water isotopologues to investigate the hydrological cycle

In the atmosphere, water vapor is transported over large distances and undergoes often several phase changes before returning to the ocean. These processes leave a characteristic imprint on the isotopic composition of atmospheric water vapor and the corresponding precipitation. From the first phase change during evaporation from the ocean surface to condensation of rain droplets and possible re-evaporation of falling raindrops, the corresponding phase changes are associated with well-known equilibrium and kinetic fractionation processes. Water isotopologue analysis becomes therefore an important tool to gain information on the hydrological cycle. For this reason, the IAEA/GNIP network has goals, which are: (1) to provide data for hydrological investigations within the scope of water resources inventory, planning and development, (2) to provide input data to verify and further improve atmospheric circulation models, and (3) to study climate change.

Plant transpiration is the largest flux from the continental land evaporation, however the fraction of transpiration over total evapo-transpiration is still under debate and poorly understood. One attractive method to partition the evapo-transpiration flux into its individual components is the use of isotope measurements. This is because the isotopic composition undergoes characteristic changes (isotope fractionation) during a number of physical processes, importantly phase changes and diffusion. As an important example, evaporation changes the isotopic composition of soil water, whereas transpiration via plants does not strongly modify the isotopic composition of root water (Ehleringer and Dawson 1992; Williams et al. 2004). Using these distinct isotope signatures allows the water isotopologue technique to qualitatively distinguish between soil evaporation and transpiration, for example studies by Yepez et al. (2003) in Arizona USA, Robertson and Gazis (2006) in Washington USA, and Sutanto et al. (2012) in the Netherlands.

It is beyond the scope of this thesis to document and exemplify each of these applications of the water isotopologues in present day hydrology but it is interesting to mention some examples. The isotope composition of precipitation has been used to reconstruct water sources in Southeast Asia, to investigate water recycling in Amazonia and to study tropical cyclones (Martinelli et al. 1996; Araguás-Araguás et al. 1998; Ichiyanagi and Yamanaka 2005; Brown et al. 2008; Gat and Matsui 1991). In more classical hydrological studies, the water isotopologues were used within two-source mixing models to estimate the contribution of isotopically separated river or groundwater flows (Wels et al. 1990; Arnold et al. 1995).

About a dozen Global Climate Models (GCMs) are already equipped with water isotopologue diagnostics. Since GCMs are highly complicated and represent non-linear models of many variables and parameters, it is often difficult to evaluate certain parameters such as regional precipitation patterns. Even a good correspondence between observations

and model results does not guarantee that the models computed the respective parameter for the right reason. Adding the water isotopologues to the water cycle of a GCM allows an independent test for the models hydrology (Hoffmann and Heimann 1997; Schmidt et al. 2005; Yoshimura et al. 2008).

But also beyond present day applications the water isotopologues were intensively used in paleo-climatology. In particular the isotope temperature and amount effects were used as modern analogues to reconstruct past climate. Information on the water isotopic composition of past precipitation is stored in many different geological archives such as polar ice caps and glaciers, calcite deposits, sweet water lake deposits or tree ring cellulose. Most famously this has provided detailed information on temperature variations during the last glacial-interglacial cycles as far back as 800,000 years (Jouzel et al. 2007; Petit et al. 1999).

Traditionally, most water isotopologue studies have investigated only water in precipitation, the end product of a multitude of evaporation, condensation and mixing processes. Isotopic measurements of water vapor are more complicated and are therefore sparse, but can give important additional information. Recent atmospheric applications focused on water isotopologues as proxy for exchange processes in the upper troposphere and lower stratosphere (Webster and Heymsfield 2003; Payne et al. 2007; Steinwagner et al. 2007), but only few in-situ measurements of the isotopic composition of lower tropospheric water vapor are available (Ehhalt et al. 1977; Lawrence et al. 2004; Schneider et al. 2006; Wunch et al. 2010). The Project for Intercomparison of Land Parameterization Schemes (PILPS) has devoted a special subproject (iPILPS) to the set-up and validation of water isotopologue schemes in land models (see e.g., Henderson-Sellers et al. 2006; Fischer and Sturm 2006).

1.5 Global water vapor isotopologues from satellites and model

Classical mass spectrometric techniques were principally used to measure liquid water samples, for example in the IAEA/GNIP network. However, measuring the isotopic composition of water vapor was much more difficult and therefore much more scarce. Comparably large air volumes had to be pumped into a cooling system to extract carefully the contained water vapor without additional fractionation. Only very few studies on the isotopic composition of water vapor were published. Most of them concentrated on the technical aspects of the extraction procedure itself (Ehhalt et al. 1989; Franz and Röckmann 2005). Moreover, isotopic measurements of extremely dry air from high altitudes or from polar sampling stations in Antarctica turned out being impossible due to these difficulties. In summary, the extraction of liquid water for subsequent spectrometric measurements was an extremely time consuming and expensive technique which basically made systematic, long term monitoring of water vapor hardly possible. This technical problem represented a major limitation for a full use of the water isotopologues. Even an extensive network such as the IAEA/GNIP only sampled precipitation, which represents less than 99 % of all water in the atmosphere. The full dynamics of the atmospheric water cycle and the bulk of atmospheric water were not accessible for isotope sampling.

It was only in the last decade that optical instruments overcame sampling difficulties of water vapor. New spectroscopic techniques have provided us with fast and comparably cheap measurements of the isotopic composition of water vapor and the number of measurement stations is quickly increasing.

Because of their global coverage, satellite measurements potentially can fill the gaps between in-situ isotopic vapor measurements. Over the last decade, new datasets from the Tropospheric Emission Spectrometer (TES) aboard the Aura spacecraft (Worden et al. 2006, 2007) and from the SCanning Imaging Absorption spectroMeter for Atmospheric CHartographY (SCIAMACHY) instrument aboard the ENVISAT satellite were published (Frankenberg et al. 2009) and revealed quantitative information about tropical water recycling such as rain evaporation (Worden et al. 2007), convection (Risi et al. 2010; Samuels-Crow et al. 2014), moistening and dehydration (Brown et al. 2013). Other remote sensing datasets delivered information on the isotopic composition of vapor at tropopause level or even in the stratosphere (the Michelson Interferometer for Passive Atmospheric Sounding (MIPAS) on Envisat; Payne et al. 2007; Steinwagner et al. 2007). These data represent important additional information on the sources and sinks of water vapor in the stratosphere, which acts as a very effective greenhouse gas at high altitudes (Solomon et al. 2010).

On the other hand, the physics of the different water isotopologues has been incorporated in general circulation models (GCM). The observed spatial and temporal variations of the isotopic content of precipitation from the GNIP network have been used to examine water sources and the relationship between the water isotopologues and climate from the GCM models (Noone and Simmonds 2002; Hoffmann et al. 1998; Jouzel et al. 1997; Yoshimura et al. 2008; Risi et al. 2010). In the following, only two satellite datasets (TES and SCIAMACHY) and the ECHAM4 (European Center HAMburg 4) model that are mostly used in the work presented in this thesis are described.

1.5.1 SCIAMACHY data

The SCIAMACHY instrument aboard the European Space Agency (ESA) environmental research satellite ENVISAT measured between 2003 and 2012 near short-wave infrared spectra, which allows the retrieval of total column abundances of H_2O and HDO (Frankenberg et al. 2009; Scheepmaker et al. 2013, 2015). SCIAMACHY has high sensitivity throughout the entire atmospheric column down to the surface. The SCIAMACHY spectrometer has relatively high spectral resolution (0.2 nm to 0.5 nm) and covers a wide wavelength range (240 nm to 1700 nm and 2000 nm to 2400 nm) with an apodized spectral resolution of 0.85 cm^{-1}, which enables SCIAMACHY to detect many different gases, clouds and aerosols. In addition, SCIAMACHY has three different viewing geometries, which are nadir, limb and sun/moon occultation. HDO data were retrieved from nadir measurements using a narrow wavelength interval from 2355 to 2375 nm (Frankenberg et al. 2009). The footprint area of an individual HDO measurement is 120 by 30 km. HDO data used in this study are temporally averaged from 2003 to 2007. Detailed information about the retrieval procedure and data processing can be found in Frankenberg et al. (2009) and Scheepmaker et al. (2015). For SCIAMACHY, the δD total column is

calculated from the retrieved HDO and H_2O columns, in contrast to TES where the δD is very close to an optimal estimation product calculated from the spectral radiances (see below).

1.5.2 TES data

The Tropospheric Emission Spectrometer (TES) aboard the Aura satellite is an infrared Fourier Transform Spectrometer (FTS), which measures the spectral infrared (IR) radiances between 650 cm^{-1} and 3050 cm^{-1} in the limb and a nadir viewing mode. HDO and H_2O abundances were obtained from TES thermal radiances between 1200 cm^{-1} and 1350 cm^{-1} (7400 to 8300 nm in wavelength) with an apodized spectral resolution of 0.1 cm^{-1} for the nadir view. The footprint is 5.3 by 8.4 km in the nadir-viewing mode. In this configuration, TES provides vertical information of abundant atmospheric species, such as O_3, CO, CH_4, H_2O and HDO (Worden et al. 2006). For the version 4 dataset, weighted mean values of the isotopic composition were provided for the height interval 500 to 850 hPa, where the HDO measurements have the highest sensitivity. Detailed information about TES data in general and the TES water isotopologue dataset can be found in Worden et al. (2004, 2006).

The TES retrieval version 5 (TES V5) has an improved sensitivity near the surface and covers the altitude range from 900 hPa to 350 hPa (Worden et al. 2012). The increased number of radiance measurements used for retrieval and the change of both the hard constraints (e.g., retrieval levels and mapping matrices) and the soft constraints (e.g., constraint matrix) in the version 5 dataset improve the TES V5 sensitivity (Worden et al. 2012). A good indicator for retrieval sensitivity is the number of degrees of freedom (DOF), which shows how well the retrieved signal is able to capture the variability of the true distribution. There number of data points at higher latitudes that pass the applied DOF criteria is much higher for TES V5 than TES V4 (see Fig. 5 in Worden et al. 2012) indicating clearly the improvement of data quality. The data used in this study are TES data measured from 2004-2011 for both satellite product version 4 and 5. During this time interval, TES had good spatial and temporal resolution. Filtering procedures have been applied to both versions with the same criteria, such as Degree Of Freedom signal, DOF > 0.5 and Species Retrieval Quality, SRQ $= 1$, in order to have an equal comparison.

1.5.3 The ECHAM4 model

The ECHAM atmospheric GCM was developed at the Max-Planck Institute for Meteorology in Hamburg. It is an atmospheric general circulation model (Röckner et al. 1996), which was used within the CMIP4 (Coupled Model Intercomparison Project; Covey et al. 2003) model inter-comparison study. Similar to the ECMWF forecast model, from which the ECHAM model was developed, it uses the spectral transform method for the "dry dynamics" (i.e., wind, temperature) but uses a semi-Lagrangian transport scheme for humidity and tracers such as the water isotopes (Williamson and Rasch 1994). The land surface scheme is based on a simple "bucket scheme" balancing the fluxes of heat and moisture over continental surfaces. Vegetation coverage and its influence on evapo-transpiration and runoff in dependence of the soils water holding capacity are parameterized in a highly

idealized way. The models cloud scheme distinguishes between stratiform clouds typical for the extensive cloud bands of the extra-tropics and a convective cloud scheme dominating in tropical regions (Tiedtke 1989). A water isotope module was added to the AGCMs model physics and tracks the different water isotopologues ($H_2^{18}O$, HDO, etc.) in each part of the AGCMs hydrology (Hoffmann et al. 1998). Each phase change is associated with temperature- and humidity-dependent isotopic fractionation processes, which are well known from laboratory experiments. The water isotope module allows therefore computing the full 4-dimensional distribution of the water isotopologues in all simulated water reservoirs of the ECHAM model.

The ECHAM4 version used in this study was run with a spatial resolution of $2.8\,°$ by $2.8\,°$ (spectral resolution T42), with a vertical sigma-pressure hybrid resolution of 19 layers extending from the surface to 10 hPa. The ECHAM4 model was "nudged" by a spectral nudging technique (von Storch et al. 2000) specifically developed for the "spectral" ECHAM model. This procedure guarantees a good representation of past atmospheric conditions since the simulated wind fields are forced to be close to the ERA40 reanalysis data. It has been shown that this approach considerably improves both, precipitation and its isotopic composition for specific months, compared to climatological means. The ECHAM4 model was nudged over the period 1971-2001. Detailed information about ECHAM4 can be found in Hoffmann et al. (1998).

1.6 Research questions and outline

The main research question addressed in this thesis is: **How can measurements and modeling of water vapor isotopologues help to study the hydrological cycle?** In the following, this study focuses on different aspects of the hydrological cycle:

- How accurate is the isotope-based approach to determine the contribution of transpiration to total evaporation? (Chapter 2).

- How good are the satellite data and an isotope-enabled global circulation model in representing the first-order isotope effects on the global-scale? (Chapter 3).

- Are changes in the isotopic composition of water useful climatic indicators for drought and flooding events? (Chapter 4).

- What atmospheric processes control the isotopic composition of water vapor in the lower and middle troposphere during ENSO (El Niño Southern Oscillation) events in the Central and West Pacific regions? (Chapter 5).

- Does the strength of lower tropospheric mixing and climate sensitivity leave an imprint in isotopic composition of water vapor (Chapter 6)?

Transpiration is the largest contributor of water to the hydrological cycle from the terrestrial ecosystem. Several approaches have been used to estimate quantitatively the relative contribution of these different fluxes. Since the isotopic composition of the transpirative flux from vegetation is different from the other fluxes, a two-flux model was

developed based on different isotopic constraints. This longtime existing isotope-based method is introduced in Chapter 2 and compared with other methods such as the hydrometric method and estimates based on land-surface models. The study discusses the limitations and accuracy of each method and analyzes to which point the isotopic method produces results that systematically diverge from the other methods.

Chapter 3 examines three different satellite datasets (TES version 4 and version 5, and SCIAMACHY) and compares them with model results focusing particularly on the first order isotope effects presented above. A major point of this analysis is the improvement of the new version of TES dataset (version 5) compared to version 4 clearly showing up when using the classical isotope effects as a benchmark to evaluate the satellite datasets. It is a central point for this analysis that the model results have to be modified so that they mimic the specific way the satellite instrument is observing the atmosphere. The humidity bias of the model relative to the observations can translate into strong biases in the modeled isotopic composition when compared to the observations. Clear differences in the performance of the observational data are identified by studying the seasonal variations of the isotopic composition of water near the Inter Tropical Convergent Zone (ITCZ).

Chapter 4 presents a correlation analysis of drought with an important ENSO index on the one hand and the isotopic composition of water on the other hand in the West Pacific (Indonesia). In this chapter, two drought indices, Standardized Precipitation Index (SPI) and Standardized Precipitation Evaporation Index (SPEI), are calculated using the ECHAM4 model outputs and compared with the calculation from in-situ observations. The relationship of droughts and ENSO, and of the droughts and the isotopic composition of water are discussed in detail. The performance of SPI and SPEI as indicators of the drought strength is validated based on data from paddy field damages during documented drought events.

Chapter 5 again discusses the relations between ENSO, the tropical hydrological cycle, and the water isotopologues. The region of interests in this chapter is the entire tropical Pacific. The focus here is in particular on the well-known changes of the tropical hydrological cycle and their link with ENSO. During an El Niño event, convective activity shifts from the West Pacific Warm Pool to the Central Pacific. The study shows that these shifts of convective activity in the tropics provoke specific patterns of the water isotopologues, which can be explained by a set of mechanisms such as re-evaporation of raindrops and associated isotopic equilibration between vapor and rain, and mixing of convectively uplifted low level air into the middle atmosphere. The proposed mechanisms link the isotopic composition of water to specific processes in the hydrological cycle. Our findings contribute to a more complete understanding of the isotope amount effect.

GCMs react quite differently when forced with the same external radiative forcing such as the rise of atmospheric greenhouse gas concentrations. For the same forcing (2 times of CO_2) the GMCs that participated in the Intergovernmental Panel on Climate Change (IPCC) model inter-comparison project computed for example a temperature range between 1.5-4.5 °C (Andrews et al. 2012; Sherwood et al. 2014). It is widely accepted that the existing spread of simulated climate sensitivities is associated to the interaction between tropical oceans, cloud dynamics and associated radiative feedbacks. In recent publications, a link was made between tropospheric mixing, low-level cloud formation and

the respective modeled climate sensitivity (Sherwood et al. 2014; Su et al. 2014). A study in chapter 6 uses the isotopic composition of water to study the inter-model spread in lower tropospheric mixing and relates this spread to the models climate sensitivity and simulated vertical isotopic gradients. This study uses results from 10 isotope-enabled GCM models and compares the model results with the TES observations. Following former studies the study focuses on one specific and simplified component of tropospheric mixing, small-scale mixing. This component is quantitatively estimated by comparably simple atmospheric indices and compared with simulated water isotope patterns. The final aim of such an approach is the future use of the isotopic composition of water in climate models to evaluate respective hydrological responses in these models, which could contribute to more reliable predictions of the future climate changes.

The last chapter (chapter 7) concludes the thesis by summarizing the main results and proposing directions for further research.

2 Continental transpiration from difference approaches

"What we are doing to the forests of the world is but a mirror reflection of what we are doing to ourselves and to one another"
Mahatma Gandhi

Abstract

Current techniques to disentangle the evaporative fluxes from the continental surface into a contribution evaporated from soils and canopy, or transpired by plants, are under debate. Many isotope-based studies show that transpiration contributes generally more than 70 % to the total evapo-transpiration, while other isotope-independent techniques lead to considerably smaller transpiration fractions. This study provides a perspective on isotope-based versus non-isotope-based partitioning studies. Some partitioning results from isotope-based methods, hydrometric measurements, and modeling are presented for comparison. Moreover, the methodological aspects of the partitioning analysis are considered, including their limitations, and explanations of possible discrepancies between the methods are discussed. We suggest sources of systematic error that may lead to biases in the results, e.g., instruments inaccuracy, assumptions used in analyses, and calibration parameters. A number of comparison studies using isotope-based methods and hydrometric measurements in the same plants and climatic conditions are consistent within the errors; however, models tend to produce lower transpiration fractions. The relatively low transpiration fraction in current state-of-the-art land-surface models calls for a reassessment of the skill of the underlying model parameterizations. The scarcity of global evapo-transpiration data makes calibration and validation of global isotope-independent and isotope-based results difficult. However, isotope-enabled land-surface and global climate modeling studies allow for the evaluation of the parameterization of land-surface models by comparing the computed water isotopologue signals in the atmosphere with the available remote sensing and flux-based data sets. Future studies that allow for this evaluation could provide a better understanding of the hydrological cycle in vegetated regions.

2.1 Introduction

Continental evapo-transpiration (including transpiration, soil evaporation, and canopy evaporation) is an important process controlling energy and mass exchange between the

terrestrial ecosystems and the atmosphere (Seneviratne et al. 2010). Transpiration is the largest contributor to the evapo-transpiration fluxes from continental areas (Lawrence et al. 2007; Blyth and Harding 2011; Jasechko et al. 2013). Therefore, many studies have been carried out to quantify the transpiration fraction through direct measurements or techniques disentangling the various evapo-transpiration components. Direct measurement of transpiration has been performed for decades, but the accuracy and separation of transpiration from total evapo-transpiration still remain a challenge. The fraction of transpiration to the total evapo-transpiration flux obviously depends upon the nature and state-of-the-surface, such as the presence of lakes or the seasonality of vegetation (growing in the spring or dormant in autumn). These conditions generate variability in each evapo-transpiration component and complicate the separation of the various components.

There are many methods and techniques to quantify this transpiration fraction. A conventional method for partitioning evapo-transpiration is the combination of hydrometric measurements such as sap flow to measure transpiration rate with other methods to calculate total evapo-transpiration (Kelliher et al. 1992; Herbst et al. 1996; Roupsard et al. 2006; Mitchell et al. 2009; Cavanaugh et al. 2011). Soil evaporation is then calculated from the difference of total evapo-transpiration and transpiration with the assumption that canopy evaporation is a small component and can be neglected. More recent methods analyze the isotopic composition of liquid water and water vapor (Yepez et al. 2003; Ferretti et al. 2003; Williams et al. 2004; Xu et al. 2008; Lai et al. 2006; Robertson and Gazis 2006; Wang et al. 2010; Sutanto et al. 2012; Jasechko et al. 2013). This method has become common since measurements of stable isotopologues in precipitation and water vapor are relatively easy and robust. Other methods use global land-surface models (Choudhury and DiGirolamo 1998; Dirmeyer et al. 2006; Oleson et al. 2004). In the land-surface models, the contribution of each evapo-transpiration component is principally simulated from the land-surface scheme due to, for example, turbulent transfer, moisture limitations, and plant physiology. Although all methods above can estimate the transpiration fraction, results from these methods vary. In general, isotope-based methods tend to result in a higher transpiration fraction than other methods. Jasechko et al. (2013) estimated the global transpiration fraction to be 80-90 % of the total evapo-transpiration from land, which implies a more dominant role of transpiration than most other previous studies. The transpiration flux in that study was calculated using the isotope mass balance method in lake catchments where the isotopic composition of the evaporative flux was estimated using an evaporation model applied to the isotopic composition of the lake water.

This study provides a perspective on the isotope-based method for isolating the contribution of transpiration to the total evapo-transpiration flux. As canopy evaporation is neglected in most isotope-based studies, the study mainly discusses evapo-transpiration as a combination of transpiration and soil evaporation only. Some partitioning results from hydrometric measurements and modeling are presented for comparison. Also how the partitioning studies have been carried out, their limitations, and the possible causes of the discrepancies between those methods are discussed briefly.

2.2 Methods to derive the transpiration fraction of evapo-transpiration

2.2.1 Isotope-based method

The use of stable water isotopologues (principally $H_2^{18}O$ and $^1H^2HO$) as tracers present a new and important technique to enable flux tracing within the soil-plant-atmosphere continuum (SPAC) system (Dawson and Ehleringer 1998; Mook 2001; Zhang et al. 2010b; Wenninger et al. 2010). Processes like water diffusion and phase changes affect the partial pressures of the different water isotopologues. The lighter isotopologues preferentially evaporate from bare ground and open water surfaces such as oceans and lakes, and leave the condensate phase enriched in the heavier isotopologue. In contrast, transpiration does not modify the isotopic composition of the remaining groundwater since there is no isotopic fractionation during water uptake and transport in roots and stems (Ehleringer and Dawson 1992; Dawson and Ehleringer 1998; Tang and Feng 2001; Williams et al. 2004). This distinct isotopic difference makes water isotope analysis an interesting diagnostic for a quantitative separation between the evapo-transpiration flux from bare soils and open water on the one hand, and plant transpiration on the other hand.

Earlier studies to measure transpiration using stable isotope measurements have been carried out on eucalyptus trees by Calder et al. (1986), Calder (1992), and Calder et al. (1992). They injected deuterated water (D) into tree roots and measured the transport of deuterium in stem water from roots to leaves as a tracer. Transpiration was calculated based on the total mass of tracer administered and the concentration in the stem water.

The isotope mass balance method is used to quantify the transpiration fraction. This method is based on a simple two-source mixing model, where evapo-transpiration (F_{ET}) is a sum of soil evaporation (F_E) and transpiration (F_T):

$$F_{ET} = F_T + F_E \tag{2.1}$$

where F denotes a flux and subscript ET stands for evapo-transpiration, T for transpiration and E for soil evaporation. When each flux has its characteristic isotopic composition δ, the isotopic mass balance is

$$F_{ET}\delta_{ET} = F_T\delta_T + F_E\delta_E \tag{2.2}$$

Transpiration and soil evaporation fluxes can be derived from Eq. (2.2) according to Zhang et al. (2010b):

$$F_E = \frac{\delta_T - \delta_{ET}}{\delta_T - \delta_E}F_{ET} \tag{2.3}$$

$$F_T = \frac{\delta_{ET} - \delta_E}{\delta_T - \delta_E}F_{ET} \tag{2.4}$$

The total evapo-transpiration flux (F_{ET}) can be directly calculated using hydrometric methods as described in Sect. 2.2.2 (eddy covariance, Bowen ratio, lysimeter, etc).

The isotopic composition in each evapo-transpiration component can be obtained from direct measurements (e.g., using a bare soil lysimeter), and calculated using empirical methods. The Craig-Gordon formulation has often been used to calculate the isotopic composition of transpiration (δ_T) and soil evaporation or open water evaporation (δ_E; Craig and Gordon 1965). The principle of this conceptual method is that the isotopic composition of the net soil evaporation or transpiration (extended Craig-Gordon model) flux can be derived as a function of environmental parameters (e.g., temperature, humidity). In this model, measurements of isotopic composition in the evaporating front of soil water (δ_e), isotopic composition in water vapor (δ_v), temperature, and relative humidity are required to calculate δ_E. For this method, the determination of the depth of the evaporating front and isotopic composition of water vapor are crucial. The soil evaporating front, which is defined as the transition zone between the liquid and vapor diffusion, can be determined from the profiles of soil water isotopic composition. This position (usually between 0.1 and 0.5 m; Barnes and Allison 1983; Dawson and Ehleringer 1998; Clark and Fritz 1997; Wang and Yakir 2000; Sutanto et al. 2012) is clearly marked by the enrichment of heavy isotopes in the soil water above the front due to soil evaporation and depletion of heavy isotopes in the soil water below the front due to diffusion and capillary rise (see Fig. 2.2). This implies that detailed measurements of the isotopic composition of soil water in the vertical soil profile are needed. The isotopic composition of water vapor can be measured directly; sometimes it is assumed that δ_v is in equilibrium with precipitation.

The isotopic composition of transpiration can be estimated from measurement of water in leaves, or calculated based on an empirical method (e.g., Craig-Gordon method). In the Craig-Gordon method, the isotopic composition of transpiration is calculated from the modeled values of leaf water enrichment (δ_L). Under steady-state conditions, the isotopic composition of leaf water is assumed equal to the isotopic composition of plant source water, being stem water or soil water in the rooting zone. However, this assumption is generally not satisfied for short (hourly to daily) timescales and not valid under rapidly changing environmental conditions (Yepez et al. 2005; Lee et al. 2007b; Welp et al. 2008; Xu et al. 2008; Zhang et al. 2010b; Wang et al. 2012a). Some studies observed that a modeled transpiration under the steady-state assumption (SSA) is similar to measurements when stomata were fully open. This condition is only met during the afternoon (Yepez et al. 2005; Farquhar and Cernusak 2005; Lai et al. 2006; Zhang et al. 2010b). Some methods exist to estimate the isotopic composition of leaf water in non-steady-state conditions. A non-steady-state model proposed by Dongmann et al. (1974), and the Farquhar-Cernusak model (Farquhar and Cernusak 2005) can be used to calculate δ_L (see also Zhang et al. 2010b). According to Farquhar and Cernusak (2005), the degree of isotopic enrichment of transpired water under non-steady-state conditions is related to the leaf water content and its isotopic enrichment above source water (isostorage), and it changes over time in the leaf. Wang et al. (2010, 2012a) describe a method to measure δ_T using a customized leaf chamber in a 100 % N_2 atmosphere. This method requires a measurement of water vapor isotopic composition and water vapor concentration to estimate the δ_L signal.

A method commonly used to estimate isotopic composition of evapo-transpiration (δ_{ET}) is the Keeling plot approach (Keeling 1958). It expresses a mass balance relationship

by plotting the isotopic values of air samples at different heights above the ground (δ_V) against the inverse of concentration of the substance of interest, for instance, water vapor mixing ratios (Yepez et al. 2003; Xu et al. 2008; Zhang et al. 2010b). This results in a linear relationship where the vertical intercept reflects the isotopic composition of evapo-transpiration (δ_{ET}). This method uses three assumptions: (1) there is no loss of water vapor from the system apart from turbulent mixing with the atmosphere, (2) the atmospheric concentration of vapor in the system combines the input from background vapor and an additional component from local evapo-transpiration, and (3) the isotopic composition of the two sources does not change during measurements. Again, this method assumes steady state for δ_{ET} over the sampling period, which is not always valid in nature.

2.2.2 Hydrometric method

Measurements of direct transpiration are available using hydrometric devices. A widely used quantity to determine continuous transpiration through tree stems and branches is sap flow (Granier 1985). However, sap flow measurements need to be combined with methods measuring total evapo-transpiration to quantify the relative contribution of transpiration to the evaporating flux. Eddy covariance, Bowen ratio techniques, and lysimeters are commonly used in combination with sap flow to calculate the evapo-transpiration.

Measurement of transpiration using the sap flow method is based on asymmetric heat transfer by upward- or downward- moving tissue moisture. There are three well-known sap flow methods, which are Heat Pulse Velocity (HPV), Heat Field Deformation (HFD), and Thermal Dissipation (TD). In the HPV and HFD methods, the Thermal Dissipation Probe (TDP) needles are implanted in the active xylem up- and downstream from a heat source, whereas in the TD method, the TDP is installed downstream from the heat source. The velocity of water through the plant is minimal when the temperature difference between two needles is maximal. On the other hand, the velocity of water increases when the temperature difference decreases.

Evapo-transpiration measured by the eddy covariance system is defined as the flux of H_2O through a horizontal plane above the canopy. Simultaneous high-frequency vertical wind speed and atmospheric water vapor measurements are needed since this method correlates fast fluctuations of vertical wind speed with fast fluctuations in atmospheric water vapor density (Nouri et al. 2013).

Another method to measure evapo-transpiration is the Bowen ratio energy balance. This is a micrometeorological method used to estimate latent heat flux, which is calculated by measurements of the temperature and humidity gradients above the canopy (Bowen 1926). Unlike the eddy covariance and lysimeter methods it is an indirect method; it uses the ratio of the temperature and moisture gradient to partition the available energy (net radiation minus soil heat flux) over latent and sensible heat fluxes.

A lysimeter measures the evapo-transpiration loss by weighing an isolated soil sample. Ideally, lysimeters should contain undisturbed soil samples to represent the direct sur-roundings. Evapo-transpiration is calculated from the weight change over time, corrected for precipitation gains and losses (e.g., drainage water and percolate water).

More methods to determine the evapo-transpiration exist (Brutsaert 1982; Shuttleworth 1993). A summary of the advantages and disadvantages of these hydrometric methods can be found in Nouri et al. (2013) (Table 2.1).

2.2.3 Evapo-transpiration components in global land-surface models

In land-surface models, a simple water balance method is commonly applied to calculate surface fluxes. Evapo-transpiration as one of the water balance components is calculated as a sum of soil evaporation, transpiration, and canopy interception. Each of these fluxes can be estimated separately using a collection of methods. The most common methods to calculate soil evaporation and transpiration are the ones developed by Priestly and Taylor (Priestly and Taylor 1972) and by Penman and Monteith (Monteith 1981). Horton's model adopted for partial canopy cover can be used to calculate interception (Horton 1919). All these methods require many parameters such as climatological and vegetation parameters, which can be obtained from the satellite data and measurements. An example of this partitioning work can be seen in Choudhury and DiGirolamo (1998).

The development of remote sensing technology has improved the representation of vegetation in these models. In recent land-surface models, Leaf Area Index (LAI) is an important component in formulating soil evaporation, transpiration, and canopy evaporation. Lawrence and Slingo (2004) described in detail the use of LAI in the land-surface model Met Office Surface Exchange Scheme (MOSES2) to estimate individual evaporation components. In this model, the distribution of soil evaporation and transpiration is controlled by two MOSES2 extinction parameters: the extinction coefficient for photosynthetically active radiation (k_{par}) and a shading factor controlling the fraction of the surface that is exposed to the atmosphere above the canopy (k_{sh}). Adjusting these two parameters leads to adjusting the transpiration fraction. Increasing k_{par} means decreasing the fraction of light for photosynthesis and therefore will decrease the transpiration fraction. On the other hand, decreasing k_{sh} increases the fraction of surface exposed to the atmosphere and therefore will increase the contribution of soil evaporation. The precise values for these two parameters in land-surface models remain a source of uncertainty (Lawrence and Slingo 2004).

Another attempt to separate the different evapo-transpiration terms is applied using the Community Land Model Version 3 (CLM3; Collins et al. 2006). Lawrence et al. (2007) noted that this model partitions the global evapo-transpiration fraction in an unrealistic manner, giving 13 % E_T, 44 % E_S, and 43 % E_I. In their study, they tried to improve the fraction of transpiration in the CLM3 model by modifying several parameters and performing a sensitivity analysis. These efforts increase the final transpiration fraction in the CLM3 model from 13 to 44 %. However, this value is still somewhat lower than results from the Global Soil Wetness Project 2 (GSWP2; Dirmeyer et al. 2006), which calculates a transpiration fraction of 48 %.

Table 2.1 Summary of hydrometric methods (adopted from Nouri et al. (2013)).

Methods	Advantages	Disadvantages
Sapflow	- direct measurement of transpiration - cheap - manual or automatic measurement	- point-based measurement -only works for woody species - some errors may occur from the space between probes, the variable geometry of stems, the variation of heat ratio, and uncertainty in measuring soil and understory evaporation
	- individual plant coefficient can be determined - accurate technique to study plant ecophysiology and water scheduling	
Eddy covariance	- direct method to study mixed vegetation	-expensive
	- Suitable for large areas	- need well-trained operators in electronics
	- feasible to predict evaporation and no need for specific evaporation equation for different species	- need a monitoring tower above canopy and a uniform fetch
Bowen ratio energy balance	- simple and cheap	- need uniform fetch for accurate measurement of net radiation and soil heat flux
	- can measure evaporation even from non-watered plantation surface	- need an adequate elevation above the canopy to collect the required meteorological data
	- proved to be a robust method in many forestry areas	- sensitive to the bias of instrument gradient and energy balance
Lysimeter	- easy for inspection - manual or automatic measurement	- point-based measurement - very sensitive to different vegetation conditions inside and outside lysimeter - not practical for mixed vegetation types at large spacing - must consider plant root development - may have edge-flow effect - difficult to install and maintenance

2.3 Results from past partitioning works

Many studies partition the evapo-transpiration fraction into basically soil evaporation and transpiration. Only few studies take the evaporation from intercepted water into account. Here, we summarize some partitioning studies using the three different methods presented above for comparison (see Fig. 2.1). It is seen that, in general, hydrometric and isotope-based methods give higher transpiration fraction values than the global land-surface models. On average, the hydrometric method calculates transpiration fractions exceeding 50 %, whereas the isotope-based method produces transpiration fractions higher than 70 %. Global land-surface models estimate the transpiration fraction to be approximately 50 %, except for a recent study by Miralles et al. (2011) (orange bars in Fig. 2.1). However, these studies have generally been carried out at different locations, for different surface types, different climatic conditions, and different seasons. For global analysis, the global modeling methods give global annually averaged results that are lower than the contribution of the transpiration fraction derived from the isotope-based method from Jasechko et al. (2013) (80-90 %).

The portion of transpiration varies as a function of many factors such as radiation, air temperature, air humidity, wind, soil water content, crop characteristic, etc. For cultivated land, the crop development stage, environment, irrigation practice, and crop management all also strongly influence the transpiration rate. Under optimal conditions the transpiration flux may reach more than 90 % of the evapo-transpiration, but it can drop to values lower than soil evaporation when plants are in a dormant or under less favorable conditions (Robertson and Gazis 2006; Cavanaugh et al. 2011).

This temporal variation has been identified in many studies (including isotope-based partitioning studies), which show that transpiration during the growing season or summer is a dominant water flux compared to other fluxes, in general more than 70 % of the total evapo-transpiration (Lee et al. 2010; Wang et al. 2010, 2012a,b; Wenninger et al. 2010; Zhang et al. 2011; Sutanto et al. 2012), with some studies (Robertson and Gazis 2006; Xu et al. 2008) reporting transpiration fractions exceeding 90 % of the total evapo-transpiration flux. For crops (Allen et al. 1998), the transpiration flux may be more than 90 % of the total evapo-transpiration at full crop cover. However, during autumn (September-November), the transpiration fraction may drop to below 30 %, the remaining moisture flux being soil evaporation (Robertson and Gazis 2006).

A seasonal cycle of hydrological recycling rates modulated by surface evapo-transpiration is evident over many of the mid-latitude regions (Dirmeyer and Brubaker 2007). At higher temperatures, the fractionation processes associated with evaporation and condensation lead to higher isotopic enrichment of precipitation during summer than winter, known as the "temperature effect". In Europe, for example, intensified recycling in spring/summer with a comparably enriched isotope value, and a reduced contribution of local evapo-transpiration to the atmospheric water vapor during autumn/winter is prominently visible in the water isotopologues. In summer, a large evapo-transpiration fraction leads to a small spatial isotope enrichment gradient from the Atlantic coast to the interior of the continent. A steeper spatial gradient of depleted heavy isotopologue in winter appears
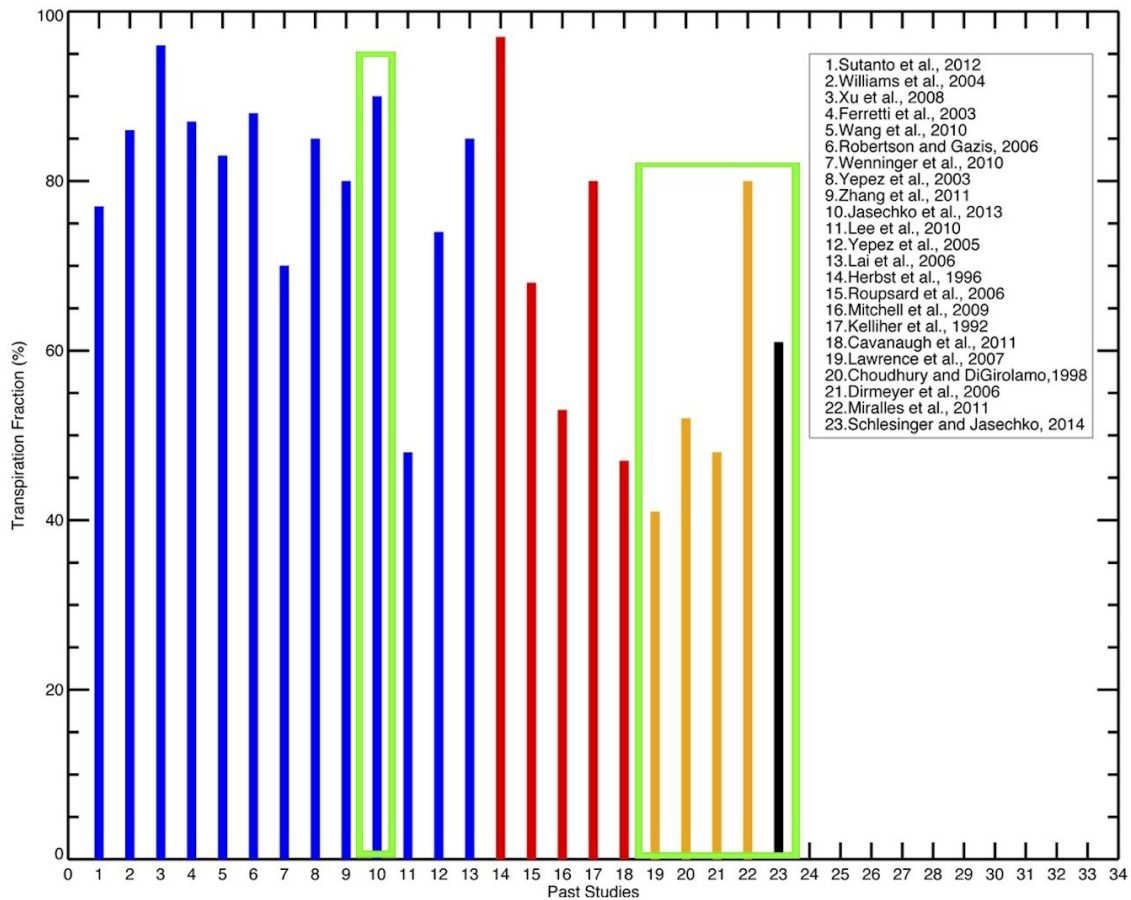
Figure 2.1 Transpiration fraction from several past partitioning studies. The plot shows maximum values of transpiration fraction from those studies. Blue is for isotope-based methods, red is for hydrometric methods, orange is for global land-surface model results, and black is a combination hydrometric and model result. The studies inside the green boxes present global average values.

from a strongly reduced contribution of continental water sources (evapo-transpiration fluxes) to the incoming water vapor masses (Rozanski et al. 1982; Hoffmann et al. 1998).

Different plant types exhibit a different transpiration fraction under similar climatic condition. Examples have been reported in some isotope studies in the US and China. In the US, studies by Yepez et al. (2003) and Ferretti et al. (2003) in Arizona and Colorado show that the transpiration fractions from savanna woodland and grass are 85 % and 76-87 %, respectively, in summer. In Washington, partitioning results in early summer from Robertson and Gazis (2006) give a transpiration fraction of 57-88 % for a steppe-forest region. In China during summer, the transpiration fractions of oaks and wheat are 96 and 80 %, respectively (Xu et al. 2008; Zhang et al. 2011). This indicates that, during summer, different plant species may have different transpiration fractions under the same climatic conditions. Savanna woodland has a higher transpiration fraction than grass in the USA and an oak stand has a higher transpiration fraction than wheat in

China. In addition, Kool et al. (2014) compile some partitioning studies and show that the transpiration fraction of a cotton field was 70-80 % and the transpiration fractions of corn, wheat, and soybean fields were lower, approximately 60-70 %.

Much lower transpiration fractions have been reported in Arizona, USA, with hydrometric methods. A study by Cavanaugh et al. (2011) during summer in a shrubland area showed a transpiration fraction of 42-47 %. This is very low compared to an isotope-based study in the same region, although different plant types are examined (85 % for savanna woodland). However, this does not necessarily imply the hydrometric method generally yields much lower results compared to the isotope-based method. In Europe during summer, results from an isotope-based method to partition the transpiration fraction from grass and a hydrometric method to partition the transpiration fraction from maize are very comparable, yielding 78 % transpiration for grass (Sutanto et al. 2012) and 77-97 % for maize (Herbst et al. 1996). Sutanto et al. (2012) also show that the evapo-transpiration rates analyzed from isotope-based and hydrometric methods are similar (3.4 and 3.5 mm d^{-1}, respectively). In addition, Williams et al. (2004) present a comparison of isotope-based and hydrometric methods in an olive tree site. Their study shows agreement between the two approaches for the midday period (10:30 to 12:30) though slightly different values are found for the late-afternoon period (14:30 to 16:30), with differences of 4 % for transpiration. In general, the difference between the isotope-based method and the hydrometric method is small if the same plants and climatic conditions are considered. The possible reasons why the isotope-based method slightly overestimates the transpiration fraction due to its limitations and assumptions are discussed in Section 2.4.

For global-scale partitioning analysis, only few studies quantify the transpiration fraction from the total evapo-transpiration. The study by Jasechko et al. (2013) is the first one that reports a global transpiration fraction based on an isotope approach. This study concluded that the transpiration fraction is 80 to 90 %. Using another set of input data, Coenders-Gerrits et al. (2014) estimate a transpiration fraction of 35-80 % globally using the same method as Jasechko et al. (2013). Moreover, a recent compilation study by Schlesinger and Jasechko (2014) results in a transpiration fraction of 61 % ($\pm$ 15 % SD). These two recent studies indicate that the estimate for the transpiration fraction of 80-90 % is likely to be biased high. In addition, these studies may not necessarily be representative for all continental areas since the calculation is derived from the isotopic composition of large lake water bodies and averaged from some studies in some places only.

Existing model and field estimates of the transpiration fraction do not support values higher than 80 % (GSWP-2, CLM3). A relatively high transpiration fraction of 80 % is simulated by Global Land-surface Evaporation: the Amsterdam Methodology (GLEAM; Miralles et al. 2011); however, in general, global land-surface models produce a lower transpiration fraction than the isotope-based method. Global averaged results may underestimate the transpiration fraction compared to field studies because they represent the global annual average and not seasonal averages. Many isotope-based and hydrometric studies have been carried out during spring and summer seasons, which have higher transpiration fractions compared to the autumn and winter seasons. Also, the transpiration

fraction is not the same everywhere, as it depends on surface types and climatic conditions. Other field measurement programs estimate the fraction of transpiration to be around 52 % globally, 65-76 % for forest, and 60 % for grasses (Choudhury and DiGirolamo 1998; Blyth and Harding 2011).

2.4 Possible discrepancies

What can explain these systematic discrepancies between the isotope and non-isotope methods? We have shown above that each technique has its own limitations and these may lead to biases in the results. The main source of inaccuracy in lysimeter methods is the edge-flow of water that can occur in the contact area between bucket and soil. This produces a significant error in the calculation of water losses from the lysimeter. Sap flow measurements suffer from leaking through the contact between tree and probes, probe misalignment, geometry of stems, the spatial variation of thermal conductivity, calibration difficulties, and the inaccuracy of the methods. According to Steppe et al. (2010), the three sap flow methods (HPV, HFD, and TD) underestimate the actual sap flux density by 35, 46, and 60 %, respectively. Some studies (Allen et al. 2011; Burba and Anderson 2007; Billesbach 2011; Nagler et al. 2005) review the errors in eddy covariance techniques, which include the assumptions used in calculations, instrument problems, frequency response, sensor time delays, noise, instrument calibration, etc. For the Bowen ratio method, a main source of uncertainty is the limited accuracy of the instrument to detect (sometimes very small) gradients (Todd et al. 2000; Nouri et al. 2013; Herbst et al. 1996).

For the isotope approach, the assumptions underlying the Keeling plot method used to calculate isotopic composition of evapo-transpiration as described in Sect. 2.2.1 are rarely met perfectly in nature. The isotopic composition of water vapor is not constant during the period of interest, which can be caused by, for example, loss of water due to condensation, influence of air mass advection, entrainment at the boundary layer, etc. The isotopic composition of leaf water also changes over time: it is generally higher during the day than during the night (Farquhar and Cernusak 2005; Yepez et al. 2005; Lai et al. 2006). The Steady State Assumption (SSA) may produce a reasonable δ_L approximation in the afternoon, when stomata are relatively open. On the other hand, plants do not transpire under SSA conditions during the night. The SSA may lead to an overestimation of the isotopic composition of leaf water compared to the measurements. Moreover, SSA is not satisfied in many field conditions when canopy climatic conditions are highly variable (Dongmann et al. 1974; Flanagan et al. 1991; Farquhar and Cernusak 2005; Yepez et al. 2005). A failure to correctly calculate the isotopic enrichment of leaf water precisely will produce a bias in the transpiration fraction analysis. Therefore the assumption of steady-state non-fractionating transpiration flux and a fractionation of all remaining surface fluxes should be critically reassessed.

According to this assumption, the isotope signature of the source water will not be altered by transpiration or by canopy and litter interception from low vegetation such as grass. However, Gehrels et al. (1998) showed that the isotopic composition of soil water in forested areas is heavier than in non-forested areas, where the isotope signature of

soil water is similar to the respective precipitation. Frequency and amount of rain will effectively modify the fractionation of interception and soil water. Over vegetated areas, precipitation is partly intercepted by the canopy, where it is exposed to open evaporation and accompanying fractionation. If followed by a new shower before the interception water is evaporated entirely, the enriched interception water is washed off and may cause an enrichment of soil water similar to a situation without the existence of a canopy with large leaves. Also, the evaporation from intercepted water on canopy or litter, which is not taken into account in many isotope-based studies, may overestimate the transpiration contribution. A study by Tsiko et al. (2012) in a savanna ecosystem shows that evaporation from intercepted water yields a 50 % interception fraction of the total evapo-transpiration.

The difference in the effective fractionation of the water isotopologues between transpiration on the one hand and evaporation from bare soils and lakes on the other is key for the isotope-based method to deliver quantitative constraints. Several studies (Yepez et al. 2005; Lai et al. 2006; Lee et al. 2007b; Cuntz et al. 2007; Ogée et al. 2007) have shown that both fluxes (from non-fractionating vegetation and fractionating soils and open waters) show a strong seasonal and diurnal variability. For instance, in a dry season, vegetation with deep roots has access to water from deeper soil layers or groundwater (Moreira et al. 1997; Wang and Yakir 2000; Lee et al. 2007b). The isotopic composition of groundwater depends on the isotopic input during the main recharge season, i.e., it is more enriched during summer than winter. Due to the fact that groundwater recharge is usually stronger in winter than in summer, the deep water will generally be more depleted than the upper layer/near-surface water. Thus, the assumption that is often used in the isotope-based method, stating that deeper water reflects the isotope composition of precipitation, is not necessarily true. In addition, near-surface water (accessible for short-rooted plants) has often undergone isotopic enrichment by evaporation from bare soils. Hence extensive transpiration from vegetation with deep roots will generally result in an atmospheric water vapor signature that is more depleted of heavy isotopes than transpiration from superficial sources (see Fig. 2.2), and may lead to an overestimation of the transpiration fraction when this is not taken into account. In isotope-based methods, the isotopic value of transpiration usually only uses isotopic composition of shallow soil water as source water.

Such effects might also contribute to the spatial patterns of isotopes in atmospheric water vapor that are becoming available via satellite-based remote sensing techniques. Water vapor over the Amazon Basin, for example, shows less deuterium enrichment than over tropical Africa in two independent data sets: TES (Worden et al. 2012) and SCIA-MACHY (Frankenberg et al. 2009; Fig. 2.3). This evidence may relate to the contribution of shallow and deep soil water to the transpiration flux: rain forest in the Amazon has access to deeper groundwater reservoirs (Miguez-Macho and Fan 2012) than most vegetation types in Africa.

Another factor that may contribute to a bias in the calculation of the transpiration fraction using the isotopic composition of open water (e.g., lakes) is the assumed similarity of the isotopic enrichment processes for soil evaporation and open water. Haverd et al. (2011) found that, after the first phase of soil drying, the value of the isotopic
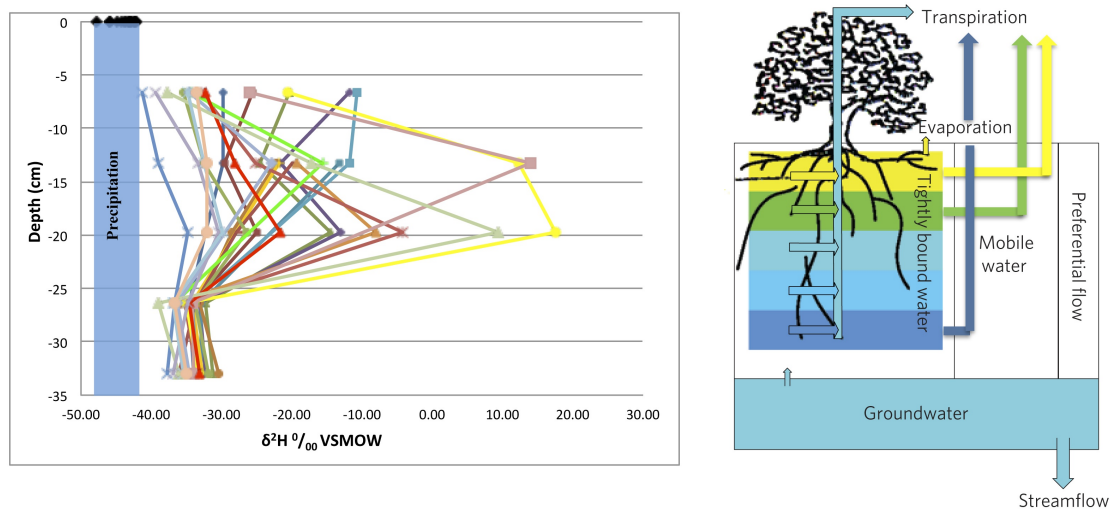
Figure 2.2 Left panel: soil water isotope profiles and evaporating front in a lysimeter experiment from a collection of soil samples from Sutanto et al. (2012); different colors represent different sampling periods. Right panel: a transpiration illustration from Brooks et al. (2010); different colors indicate different soil water isotopic values, with enriched isotopic values close to the surface and more depleted isotopic values in the bottom layers.

enrichment of evaporated soil water rapidly reaches a steady-state value, which is approximately equal to that of the transpired water vapor. Thus the top soil layer may act as an isotopically enriched conduct for water from deeper layers without strong overall fractionation between the soil water and evaporated water, similar to the enrichments in leaves during transpiration. This does not apply to the isotopic enrichment of lakes. Partitioning of evapo-transpiration using the isotope-based method on the global scale is highly sensitive to the input data and its isotopic composition. Coenders-Gerrits et al. (2014) show that the transpiration fraction calculated using the same method as Jasechko et al. (2013) reduces to 50-80 % if the input data are different, and to 35-80 % if the isotopic composition of transpiration is different.

The discrepancies between transpiration fractions calculated from different models can also be caused by the use of different averaging techniques. Some models include the desert regions (e.g., Sahara and Australian deserts), whereas in other approaches, deserts are ignored. The global transpiration fraction will be lower if the desert regions are included in the calculation. Based on observations, Haverd et al. (2013) estimate that 50 % of the Australian rainfall is lost as bare soil evaporation, which means that less than 50 % of the rainfall is used for transpiration. Moreover, global land-surface-model-based estimates can be strongly biased due to systematic errors and poor representation of relevant processes. The representation of tiling bare ground versus vegetated fractions in models deviates strongly from the true organization of vegetated or bare fractions of natural surfaces. Litter or moss layers are often missing, and the coarse vertical discretization of the soil does not allow for steep moisture gradients near the surface. The relatively low transpiration fraction in current state-of-the-art land-surface models (Dirmeyer et al. 2006) calls for a
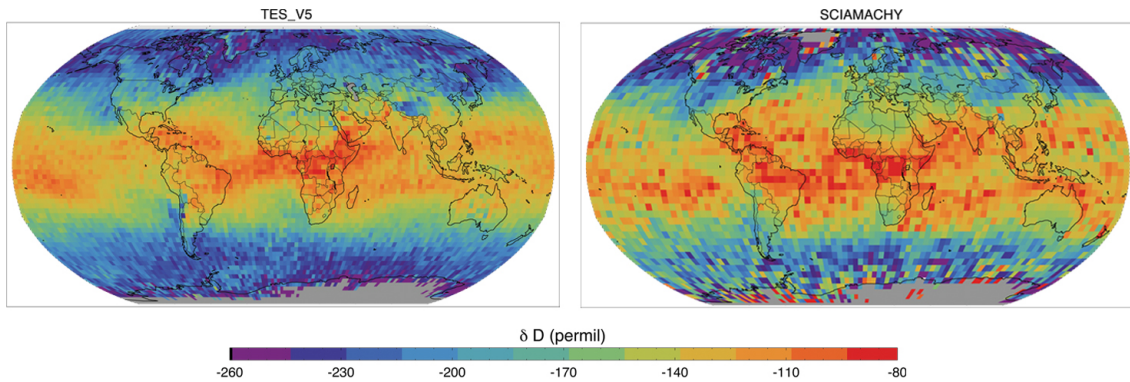
Figure 2.3 Water vapor isotopic composition (δD) measured from TES (version 5, year 2006, weighted averaged from 900 to 425 hPa, left panel) and SCIAMACHY (average over 2003 to 2005, total column, right panel) satellites. Red colors indicate an enrichment in heavy isotopes and blue and purple colors indicate a depletion in heavy isotopes.

reassessment of the skill of the underlying model parameterizations. A proper physical interpretation of (tuned) model parameters is still a difficult task (Lawrence and Slingo 2004).

2.5   Conclusion

Different approaches exist to infer the transpiration fraction of the continental evapotranspiration flux. In general, estimates based on water isotope balance calculations tend to allocate a fairly large contribution of transpiration to the total moisture flux (generally exceeding 70 % of the evapo-transpiration fluxes). These results are at or above the upper estimates of the transpiration fraction using other isotope-independent techniques (models, in situ physical flux data). The comparability is limited due to incomplete temporal and spatial coverage of most isotope-based analyses. However, a few studies that compare estimates of evapo-transpiration at the same location and conditions using the isotope-based and hydrometric methods show that the results are in good agreement. The relatively low transpiration fraction in land-surface models shows that a reassessment of model parameterizations must be carried out.

The lack of global evapo-transpiration partitioning estimates using the isotope-based method and validation of global isotope-independent techniques using isotope-based results remain a challenge. Continued measurements of global isotopic composition of soil water and water vapor around leaves are needed to put the isotope-based results into context. Isotope-enabled land-surface and global climate modeling studies such as isotopes in the Project for Intercomparison of Land-surface Parameterization Schemes (iPILPS; Henderson-Sellers et al. 2006) and (SWING; Noone 2007) allow for the evaluation of the parameterization of land-surface models by comparing the computed water isotopologue signals in the atmosphere with the available remote sensing and flux-based data sets. A validation of modeled water isotopologue signals in the atmosphere is needed. We

suggest that future studies should perform this evaluation in order to provide a better understanding of the hydrological cycle in vegetated regions.

3   Global-scale water isotopologues: satellite and model comparison

"Satellite would be more important than sending a man into space because this satellite will send ideas into space, and ideas last longer than men"
Newton N. Minnow

Abstract

Over the last decade, global-scale datasets of atmospheric water vapor isotopologues (HDO) have become available from different remote sensing instruments. Due to the observational geometry and the spectral ranges that are used, few satellites sample water isotopologues in the lower troposphere, where the bulk of hydrological processes within the atmosphere take place. Here, the study compares three satellite HDO datasets, two from the Tropospheric Emission Spectrometer (TES retrieval version 4 and 5) and one from SCIAMACHY, with results from the atmospheric global circulation model ECHAM4. A list of known isotope effects to qualitatively benchmark the various observational datasets is examined. TES version 5 (TES_{V5}), TES version 4 (TES_{V4}), SCIAMACHY, ECHAM, and ECHAM convolved with averaging kernels of TES version 5 ($ECHAM_{AK5}$) successfully reproduced a number of established isotope effects such as the latitude effect, the amount effect, and the continental effect. The improvement of TES_{V5} over TES_{V4} is confirmed by the steeper latitudinal gradient at higher latitudes in agreement with SCIAMACHY. Also the representation of other features of the water isotopologue cycle such as the seasonally varying signal in the tropics due to the movement of the Inter Tropical Convergence Zone (ICTZ) is improved in TES_{V5} and SCIAMACHY compared to TES_{V4}. A known humidity bias due to the cross correlation of H_2O and HDO measurements, which is of particular importance for instruments with low sensitivity close to the surface, was analyzed by applying either a humidity bias correction or a suitable a posteriori analysis. The study suggests that the qualitative and quantitative tests carried out in this study could become benchmark tests for evaluation of future satellite isotopologue datasets.

3.1   Introduction

Heavy isotopologues of atmospheric water (principally HDO and $H_2^{18}O$) are important tracers that are widely used to derive information on moisture recycling (Worden et al.

2007; Risi et al. 2013), cloud physics (Webster and Heymsfield 2003), troposphere-stratosphere exchange (Kuang et al. 2003; Moyer et al. 1996; Steinwagner et al. 2010), climate studies (Gedzelman et al. 2003; Lawrence et al. 2002), and paleoclimate (Jouzel et al. 1997; Field 2010). Equilibrium and kinetic isotope effects in the hydrological cycle, associated mainly with evaporation, condensation, and diffusion can be measured in the laboratory with high precision.

Due to the potential of these measurements for evaluating hydrological cycle processes, the GNIP network has supported the evaluation and storage of precipitation isotope measurements (Aggarwal et al. 2007). Compared to this global-scale international activity directed at precipitation, only very few measurements were directed at measuring water vapor, because of the logistical effort required for sampling water vapor using mechanical cold trap devices (Ehhalt et al. 1989; Franz and Röckmann 2005). Nevertheless, the bulk of water in the atmosphere is in the vapor phase and the liquid fraction of atmospheric water amounts only to a very small percentage of the total water.

With the development of faster and more robust in-situ measurement methods for water vapor isotopologues, the number of measurements has been strongly increasing in the last years. Available techniques include Tunable Diode Laser (TDL) absorption spectroscopy (Lee et al. 2005), in-situ Fourier Transform Infrared (FTIR; Griffith et al. 2006), cavity ringdown spectroscopy (Gupta et al. 2009) and integrated cavity output spectroscopy (Wang et al. 2009; Sturm and Knohl 2010). These techniques are now operational at several ground sites, and have been installed on mobile platforms like balloons, ships, and aircraft. In addition, ground-based FTIR remote sensing observations are made within the MUltiplatform remote Sensing of Isotopologues for investigating the Cycle of Atmospheric water/Network for the Detection of Atmospheric Composition Change (MUSICA/NDACC; Schneider et al. 2006, 2012) and Total Carbon Column Observing Network (TCCON; Wunch et al. 2010).

In addition, global water isotopologue data have become available using remote sensing techniques installed onboard satellite platforms: the Interferometric Monitor for Greenhouse Gases (IMG) on ADEOS (Zakharov et al. 2004; Herbin et al. 2007), the TES on Aura (Worden et al. 2006), the Michelson Interferometer for Passive Atmospheric Sounding (MIPAS) on Envisat (Payne et al. 2007; Steinwagner et al. 2007, 2010; Lossow et al. 2011), the SCIAMACHY on Envisat (Frankenberg et al. 2009; Scheepmaker et al. 2013), the Infrared Atmospheric Sounding Interferometer (IASI) on Metop (Lacour et al. 2012; Schneider and Hase 2011; Wiegele et al. 2014), and the Greenhouse gases Observing SATellite (GOSAT) launched by the Japanese Space Agency in January 2009 (Boesch et al. 2013; Frankenberg et al. 2013). These instruments are sensitive to different parts of the atmosphere. For example, MIPAS has significant sensitivity to the water vapor isotope distribution in the upper troposphere and stratosphere as it is a limb thermal infrared sounder, TES is a nadir-looking thermal infrared sounder with sensitivity from 850 hPa to 500 hPa (version 4) or from 900 to 350 hPa (version 5), while SCIAMACHY measurements are sensitive to the total atmospheric column as it is a nadir looking short-wave infrared (SWIR) sensor.

Global-scale water isotopologue measurements also provide invaluable information to validate isotope-enabled atmospheric general circulation models (Iso-AGCMs), such as:

ECHAM (Hoffmann et al. 1998; Werner et al. 2011), GISS-E2 (Goddard Institute for Space Studies; Schmidt et al. 2005), MUAGCM (Melbourne University General Circulation Model; Brown et al. 2006), IsoGSM (Isotopes-incorporated Global Spectral Model; Yoshimura et al. 2008), and LMDZ iso-GCM (the Laboratoire de Météorologie Dynamique atmospheric general circulation model with Zooming capability; Risi et al. 2010). These models integrate the well-known fractionation physics in the models hydrological cycle. The main objective of water isotope studies is to test the parameterization of the hydrological cycle in AGCMs with isotope data as an independent and sensitive tracer of the models hydrology. Until recently, the isotopic distribution of water in most climate models has been compared to data from the GNIP surface network (Hoffmann et al. 1998; Noone and Simmonds 2002; Schmidt et al. 2007; Yoshimura et al. 2008).

In recent years, several studies have been carried out to investigate the use of new datasets of water isotopes retrieved from satellite measurements. Frankenberg et al. (2009) compared the SCIAMACHY HDO measurements with the IsoGSM model. Yoshimura et al. (2011) extensively compared the HDO measurements from SCIAMACHY, and TES version 4 with IsoGSM results, Werner et al. (2011) compared the ECHAM5 model with SCIAMACHY, Risi et al. (2012a) conducted an inter-comparison study between models and observations, both ground-based and from satellites. Recently Frankenberg et al. (2013) compared GOSAT with LMDZ model outputs. Those studies conclude that in general the model can reproduce the geographical variability of the mean climatological δD very well. However, models tend to underestimate the amplitude and the gradient of seasonal variations of δD in the mid latitudes at all atmospheric levels (Risi et al. 2012a).

When comparing satellite data with model results, the sensitivity of the satellite sensor to the different layers of the atmosphere has to be taken into account. For example, the TES V4 dataset is sensitive only to a limited altitude range (mid troposphere, 850-500 hPa), in order to reduce the impact of non-linearities within the retrieval process (Worden et al. 2006). Therefore TES V4 is not sensitive to humidity and isotopologues in the lower troposphere. A low sensitivity means that the measured signal receives a low weight in the retrieval compared with the a priori assumed profile.

The retrieval process provides us with a quantitative measure of how much the a priori profiles have been modified by the actual satellite observations, i.e., the averaging kernel (AK). For a meaningful satellite-model comparison, the instrument operator, which is composed of the retrievals AK and a priori constraint, must be applied to the model. The principle of applying the instrument operator to the model output can be formulated as: $X_{GCM}^{New} = X_a + A[X_{GCM} - X_a]$, where A is the averaging kernel vector obtained from the satellite retrieval, X_a is a priori information that is used for the satellite retrieval and X_{GCM} is the original model field. If the satellite retrieval represents the atmospheric conditions perfectly (AK = 1), applying the AK has no effect on the model results. On the other hand, if the sensitivity of the satellite retrieval is negligible, applying the AK to the model will yield the a priori profile (as does the measurement in this case).

This chapter compares the TES V4 and V5 datasets to the ECHAM4 model output. The TES V5 dataset has greatly improved sensitivity over the V4 dataset because of the use of an improved retrieval approach that depends on a larger number of HDO absorption lines, while minimizing spectral interferences from other tropospheric trace gases Several

of the studies mentioned above were carried out using the TES V4 dataset. The transition between use of the TES V4 and TES V5 (Worden et al. 2012) data in the scientific studies occurred without detailed investigation of the differences and improvements between V4 and V5. Here the study presents the implications of the improved sensitivity of TES V5 data in terms of the isotope effects. For example, we show that the TES V5 data set is more sensitive to variations in the HDO/H_2O ratio caused by the isotope amount effect in the tropics. In addition, how humidity biases in the models affects model/data comparisons is investigated and methods to avoid these biases are discussed. The results are compared with data from SCIAMACHY, which should be less affected by the humidity bias due to its larger sensitivity near the surface.

This chapter is organized as follows. In section 3.2 we describe the application of satellites AK to the model and bias correction. In section 3.3 we compare the remote sensing δD datasets with the model results. In particular we discuss the consequences of applying the AK from both TES versions to the ECHAM4 model output. Conclusions are presented in section 3.4 and an appendix is presented in section 3.5.

3.2 Methods

All HDO data from observations and model are presented as deviation (delta deuterium, δD) from the isotopic composition of the international standard Vienna Standard Mean Ocean Water (VSMOW) expressed in per mil (‰). Since the water vapor mixing ratio and δD decrease with altitude, the total column value of δD is calculated as a weighted mean:

$$\overline{\delta D} = \frac{\sum_{i=0}^{n}(\delta D_n \cdot H_2O_n)}{\sum_{i=0}^{n} H_2O_n} \tag{3.1}$$

Where n is the number of layers. All results are given as weighted means $(\overline{\delta D})$.

3.2.1 Application of satellite AK to model results

In order to compare the model results to satellite observations, the ECHAM model output is convolved with the instrument operator (composed of the averaging kernel and constraint vector) from the TES satellite datasets. Unlike for real atmospheric observations, in the model the "true state" is explicitly available. By applying the AK to the model results we mimic the way in which the satellite observes the atmosphere, to allow a meaningful comparison with the model (Rodgers 2000; Worden et al. 2004; Bowman et al. 2006).

The monthly TES data are interpolated on the horizontal grid of the model, while in the vertical the model levels are interpolated onto the TES levels. The TES DOF and SRQ data filtering are carried out during the interpolation of all TES data into horizontal model grid including the AK values. This study does not sample the model outputs coincident

with the orbital paths of the satellite since we use the monthly TES LITE dataset and monthly model outputs. One should note that the AK convolution must account for the cross correlations in the joint HDO/H_2O profile retrieval (Yoshimura et al. 2011; Worden et al. 2006, 2011). The basic application of the AK to the model is presented in Eq. (3.2) and Eq. (3.3). These equations can be re-formulated into Eq. (3.4) for the HDO/H_2O ratio, and to Eq. (3.5) for H_2O (see also supplementary material of Risi et al. 2013).

$$ECHAM_{AK} = X_a + A_{TES}[X_m - X_a] \tag{3.2}$$

$$A_{TES} = \begin{bmatrix} A_{DD} & A_{DH} \\ A_{HD} & A_{HH} \end{bmatrix} \tag{3.3}$$

$$ln(ECHAM_{AK}^R) = ln(R_a) + ((A_{DD} - A_{HD}) \cdot ln(\frac{R_m}{R_a}) + (A_{DD} - A_{HD} - A_{HH} + A_{DH}) \cdot ln(\frac{q_m}{q_a}))$$
$$\tag{3.4}$$

$$ECHAM_{AK}^H = X_a^H + A_{HH}(X_m^H - X_a^H) + A_{HD}(X_m^D - X_a^D) \tag{3.5}$$

D and H stand for HDO and H_2O, respectively while m and a stand for the model field and the a priori field, respectively. R is the ratio of volume mixing ratios of HDO and H_2O (i.e., R_a = (HDO/H_2O) of TES a priori). q is the specific humidity; A_{DD} and A_{HH} are the averaging kernel sub-matrices for HDO and H_2O; A_{HD} and A_{DH} are the cross correlation AK matrices between H_2O and HDO and the reverse (see also Worden et al. 2006; Yoshimura et al. 2011; Risi et al. 2013). $ECHAM_{AK}^R$ is the new HDO/H_2O ratio R as a function of pressure grid for the convoluted ECHAM.

The application of the averaging kernel to the model output has two components (see Eq. 3.4). The first depends on the difference between the a priori HDO/H_2O ratio profile and the model HDO/H_2O ratio profile. The second depends on the difference between the a priori humidity profile and the model humidity profile. If there is a model bias in humidity, the difference between model humidity and a priori humidity will affect the model-data comparison of δD. The model humidity bias commonly occurs in the upper troposphere, also in the ECHAM model. This bias may then be propagated to the lower-tropospheric δD through the averaging kernels (Worden et al. 2012; Risi et al. 2013). The effect of the model humidity bias can be eliminated by assuming that the model correctly captures the satellite a priori humidity profile (see Eq. 3.6). Based on this assumption, the second component, which includes the humidity term in Eq. (3.4), is neglected. However, this assumption also incurs an uncertainty related to the uncertainty in the a priori error in the humidity, propagated through the HDO component of the averaging kernel. In general, this error is much smaller than that due to the humidity bias and is typically less than 8 ‰ (Risi et al. 2013).

$$ln(ECHAM_{AKBcorr}^R) = ln(R_a) + ((A_{DD} - A_{HD}) \cdot ln(\frac{R_m}{R_a}) \tag{3.6}$$

Schneider et al. (2012) discussed the complexity of isotopologue remote sensing datasets in detail. They introduced an a posteriori method to reduce the cross dependence

of retrieved δD on atmospheric humidity and to assure similar AKs for humidity and δD. The ratio of water vapor isotopologues is much smaller than the variability of humidity and the a posteriori data treatment reduces the risk of misinterpreting the remote sensing data (Schneider et al. 2012; Pommier et al. 2014; Wiegele et al. 2014). Similar AKs guarantee that the retrieved isotopologue ratio and humidity are sensitive to the same atmospheric air mass and the cross dependence of atmospheric humidity on the retrieved δD is significantly reduced (see the appendix for details of the AK computation results). In this chapter, we present results for both an a posteriori analysis of the TES version 5 dataset (TES$_{\text{V5Pos}}$) and the application of AK to the ECHAM model (ECHAM$_{\text{AK5Pos}}$), following Schneider et al. (2012) and Risi et al. (2013).

The correction of the AK by a posteriori analysis (A'') is described as:

$$A'' = CA'$$

(3.7)

with C and A' as follow:

$$C = \begin{pmatrix} A'_{\text{DD}} & 0 \\ -A'_{\text{DH}} & \mathbb{I} \end{pmatrix}$$

(3.8)

$$A' = PAP^{-1}$$

(3.9)

and P is described as:

$$P = \begin{pmatrix} \frac{1}{2}\mathbb{I} & \frac{1}{2}\mathbb{I} \\ -\mathbb{I} & \mathbb{I} \end{pmatrix}$$

(3.10)

Here, P is the orthogonal basis for describing the tropospheric water vapor state: the first rows contain the $\{(\ln(H_2O)+\ln(HDO))/2\}$-state, and the second rows contain the $\{\ln(HDO)-\ln(H_2O)\}$-state. $\mathbb{I}$ is the identity matrix, A is the averaging kernel, and C is a matrix transformation for a posteriori corrected kernels. ECHAM$_{\text{AK5Pos}}$ is calculated based on Eq. (3.2) by replacing A with A'' and TES$_{\text{V5Pos}}$ is calculated based on Eq. (20) in Schneider et al. (2012). An example for the effect of the a posteriori correction on humidity and δD AKs is shown in the appendix.

In the case of SCIAMACHY, full AKs are not provided and thus we cannot apply the AK correction to the model. We therefore have to consider throughout this work that some effects of the cross-dependency between H_2O and δD and differences in the sensitivity for H_2O and δD might affect the interpretation of the SCIAMACHY data.

3.2.2 Bias correction

A bias of $\sim$5 % on average and $\sim$15 % maximum, evaluated from ground and aircraft measurements, in the TES HDO vapor data has been attributed to uncertainties in the spectroscopic line strengths (Worden et al. 2006, 2007, 2011; Herman et al. 2014). A correction for this bias is already included in the version 5 dataset (Worden et al. 2012) but not in version 4. The sensitivity of the measurements must be accounted for in the application of the bias correction to the TES V4 data (Lee et al. 2011; Risi et al. 2013) according to:

$$X_{\text{corrected}}^{\text{HDO}} = X_{\text{original}}^{\text{HDO}} - A_{\text{DD}}(\delta_{\text{bias}}) \tag{3.11}$$

$X_{\text{corrected}}^{\text{HDO}}$ is the logarithm of the volume mixing ratio of the HDO profile after bias correction, $X_{\text{original}}^{\text{HDO}}$ is the logarithm of the original volume mixing ratio of the model or satellite, and δ_{bias} is a column vector of the same length as $X_{\text{original}}^{\text{HDO}}$ that contains the bias correction values. Note, that this correction is only applied to HDO and not to H_2O. We applied the bias corrections of 5 % to TES_{V4} (Worden et al. 2006; Herman et al. 2014) and no bias correction was applied to TES_{V5} since it has already been corrected by 6.5 % (Worden et al. 2012). To improve the agreement amongst the dataset in the tropics, bias corrections of 3 % and 5 ‰ were applied to $ECHAM_{AK4}$ and SCIAMACHY.

3.3 Results and discussion

3.3.1 Spatial isotope distribution

The annual mean δD isotope distributions of the different satellite and model datasets and the a priori are shown in Figure 3.1 and 3.2. The TES and SCIAMACHY prior profiles that are used as an initial guess for HDO and H_2O to constrain the HDO/H_2O estimation do not show a latitudinal effect (Fig. 3.1a and b). The TES prior for HDO (HDO_{prior}) was calculated based on atmospheric H_2O profiles from re-analysis data, multiplied by a single a priori profile of the HDO/H_2O ratio, which was obtained from a run of the National Center for Atmospheric Research (NCAR) Community Atmosphere Model (CAM), augmented with an isotope physics approach developed by Noone and Simmonds (2002) (Worden et al. 2006, 2012; Zhang et al. 2010a). This prior HDO profile is representative for the tropical HDO/H_2O ratio and as a result, the TES δD prior is strongly biased high at high latitudes. The TES prior does include an altitude effect (Fig. 3.1a), which is clearly visible in the Himalayas, the Andes, the Rocky Mountains, and Greenland. The prior for TES version 5 is not significantly different from version 4.

The SCIAMACHY prior shows a similar pattern as the TES prior (Fig. 3.1b) but generally lower δD values of -140 to -160 ‰. It does not include a latitudinal gradient and altitude effect. The sensitivity to the weak HDO absorber is close to unity throughout the column (Frankenberg et al. 2009; Scheepmaker et al. 2013), so it is sensitive to near-surface water vapor. The SCIAMACHY prior was constructed from ECMWF water vapor profiles and a fixed prior depletion profile that decreases from -100 ‰ at the lowest layer to -500 ‰ at the highest layer. This results in the prior H_2O-weighted total column δD value of approximately -150 ‰.

Figures 3.1c to 3.1f and 3.2a to 3.2e present modeled and observed patterns (isoscapes) of total column δD of atmospheric water vapor. The first order isotope feature shown in all figures is the significant difference in δD between low, mid and high latitudes roughly following global temperatures. The latitude effect is stronger in the observed global isotope pattern of the TES version 5 (TES_{V5}) and of the SCIAMACHY dataset than in the TES version 4 (TES_{V4}). It is also present in the modeled results of ECHAM. ECHAM results convolved with the instrument operator of TES version 4 ($ECHAM_{AK4}$) shows a smaller latitude gradient than for version 5 ($ECHAM_{AK5}$). Another feature, visible in these global
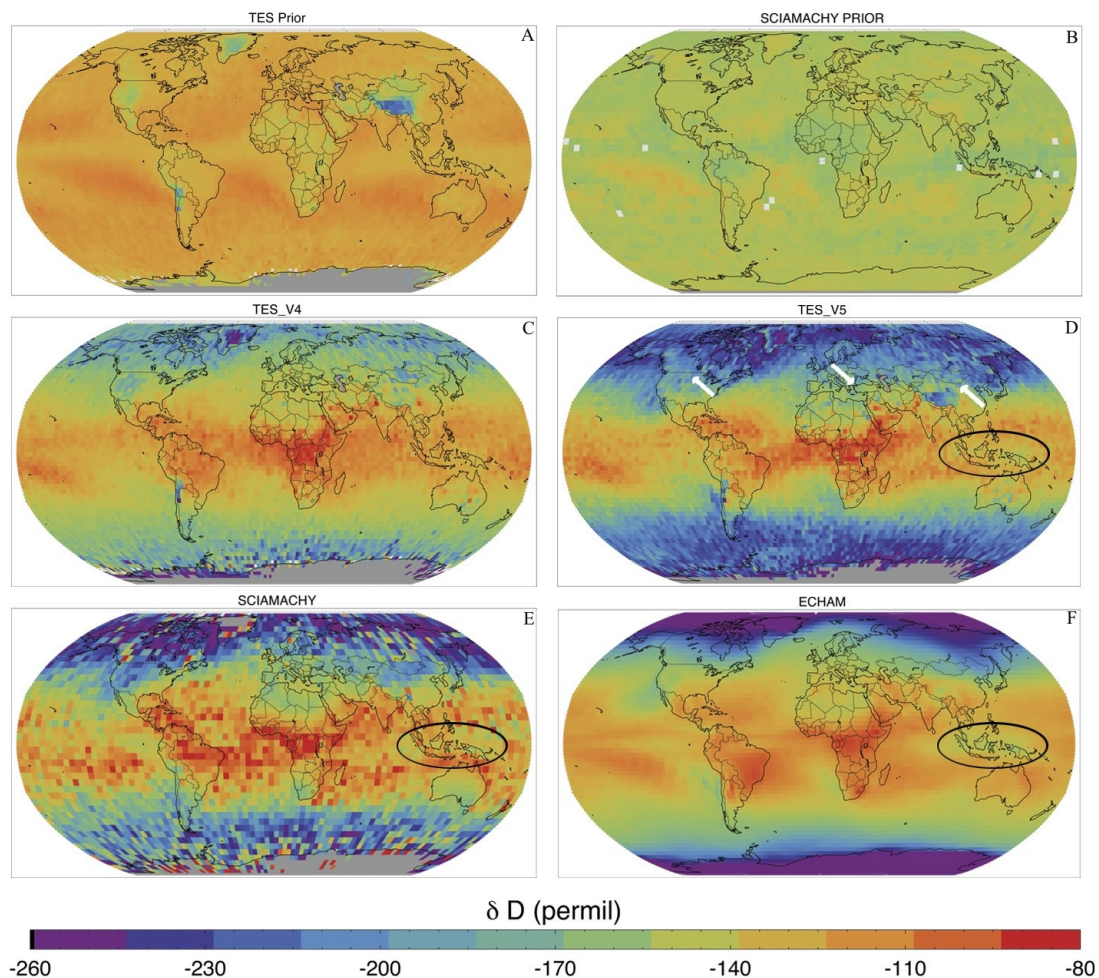
Figure 3.1 TES prior version 4 (a), SCIAMACHY prior (b), δD product from TES$_{V4}$ (c), TES$_{V5}$ (d), SCIAMACHY (e), ECHAM (f). The figures of TES prior, and TES$_{V4}$ are weighted averaged from 850 to 500 hPa, and TES$_{V5}$, and ECHAM from 900 to 425 hPa. The results are bias corrected by 5 % and -5 ‰ for TES$_{V4}$ and SCIAMACHY, respectively. Arrows in 3.1d point out the continental effect and ellipses in 3.1d, e, f show the region with a strong isotope amount effect around Indonesia. All plots are annual average δD

isoscapes, is that the tropical and sub-tropical zones with enriched values are wider in the ECHAM model results (Fig. 3.1f, 3.2a, 3.2b, 3.2c, and 3.2d) compared to the TES$_{V5}$ and SCIAMACHY satellite observations (Fig. 3.1d and 3.1e).

A strong latitude effect of the order of $\sim$150 ‰ for δD between the tropics and the cold and isotopically depleted polar regions of both hemispheres is well established in the literature. Isoscapes based on an interpolated multi-variable regression of GNIP precipitation data also show such strong latitudinal gradients (Bowen and Wilkinson 2002). Also the few existing near surface vapor measurements (Uemura et al. 2008) indicate a strong isotopic gradient between low and high latitudes. This principal geographical pattern is better represented in TES$_{V5}$ compared to TES$_{V4}$, which has a stronger influence

from the a priori field at higher latitudes. It clearly indicates a substantial improvement of the version 5 retrieval over version 4.

The altitude effect is apparent in all datasets. Major mountain chains such as the Andes, Rocky Mountains or the Himalayas together with the Tibetan Plateau are easily recognizable by lower δD values. $ECHAM_{AK5}$, however, shows unrealistically high δD values over the Tibetan plateau (Himalayas; Fig. 3.2b). This unrealistic pattern is due to a high bias in the model humidity profile as discussed in section 3.2 (Risi et al. 2012b, 2013) and the effect of limited vertical resolution and a priori constraints on retrieved δD over the Himalaya region. Therefore, this problem disappears when we leave out the humidity term in the application of the instrument operator (Eq. 3.6), and the resulting $ECHAM_{AK5BCorr}$ shows a local isotope minimum over the Tibetan Plateau again (Fig. 3.2d). Thus, the humidity bias can have a large effect on the isotope results of a model convolved with the averaging kernel of a satellite instrument.

The unrealistically high δD values over the Tibetan plateau also disappear if the a posteriori analysis suggested by Schneider et al. (2012) and Pommier et al. (2014) (Fig. 3.2c) is performed. The a posteriori data treatment results in δD and H_2O profiles that are sensitive to the same atmospheric airmass. The AK application to the model with applied a posteriori analysis produces a similar result as the humidity correction (Fig. 3.2c and 3.2d). Latitudinal profiles from both $ECHAM_{AK5Corr}$ and $ECHAM_{AK5Pos}$ show very similar δD values in the tropics and only 2-5 ‰ differences at the higher latitudes (Fig. 3.3c). Both correction procedures thus show that humidity biases have to be taken into account when the satellite AKs are applied to model results, either by a humidity correction or an a posteriori processing.

The isotopically most enriched water vapor is found over tropical South America and tropical Africa, and is associated with the Amazon and Congo River basins. The intense recycling and very strong evapo-transpiration over these rainforest regions, in combination with shallow convection is responsible for this pattern (Worden et al. 2007; Yoshimura et al. 2011). The location and extension of these isotope maxima are relatively robust throughout all datasets. Since these large areas with δD between -110 and -100 ‰ are not apparent in the TES and SCIAMACHY a priori fields (Fig. 3.1a and b) but clearly appear in the final products (Fig. 3.1c, d, and e), they are a robust result of the added information from the satellite measurements and not an artificial product of the retrieval procedure. This result is consistent with the previous studies from Yoshimura et al. (2011), Werner et al. (2011), and Risi et al. (2012a), which yield δD values between -80 ‰ and -110 ‰. A study from Brown et al. (2008), however, shows that lower δD values of -150 ‰ to -165 ‰ are also observed in these regions but these lower values are related to seasonal tropical convection and the corresponding amount effect.

In the scientific literature, many examples of the continental effect are documented, e.g., the Southwestern USA or Western/Central Europe, based on measurements in ground waters (Rozanski 1985) and precipitation (Aggarwal et al. 2007). The continental effect appears in all datasets with varying intensity, except for ECHAM convoluted with AK version 4. TES_{V4}, TES_{V5}, TES_{V5Pos}, SCIAMACHY, ECHAM, $ECHAM_{AK5}$, $ECHAM_{AK5Corr}$, and $ECHAM_{AK5Pos}$ results clearly show the continental effect (white arrows in Fig. 3.1d and Fig. 3.2d).
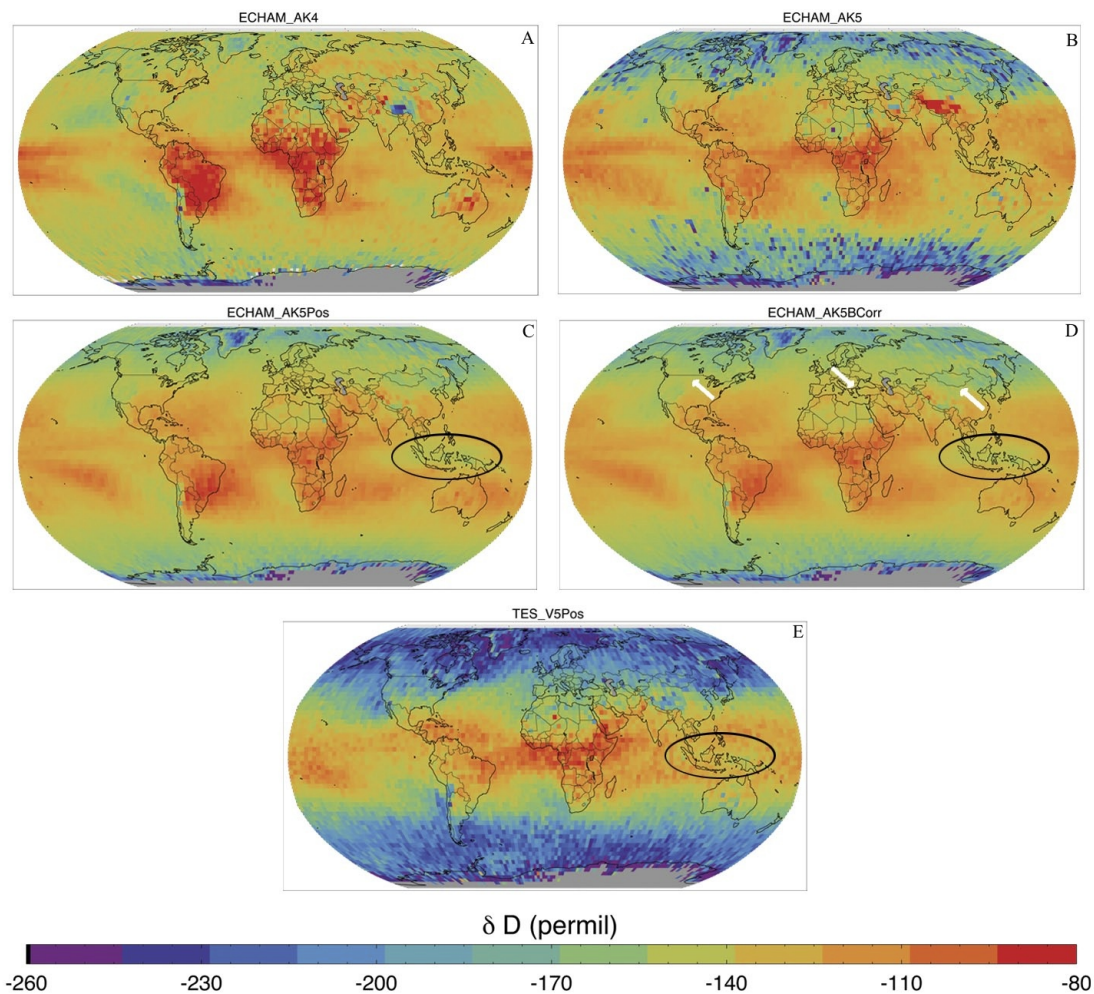
Figure 3.2 δD product from ECHAM$_{AK4}$ (a), ECHAM$_{AK5}$ (b), ECHAM$_{AK5Pos}$ (c), ECHAM$_{AK5Corr}$ (d), and TES$_{V5Pos}$ plot (e). All figures are weighted averaged from 900 to 425 hPa. The ECHAM$_{AK4}$ result is bias corrected by 3 %. Arrows in 3.2d point out the continental effect and ellipses in 3.2c, d, e show the region with a strong isotope amount effect around Indonesia. All plots are annual average δD

The Hadley-Walker Circulation defines the seasonally varying zones of strong convective activity in the tropics. Three rising branches of the meridional Walker circulation are situated over tropical South America, tropical Africa and the Western Pacific Warm Pool (Oort and Yienger 1996). As described above, the strong isotope enrichment over the continental parts of the Walker circulation is due to the intense recycling of continental water. These yearly averages are on balance weighted towards these enriching effects as opposed to depleting effects associated with seasonal convection that are also observed by TES (Brown et al. 2008; Samuels-Crow et al. 2014). However, over the Pacific warm pool one recognizes a zone with slightly lower δD (ellipses in Fig. 3.1d, e, f, and Fig. 3.2c, d, e). This area of very high Sea Surface Temperature (SST), persistent strong convection

and rainfall and more depleted vapor extends over the Inner Tropics and is surrounded by a zone of descending air, less rainfall (Oort and Yienger 1996; Jo et al. 2014), and more enriched vapor. We consider this pattern as a manifestation of the isotope amount effect since the isotopic pattern anti-correlates with regional rainfall (Brown et al. 2008; Dansgaard 1964; Kurita et al. 2011; Lee and Fung 2007; Lee et al. 2011; Risi et al. 2008; Worden et al. 2007). Apparently, TES_{V4} and $ECHAM_{AK4}$ (Fig. 3.1c and Fig. 3.2a) do not pick up this important feature of the tropical water cycle. TES_{V5} clearly shows the depletion of water vapor over this region with δD value difference of $\sim$22 ‰ compared to V4.

Figure 3.3 presents a comparison of zonal mean δD values for all datasets. As discussed above, δD decreases to -200 ‰ in the TES_{V4} product at high northern latitudes, whereas it decreases to -250 ‰ for TES_{V5}, the latter in agreement with SCIAMACHY, and with other independent observations (Uemura et al. 2008). The differences between ECHAM4 and SCIAMACHY in this study are consistent with results from Werner et al. (2011) for ECHAM5 and SCIAMACHY. The difference between ECHAM5 and SCIAMACHY is $\sim$20 ‰ in the tropics and $\sim$25 ‰ at higher latitudes (60 °N-S; Werner et al. 2011). Here, the differences between ECHAM4 and SCIAMACHY amount to between 10 ‰ to 20 ‰ in the tropics and at higher latitudes (60 °N-S), respectively. TES_{V4} displays much weaker δD gradients at mid latitudes compared to SCIAMACHY and TES_{V5}. As mentioned earlier, the tropical and sub-tropical isotope maximum in the ECHAM model is significantly wider than for SCIAMACHY and TES_{V5} (Fig. 3.3b). This issue is aggravated when the ECHAM results are convolved with the TES averaging kernels. The $ECHAM_{AK4}$ product shows the smallest latitude gradient and highest δD values at high latitude of all datasets. The small AK values of version 4 enhance the influence of the a priori field, which consequently leads to larger δD values. This high-latitude problem has been improved in the version 5 datasets (Fig. 3.3b), but still the $ECHAM_{AK5}$, $ECHAM_{AK5Corr}$, and $ECHAM_{AK5Pos}$ results are significantly higher than the model state of ECHAM at northern high latitudes (Fig. 3.3c). TES_{V5} and TES_{V5Pos} are in good agreement with SCIAMACHY.

We note that the different climatological periods that are used in the comparison between TES (2006), ECHAM4 (2001) and SCIAMACHY (2003-2005) can also contribute to the difference between these datasets, although the general latitudinal distribution is not expected to show strong interannual variations.

Although, there are significant discrepancies at mid and high latitudes, all data products agree fairly well in a tropical/subtropical band between 30 °N and 30 °S with values around -100 ‰, similar to the results of Webster and Heymsfield (2003), Lawrence et al. (2004) and Zakharov et al. (2004). It seems therefore that different remote sensing datasets and model results (with AK applied) coincide in the tropics, which means that the isotope measurements there can be exploited to examine smaller scale effects (see below).

3.3.2 Seasonal isotope distribution

Above we analyzed the spatial structure of the dominant annual average isotope patterns. In addition, both satellite data and model simulations allow to study the seasonality of
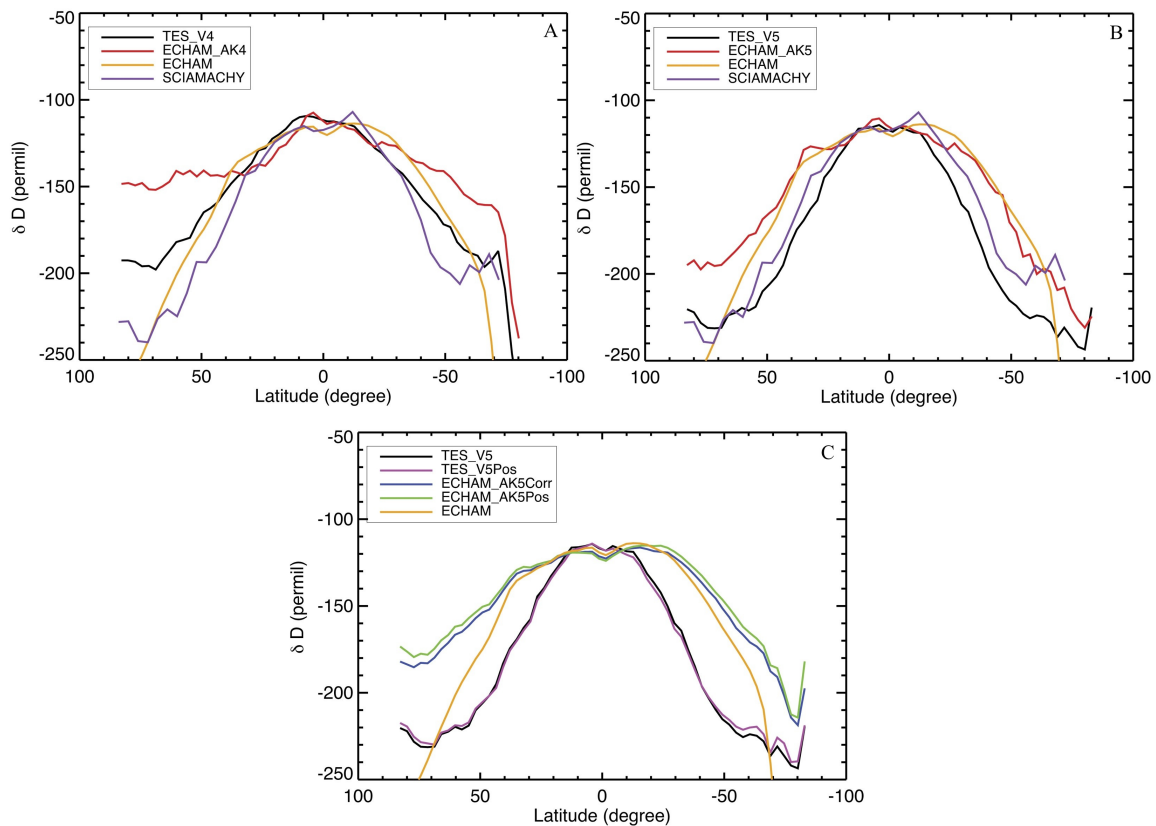
Figure 3.3 Annual average latitude profile of δD in water vapor from TES, TES$_{\text{V5Pos}}$, ECHAM, ECHAM$_{\text{AK}}$, ECHAM$_{\text{AK5Corr}}$, ECHAM$_{\text{AK5Pos}}$, and SCIAMACHY. In (a) the TES for version 4 datasets are shown and in (b and c) the TES version 5 datasets. Fig. 3.3a is weighted averaged from 850 to 500 hPa, and Fig. 3.3b and c are weighted averaged from 900 to 425 hPa.

δD patterns and to identify the leading processes on this time scale. Zonal means of all datasets are computed for the mean winter (DJF) and summer season (JJA) of the respective annual time period (Fig. 3.4). TES$_{\text{V5}}$ shows similar results as SCIAMACHY during summer and winter in the northern hemisphere and both datasets show a clear and consistent seasonal isotope difference between the two seasons in the northern hemisphere. In the southern hemisphere, however, the difference between the two seasons is much smaller for both datasets. In addition, in the southern hemisphere there appears to be a significant difference between the instruments. TES$_{\text{V5}}$ δD values are consistently lower compared to SCIAMACHY (Fig. 3.4a). It is unlikely that the different simulation and observation periods in our analysis can explain these large discrepancies.

Due to the high solar zenith angle (low sun), SCIAMACHY data are seasonally scarce at mid and high latitudes. Therefore, there are not many measurements above 50 °N or 50 °S in the respective winter season (Fig. 3.4a). Also, large parts of the oceans are not covered due to the low albedo of the ocean and the signals from oceanic regions are primarily above low-level clouds. For our analysis we use the same data filtering procedure of SCIAMACHY
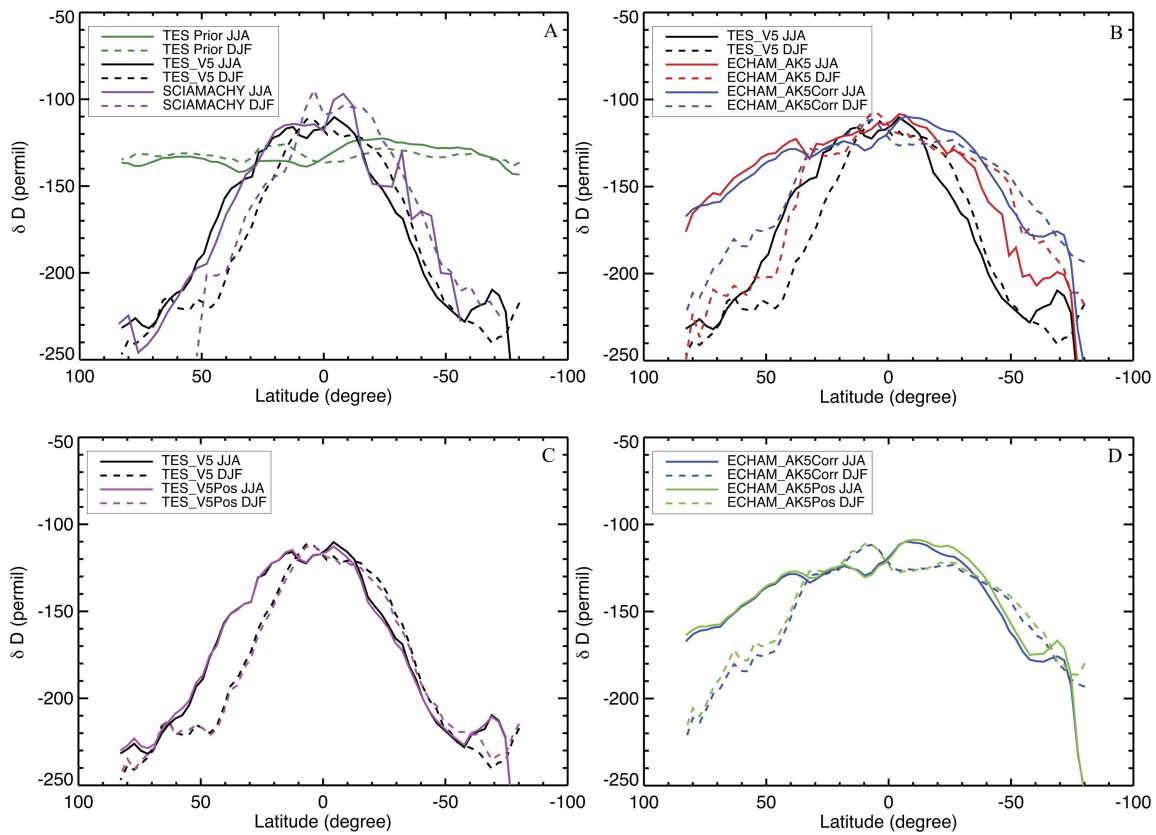
Figure 3.4 Seasonal comparison of zonal means of δD from TES prior, TES$_{V5}$ and SCIAMACHY (a), from TES$_{V5}$, ECHAM$_{AK5}$, and ECHAM$_{AK5Corr}$ (b), from TES$_{V5}$ and TES$_{V5Pos}$ (c), and from ECHAM$_{AK5Corr}$ and ECHAM$_{AK5Pos}$ (d). Solid lines show NH summer profiles and dashed lines NH winter profiles. All figures are weighted averaged from 900 to 425 hPa.

data as in Frankenberg et al. (2009), which only accepts water isotopologue measurements if the H$_2$O total column corresponds to at least 70 % of the ECMWF total water column. This constraint excludes profiles with high clouds, but accepts profiles with low clouds (up to 1 km). Thus all SCIAMACHY measurements are biased towards clear sky or low cloud conditions. The δD seasonality of SCIAMACHY shown in Figure 3.4a (especially in the Southern Hemisphere during the Northern Hemisphere Summer) is therefore neither temporally nor spatially fully representative of the mean state of the atmosphere. These issues are not applicable to TES data. However, TES measurements are also less sensitive at higher latitudes, especially the version 4 dataset.

The wider tropical maximum of ECHAM is seen in both seasons (Fig. 3.4b and d). It is apparent that in the summer season the ECHAM$_{AK5}$ results show considerably higher δD values than TES$_{V5}$ in the northern hemisphere and vice versa for the winter season in the southern hemisphere. This shows that the annual bias in ECHAM as discussed above, originates to a large degree from the summer season. The mid latitude bias found in the ECHAM model is a common bias that is present in many GCMs. In general, most

GCMs tend to overestimate humidity in the tropics and subtropics due to inadequate representation of cloud processes or of the large-scale circulation, or to excessive diffusion during the transport of water vapor (Risi et al. 2012a,b). The overestimation of humidity in the subtropics affects the enrichment of δD in the mid and high troposphere.

Whereas there are still some discrepancies between the different data products at mid and high latitudes, isotope data within a zonal band from $30\,°N$ to $30\,°S$ are roughly consistent, both for the annual average and the summer and winter profiles. An interesting feature of all datasets except for TES_{V4} (not shown) is a seasonal seesaw behavior of the latitudinal δD profiles in the inner tropics: in both seasons, the δD values close to the equator are lower in the respective summer hemisphere than in the winter hemisphere. The absolute δD variations are small and extend over different ranges in the respective hemispheres, but the δD latitude profiles for the two seasons (solid and dashed lines of each color) intersect very close to the equator.

This seasonal variation of δD in the tropics is a robust feature of the TES V5 dataset and a consequence of the seasonal displacements of the ITCZ Tropical rainfall bands and corresponding convective activity, which closely follow the maxima of insolation. The ITCZ is displaced towards the north during northern hemisphere summer and towards the south during southern hemisphere summer. Due to the isotope amount effect, the convectively active regions within the ITCZ to be associated with lower δD values are expected. Therefore, areas north (south) of the equator are isotopically more (less) depleted during NH summer, and vice versa during NH winter. The isotope amount effect therefore leads to the seesaw behavior of the zonal δD means where the latitudinal profiles in the two seasons have their lower values in the summer hemisphere (see the crossing lines in Fig. 3.5). This seesaw behavior has already been recognized in precipitation data (Waliser and Gautier 1993; Wu et al. 2003; Back and Bretherton 2005).

SCIAMACHY and TES_{V5}, show this isotope feature with varying intensity (Fig. 3.5a). The amount effect due to the movement of ICTZ is more pronounced in SCIAMACHY than in TES_{V5}. The original ECHAM model, $ECHAM_{AK5Corr}$, TES_{V5Pos} and $ECHAM_{AK5Pos}$ also show this seesaw pattern (Fig. 3.5b and c). The seesaw pattern seen in TES_{V5Pos} indicates that the cross dependency of H_2O on δD has no influence in this seesaw behavior.

A possible reason why SCIAMACHY shows this seesaw pattern more clearly is SCIA-MACHY's higher sensitivity at lower altitudes where many processes contributing to the amount effect occur (such as re-evaporation of raindrops in more/less humid air, etc). In order to investigate this further, ECHAM, TES_{V5} and $ECHAM_{AK5Corr}$ were separated into two layers (Fig. 3.6). Figure 3.6b confirms that seesaw pattern in the TES_{V5} originates from the lower layer. This is qualitatively in line with the fact that SCIAMACHY is sensitive down to the surface and the seesaw pattern nicely shows up in the SCIAMACHY dataset. This was not necessarily expected since the seesaw phenomenon is largely produced by displacements of the ITCZ over the oceans, where the SCIAMACHY coverage is relatively low (due to the requirement of low-level clouds) compared to the coverage over land. In contrast, ECHAM and $ECHAM_{AK5Corr}$ show the seesaw pattern throughout the entire atmospheric column, both at the lower and high layers (Fig. 3.6a and c). It seems that the model overestimates the correlation between lower and higher layers compared to the observations. It was speculated that GCMs in general show strong coherence between
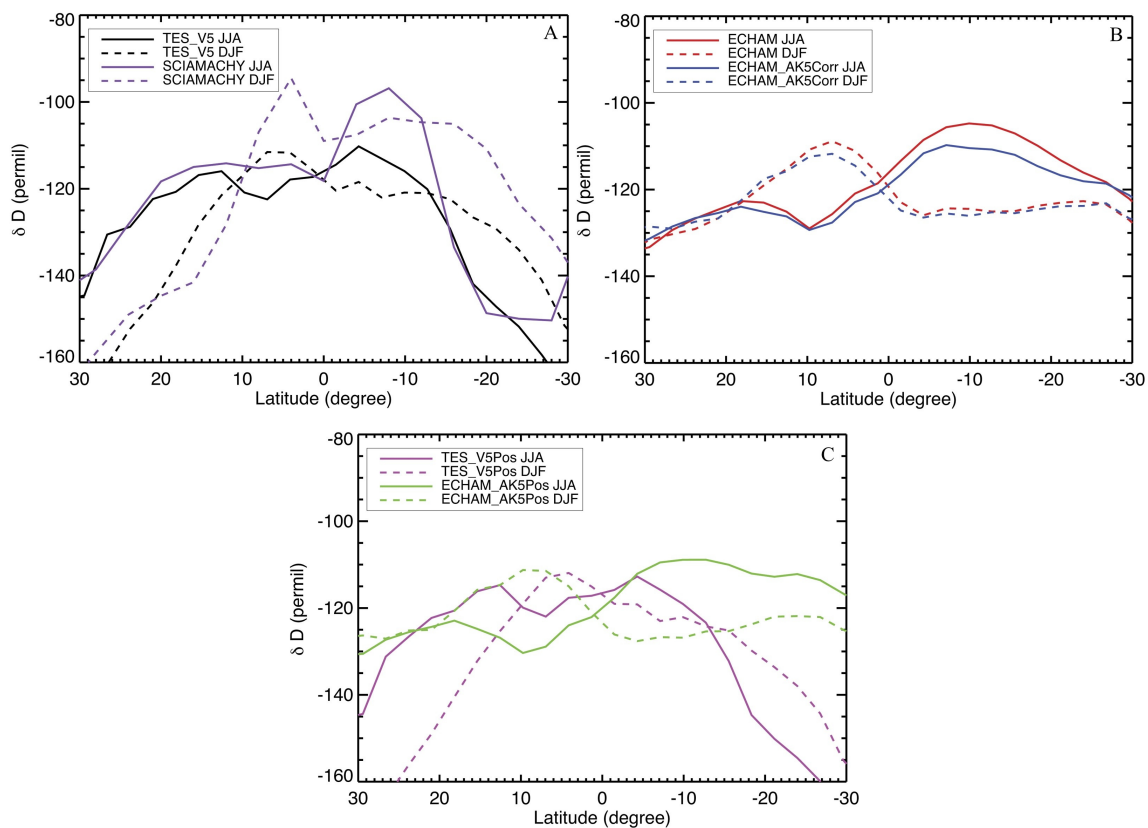
Figure 3.5 Latitudinal δD profiles between $30\,°$N and $30\,°$S in northern summer (JJA, solid lines) and northern winter (DJF, dashed lines) of TES$_{V5}$ and SCIAMACHY (a); ECHAM and ECHAM$_{AK5Corr}$ (b); TES$_{V5Pos}$ and ECHAM$_{AK5Pos}$ (c). All figures are weighted averaged from 900 to 425 hPa.

processes at lower altitudes (such as Sea Surface Temperature variations) and associated features at high altitudes (such as high convective cloud formation). In this case the common isotope seasonality at low and high altitudes in the model might be a further consequence of these known model problems (Risi et al. 2012a; Conroy et al. 2013).

The representation of this "fine structure" in the tropics is an important feature, which needs further investigation in remote sensing datasets of water isotopologues. It should be noted that the cloud height issue might contribute to or even cause the seesaw pattern seen in the satellite datasets. Satellites in general measure above thick clouds, but can measure through optically thin clouds (Lee et al. 2011). Thus, above convection, the satellite data are representative for δD at higher altitudes where δD is lower.

3.3.3 Relation of water vapor and δD

Already in 1964, Dansgaard (1964) described the water isotopologues within the global water cycle by means of a Rayleigh-type distillation model. Each condensation process extracts a certain quantity of water from an air mass and fractionates the water isotopo-
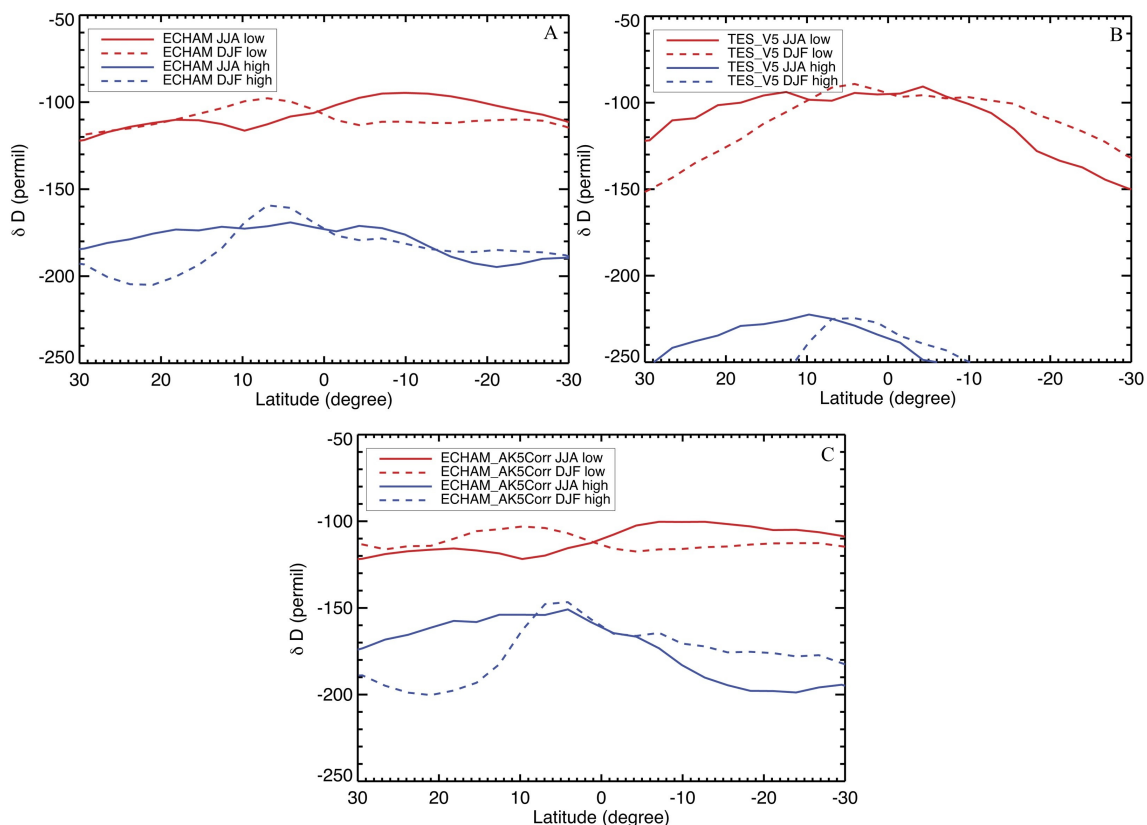
Figure 3.6 Latitudinal profiles between $30\,°\mathrm{N}$ and $30\,°\mathrm{S}$ in northern summer (JJA, solid lines) and northern winter (DJF, dashed lines) of ECHAM weighted averaged from 900 to 680 hPa and from 618 to 425 hPa (a), of $\mathrm{TES_{V5}}$ from 900 to 680 hPa and from 618 to 425 hPa (b), and of $\mathrm{ECHAM_{AK5Corr}}$ from 900 to 680 hPa and from 618 to 425 hPa (c).

logues according to the respective temperature. This successive extraction of the heavier isotopologues by distillation happens both during transport from the tropical/subtropical source regions to higher latitudes (Yoshimura et al. 2011; Frankenberg et al. 2009) and from lower to higher altitudes (Schneider et al. 2010; Worden et al. 2007; Brown et al. 2008). Assuming that this process is exclusively temperature dependent and controlled by a moist adiabatic lapse rate, a qualitative explanation of the isotope temperature effect over a wide temperature range is straightforward. It is instructive to check to what degree the atmosphere corresponds to this simple temperature dependent scheme: how Rayleigh-like is the earth's atmosphere?

Temperature gradients from the surface to higher altitudes and from the tropics to mid and high latitudes dry the corresponding air masses and lead to both lower total precipitable water (TPW) and, via the Rayleigh mechanism, to more depleted isotope values. In a pure Rayleigh distillation system, $\ln(\mathrm{HDO}/\mathrm{H_2O})$ is linearly related to $\ln(\mathrm{TPW})$ and the slope corresponds to the effective equilibrium fractionation, α_{eff}-1 (Frankenberg et al. 2009; Schneider et al. 2010; Yoshimura et al. 2011). Here, α_{eff} refers to a mean frac-

tionation over the entire distillation process with an "effective fractionation temperature" (Frankenberg et al. 2009; Yoshimura et al. 2011).

In the following, whether the atmosphere follows such a Rayleigh distillation model is investigated. Globally, a $\ln(HDO/H_2O)$ versus $\ln(TPW)$ plot (see Fig. 3.7a and b) is dominated by the latitudinal gradient of both quantities (i.e., the latitude effect). Lower $\ln(TPW)$ values and more depleted isotopic values are largely organized along a gradient from lower to higher latitudes. At high $\ln(TPW)$ (> 3), the different datasets agree rather well, but below 3, significant differences become apparent. Between $\ln(TPW)$ values of 2 and 3, SCIAMACHY appears to have lower $\ln(HDO/H_2O)$ values than ECHAM and TES. Below a $\ln(TPW)$ of 2, SCIAMACHY also displays a group of very high $\ln(HDO/H_2O)$ values, which show a larger scatter and deviate strongly from the linear correlation. The ECHAM model shows two separated branches at the lower end of the global distillation chain, which corresponds to air masses over Antarctica and the Arctic (Fig. 3.7b). This feature does not present in any available observational dataset since observations in these regions are absent.

It is evident that these structures influence the linear regression lines shown in Figure 3.7. The original ECHAM model simulates steeper overall slopes than observed by the satellites, mainly because the model results include strongly depleted water vapor at higher and polar latitudes, where no satellite data are available. TES_{V5} data result in a steeper slope than TES_{V4}, which again reflects the smaller latitude gradient in TES_{V4}, and convolution with the version 4 AK leads to a similarly low slope for $ECHAM_{AK4}$. The slope for the $ECHAM_{AK5}$ dataset is lower than TES_{V5}. However, both TES products disagree with ECHAM and SCIAMACHY for $\ln(TPW)$ lower than 2.5. The differences between datasets for lower $\ln(TPW)$ reflect the differences discussed in section 3.3.1 for the latitudinal δD gradients at mid and high latitudes. In the following, the study focuses on the tropical region (high $\ln(TPW)$) where the latitudinal profiles are in good agreement.

In the tropics, the differences between the datasets in the $\ln(HDO/H_2O)$ versus $\ln(TPW)$ correlation plot are smaller, but the correlation between $\ln(TPW)$ and the isotopes and the respective slope of this correlation is lower as well (Fig. 3.7c and d). These low slopes imply unrealistically high "effective" condensation temperatures for the satellite datasets (TES_{V5} and SCIAMACHY) and even more for the ECHAM model (up to almost 60 $^\circ C$). Apparently, a description of the relatively small isotopic variance by a simple overall distillation process is not suitable. This is likely due to the dominance of convective activity there, which affects the isotopic composition by many large scale (e.g., low level humidity confluence) and sub-scale processes (e.g., entrainment/detrainment of vapor in convective systems) that are not sufficiently described by Rayleigh fractionation. The isotope amount effect in the tropics is another factor contributing to the relatively flat slope because it leads to lower δ values at higher humidity (Fig. 3.7d). This feature is more prominent in the V5 dataset and less in the V4 dataset.

Figure 3.7e and f show $\ln(HDO/H_2O)$ vs $\ln(TPW)$ from satellites and model simulations over the Sahel region (0-10 $^\circ E$, 15-30 $^\circ N$). The Sahel has been chosen because SCIAMACHY shows the best performance here and has recorded most measurements ($>$ 6000 measurements, see also Frankenberg et al. 2009) allowing therefore a more complete comparison with the TES data. The slopes from all datasets in the Sahel are relatively flat

except for SCIAMACHY. This may again be related to the diverging vertical sensitivity of the different datasets. Based on a network of FTIR HDO/H_2O observations, Schneider et al. (2010) conclude that ln(HDO/H_2O) versus ln(TPW) slopes are steeper in air masses close to the surface and decrease progressively with height. In our observations, the slope is highest for SCIAMACHY, which also has the highest sensitivity close to the surface. The slope is high for TES$_{V4}$ and higher for TES$_{V5}$, which has the lowest sensitivity in the lower troposphere. Interestingly, the slope from SCIAMACHY (0.093) is in the range of a typical Rayleigh distillation process slope, which is between 0.08-0.15 ($+20 \sim$ -20 °C) depending on evaporation/condensation temperatures (Majoube 1971a,b; Yoshimura et al. 2011). The SCIAMACHY slope would correspond to an effective condensation temperature of 281.8 K. The slopes from TES$_{V5}$, ECHAM, ECHAM$_{AK5}$, and ECHAM$_{AK5Corr}$, ECHAM$_{AK5Pos}$ and TES$_{V5Pos}$ correspond to 314.2 K, 317.7 K, 313.9 K, 322.6 K, 311.1 K and 325.1 K, respectively (Fig. 3.7f and g).

In Figures 3.7h ln(HDO/H_2O) vs ln(TPW) scatter plots over the Sahel area are shown for all model layers from 900-425 hPa (900, 825, 749, 681, 618, 510 and 425 hPa). Since SCIAMACHY only provides total column data, it is not included in this analysis. All slopes from single altitude layers are steeper than the slopes from the total column ln(HDO/H_2O) vs ln(TPW) data. The TES$_{V5}$, ECHAM, ECHAM$_{AK5}$, and ECHAM$_{AK5Corr}$ slopes increase from $\sim$0.05 to $\sim$0.08, which lies in the range of typical Rayleigh distillation slopes. The a posteriori analysis products produce similar results as the original TES$_{V5}$ and ECHAM$_{AKCorr}$. The outlier data point with ln(HDO/H_2O) above 0 may cause the highest slope of ECHAM$_{AK5}$.

The low slopes of the ln(HDO/H_2O) vs ln(TPW) total column correlations imply that the total column data is inadequate to describe the Rayleigh model from the tropics to higher latitudes. It is suggested to use single altitude layers although in the atmosphere, there are many factors influencing this process such as mixing of various air parcels (Gedzelman 1988; Johnson et al. 2001), evaporation of condensate water (Smith 1992; Galewsky et al. 2007), kinetic effects (Keith 2000), or active convection (Smith et al. 2006; Moyer et al. 1996). Worden et al. (2007) and Brown et al. (2008) studies show that the amount effect plays an important role in the tropics. The isotopic composition of water vapor is lower than the predicted by the Rayleigh condensation curve. Apparently these processes have an important influence on the isotope-concentration correlation that overrules the condensation temperature-induced correlation.

3.3.4   Weighted versus non weighted average of δD

All δD total column data in the previous chapters were computed as averages weighted with the respective water vapor mixing ratio (see Eq. 3.1). This appears as a logical choice since it considers the total amount of the respective isotopologues in the atmospheric column. However, this weighted δD (δD$_{Col}$) is influenced by the vertical distribution of H_2O and its uncertainties. Weighted this way, the δD$_{Col}$ value is biased to near-surface levels where most of the total humidity is located. This means that the variability and the respective uncertainties of low level water vapor will affect δD$_{Col}$. Here we discuss briefly
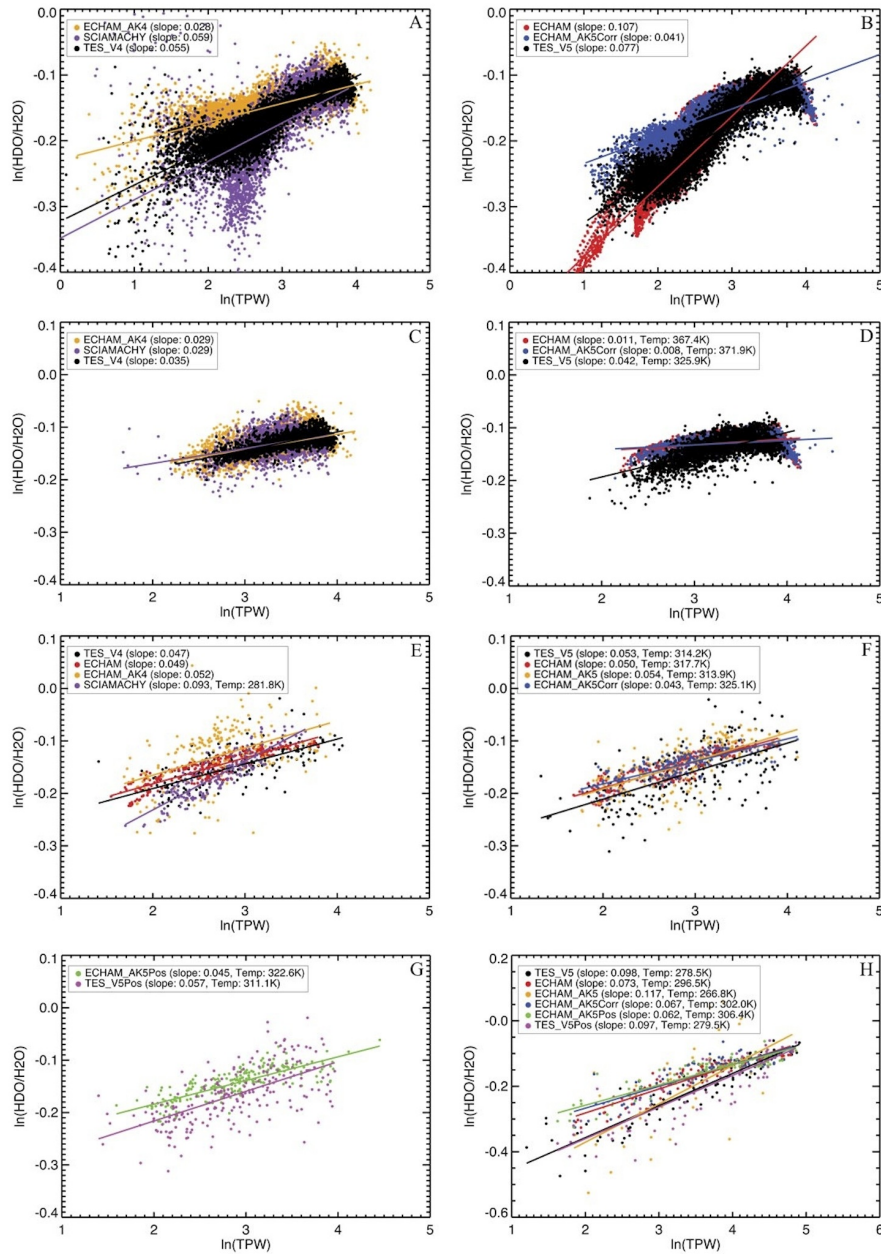
Figure 3.7 Correlation plot of ln (TPW; Total Precipitable Water derived from specific humidity) versus model simulated and satellite retrieved ln(HDO/H_2O). (a and b) Global correlations. (c and d) Correlations in the tropics (30 °N-30 °S). (e, f, g and h) Correlations in the Sahel region. Panels a, c, and e show the version 4 TES datasets and SCIAMACHY. Panels b, d, f, g, h show the version 5 TES datasets, both together with $ECHAM_{AK}$. Panels a, c, e are weighted averaged from 850 to 500 hPa and Panels b, d, f, g are weighted averaged from 900 to 425 hPa. Panel h is correlation plot at each layer from 900 to 425 hPa (900, 825, 749, 681, 618, 510 and 425 hPa).
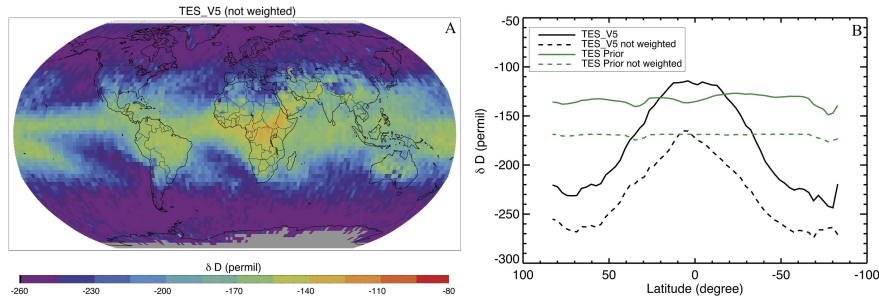
Figure 3.8 a: Arithmetically averaged δD product from TES_{V5} for the vertical region 900-425 hPa; b: Annually averaged latitude distribution of the H_2O-weighted (solid lines) and arithmetically averaged (dashed lines) δD value (900-425 hPa) from TES_{V5} and the respective values for the prior (green).

the differences between H_2O-weighted values of δD_{Col} and a simple arithmetic average (see Figure 3.8).

As expected, the arithmetically averaged δD values (900-425 hPa) are considerably lower than humidity weighted values (Fig. 3.8a). The difference between the two computations of δD amounts to about 60 ‰ in the tropics (Fig. 3.8b). The latitudinal distribution of the arithmetically averaged δD is more depleted than δD_{Col}, since the later is strongly determined by near surface water vapor. The δD_{Col} of TES_{V5} and TES prior values in the tropics show fluctuations, indicating the influence of H_2O variability close to the surface. SCIAMACHY does not measure vertical profiles of δD, therefore the SCIA-MACHY δD total column values shown in this paper are dominated by δD close to the surface and may additionally be influenced by the H_2O variability in the vertical column of water vapor.

3.4 Conclusions

Over the last years, water isotope retrievals have become available from different global satellite instruments. Here comparisons of the HDO/H_2O data from TES version 4, TES version 5, and SCIAMACHY with each other and with large-scale isotope patterns from the ECHAM model were carried out. The study systematically assessed how first-order water isotope effects (temperature-, latitude-, altitude-, continental-, and amount-effect) are represented in the respective remote sensing datasets.

The geographical and temporal patterns in the respective water isotopologue fields reproduced the different "classical" large-scale isotope effects to a varying degree. Our analysis confirmed the improvement of TES_{V5} compared to TES_{V4} for the first-order global isotope signals investigated. Similarly, when the model results are convoluted with the AK, ECHAM_{AK5} outperforms ECHAM_{AK4}. Nevertheless, the study identified a problem of ECHAM_{AK5} over the Himalayas region. The large positive isotope anomalies were shown to be caused by a high humidity bias of the ECHAM. A humidity correction or an a posteriori processing is necessary for model-data comparison because of cross dependence

between H_2O and δD in the application of the AK to the model. Furthermore, ECHAM overestimates δD values at mid latitudes compared to SCIAMACHY and TES_{V5} and the tropical and sub-tropical band of high δD values is wider in the model than in the satellite datasets. This is a common problem in many GCM models since the models tend to have a high moist bias in the tropical and subtropical regions associated with errors in cloud processes, large-scale circulation and diffusion during water vapor transport.

When examining the seasonally varying δD signal in the tropics associated to the movement of the ITCZ, SCIAMACHY, TES_{V5}, ECHAM, and $ECHAM_{AK5}$ showed the expected seasonal covariation of the latitudinal δD minima and maxima in water vapor with insolation and rainfall. Some of the isotopologue effects are difficult to identify in SCIAMACHY because of its limited coverage of large parts of the respective winter hemispheres and oceans.

This chapter also tested to what extent the atmosphere in the different datasets can be described as a Rayleigh distillation system. The results show that the humidity-isotope correlations based on the total column values cannot be explained with a simple Rayleigh distillation model. For small regions, e.g., in the Sahel, the observations from TES_{V5} and SCIAMACHY imply a more Rayleigh type behavior than what is modeled in ECHAM. However, none of the effective condensation temperatures deduced from the observed slopes reflect pure Rayleigh condensation temperatures. This comes not as a surprise since many processes influence this condensation process, such as mixing of the air parcel, evaporation of condensate water, kinetic effects, and active convection, which are not controlled by a single effective condensation temperature. However, when the vertical profiles of humidity and δD plot is made, the correlation slopes from all data are close to Rayleigh condensation slopes.

As the vertical resolution of the present satellite remote sensing products is very limited, it is not possible investigate the differences between the vertical and the horizontal dimension in more detail yet. To study this further, remote sensing data of the water isotopologues are needed that faithfully resolve single atmospheric levels. This should also help to reduce the influence of H_2O distribution in the computation of total column values (humidity bias). For model and satellite comparison, however, we can use total column of δD as long as both the model and satellite are equally treated and the adequate averaging kernels is applied to the model.

One central application of existing and future water isotopologue datasets will be the evaluation of global observations and models. It is suggested to use the qualitative and quantitative tests carried out in this study as a benchmark for the different data products and to evaluate their strengths and weaknesses.

3.5 Appendix

In this appendix, the TES averaging kernels over Tenerife before applying the a posteriori correction (A) and after applying the a posteriori correction (A$''$) are presented. The vertical sensitivity of the satellite is higher for water vapor compared to HDO. This is seen from the higher averaging kernel values of A_{HH} than A_{DD}. The a posteriori analysis aims
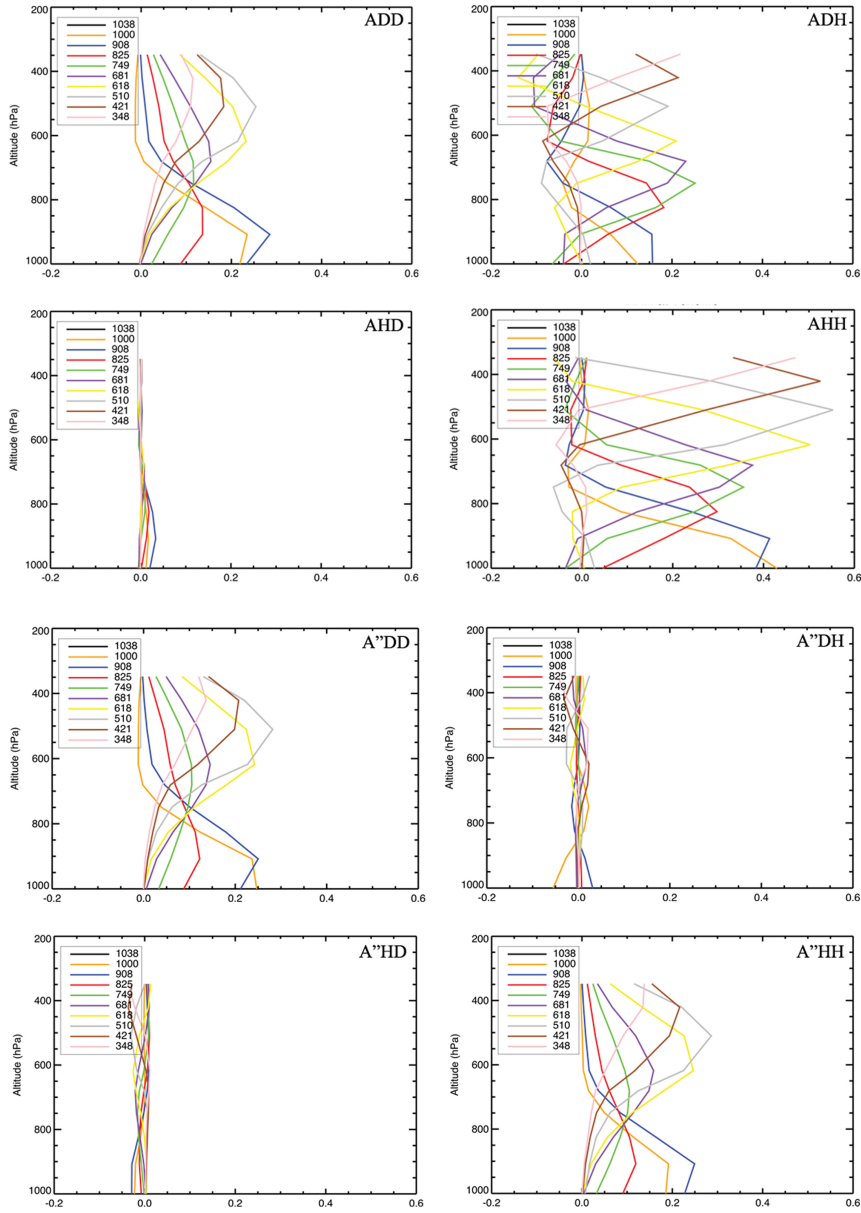
Figure 3.9 Averaging kernels in the $\{\ln(H_2O), \ln(HDO)\}$-basis for A_{DD}, A_{DH}, A_{HD} and A_{HH}, and in the $\{(\ln(H_2O)+\ln(H_2O))/2, \ln(HDO)-\ln(H_2O)\}$-proxy state after a posteriori correction $(A_{DD}'', A_{DH}'', A_{HD}'', A_{HH}'')$.

for the best possible degree of consistency between H_2O and δD profiles. The vertical resolution and sensitivity of the humidity (HHO) product need to be adapted to the vertical resolution and sensitivity of the isotopologue ratio product. After this a posteriori correction the retrieved humidity and isotopologue ratio represent the same atmospheric air mass $(A_{DD}'' \approx A_{HH}''$, Fig. 3.9).

4 The correlation of drought to ENSO and water isotopologues

"When the well's dry, we know the worth of water"
Benjamin Franklin

Based on: Sutanto, S. J., Adidarma, W., Hoffmann, G., and Röckmann, T (2013), Correlation of drought related to ENSO and water isotopes in Indonesia. conference proceeding, 4th International Seminar of HATHI, 6-8 September 2013, Yogyakarta, Indonesia.

Abstract

ENSO affects mainly the hydrological cycle and produces in particular droughts during El Niño and floods during La Niña in Indonesia. In order to have a better understanding on drought and its link with ENSO and water isotopologues, the ECHAM model has been used to simulate drought conditions by computing two drought indices, SPI and SPEI. These drought indices are commonly used in the empirical studies and have been successfully applied in Indonesia. The correlation of drought and water isotopologue during ENSO events shows that the ECHAM model is capable to simulate the ENSO associated droughts realistically. The SPI index reproduces the extreme droughts in Indonesia such as in 1994, where there were 19,817 ha paddy fields damaged. On the other hand, SPEI only shows severe drought due to low evapo-transpiration. The correlation of drought indices and water isotope is remarkably good (R = -0.926), whereas, the correlation of drought indices and Niño-3 is weak (R = -0.436). This indicates that δD is a good climatic indicator for drought and flooding events and it outperforms the Niño-3 index. In addition, the correlation of Niño-3 index and δ_v shows a strong correlation over Indonesia, pointing to the isotope amount effect as a dominant factor for the regional isotope signature.

4.1 Introduction

In Indonesia, prolonged dry and wet periods are mainly connected to ENSO (El Niño-Southern Oscillation) variability. Therefore, it is believed that extreme drought and flooding events occurred in Indonesia are caused by the higher ENSO variability. ENSO is a quasi climate oscillation between two states, La Niña and El Niño. El Niño and La Niña events are associated with anomalously warm and cold sea surface water temperatures (SST) for long periods in the tropical eastern Pacific Ocean (the coast of Peru), respectively. The Southern Oscillation refers to major changes in surface pressure gradients over the entire Pacific, which results during an El Niño (La Niña) event in anomalously high (low) surface pressures in the tropical western Pacific and over Indonesia. Because of its large associated SST patterns, and numerous associated teleconnection patterns

affecting temperature, precipitation and circulation anomalies, ENSO is considered as the dominating source of inter-annual variability.

Different methods and climatological indices have been developed to measure the strength of drought, such as Palmer Drought Severity Index (PDSI; Palmer 1965; Alley 1984), a modification of PDSI called Self-Calibrating Palmer Drought Severity Index (SC-PDSI; Wells et al. 2004), Standardized Precipitation Index (SPI; McKee et al. 1993), and Standardized Precipitation Evaporation Index (SPEI; Vicente-Serrano et al. 2009). These methods, especially PDSI, are robust and have been widely used in many countries as national drought indicators. In this study, the magnitudes of droughts in Indonesia were calculated using SPI and SPEI indices and compared with in-situ observations. In this chapter, the results from both indices will be compared with the simulated isotopic composition of precipitation and atmospheric water vapor isotopologue.

The modeling was carried out using the ECHAM model (Hoffmann et al. 1998), a general circulation model equipped with an isotope module allowing the computation of all related fractionation processes between the different water isotopologues in function of the simulated climate. Some other studies analyzed the correlation of ENSO and water isotopes using GCMs (Vuille and Werner 2005; Tindall et al. 2009). However, no study using GCM correlates the strength of drought with ENSO, the isotopic composition of water vapor, and the isotopic composition of precipitation. Thus, this study has an objective to study the correlation of droughts and ENSO, and their consequences for the water isotopologue signature in the region of Indonesia.

4.2 Methods

To describe drought severity in the region of Indonesia, two well-established indices, SPI and SPEI, are used. The ECHAM model simulates the monthly precipitation and temperature data used in the analysis. Validation of the model performance to realistically reproduce ENSO related drought events in Indonesia are carried out using the same indices computed with in-situ meteorological data from Empang (1967-2006) and Gunung Mas (1978-2012) stations. The averaged indices from both stations are then compared with the model result of the two grid points including the corresponding climatological stations. In addition, documentary of evidence on the area of paddy fields affected by droughts is collected to confirm the drought occurrences. Exceeded probability analysis for drought and flooding events is performed using the Gumbel distribution.

The isotopic composition of water vapor (δD_v) is computed by the ECHAM model. Correlation analyses of model results and observations are performed between the drought indices and the Niño-3 index, the drought indices and the isotopic composition of water vapor, and between the Niño-3 index and the isotopic composition of water vapor.

4.2.1 The Niño-3 index

The Niño-3 index is an average of the sea surface temperatures (SST) in the region of $150\,°\mathrm{W}$ to $90\,°\mathrm{W}$ (longitude) and $5\,°\mathrm{N}$ to $5\,°\mathrm{S}$ (latitude; see Fig. 4.1). When the index is positive (red), water is warmer than normal and when the index is negative (blue), water
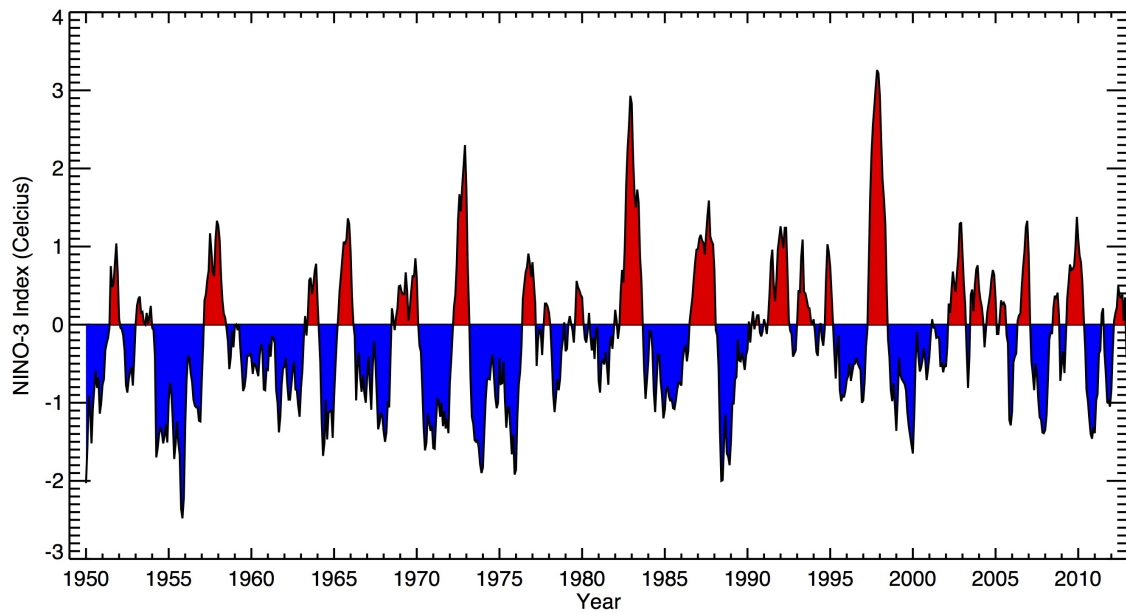
Figure 4.1   The Niño-3 index from January 1950 to December 2012 obtained from National Aeronautics and Space Administration (NASA).

is cooler than normal. El Niño occurs when the water is much warmer than normal for a sustained period of time and vice versa for La Niña. Strong El Niño events occurred in years 1972, 1982 and 1997.

4.2.2   The SPI drought index

The SPI drought index was developed by McKee et al. (1993) based on standardized precipitation data. Unlike PDSI, SPI was designed to quantify a precipitation deficit at different time scales. The advantages of SPI index are simple, spatially consistent (invariant) in its interpretation, does not need a fixed time scale, and only precipitation data is required (McKee et al. 1993; Vicente-Serrano et al. 2009). However, the SPI method does not include evapo-transpiration and therefore does not reach to temperature changes.

SPI calculation requires minimum 30 years of precipitation data record (McKee et al. 1993; Bordi et al. 2001; Wu et al. 2005), though a study from Guttman (1994) concludes that 40-60 years of precipitation data are needed in order to get an accurate and stable result. In the calculation of SPI, an essential step is a determination of a probability density function (PDF) using two-parameter gamma distribution. The gamma probability density function for a given frequency distribution of precipitation is fitted as (for precipitation more than 0):

$$g(x) = \frac{1}{\beta^{\alpha} \Gamma(\alpha)} x^{\alpha-1} e^{-x/\beta} \tag{4.1}$$

where x is the precipitation amount, α is a shape parameter, β is a scale parameter, and $\Gamma(\alpha)$ is the gamma function.

$$\alpha = \frac{1}{4A}\left(1 + \sqrt{1 + \frac{4A}{3}}\right) \tag{4.2}$$

$$\beta = \frac{\overline{x}}{\alpha} \tag{4.3}$$

$$A = ln(\overline{x}) - \frac{\sum ln(x)}{n} \tag{4.4}$$

n is number of precipitation events, and $\overline{x}$ is mean precipitation over the time scale of interest. The estimated parameters are used for calculating the cumulative probability distribution for a specific precipitation event observed in a defined time scale (e.g., months, Eq. 4.5).

$$G(x) = \int_0^x g(x)dx = \frac{1}{\beta^\alpha \Gamma(\alpha)} \int_0^x x^{\alpha-1}e^{-x/\beta} \tag{4.5}$$

The gamma function cannot be defined when there is no precipitation ($x = 0$). In reality, however, there are few times when there is no precipitation occurrence in a week or even in a month during dry season. The cumulative distribution needs to be modified to include these events:

$$H(x) = q + (1 - q)G(x) \tag{4.6}$$

where q is the probability of having no precipitation event on a specific time scale.

Finally, the SPI index is calculated from the cumulative probability distribution $H(x)$, transformed into standardized normal distribution Z.

$$Z = SPI = -\left(t - \frac{c_0 + c_1 t + c_2 t^2}{1 + d_1 t + d_2 t^2 + d_3 t^3}\right) \tag{4.7}$$

$$Z = SPI = +\left(t - \frac{c_0 + c_1 t + c_2 t^2}{1 + d_1 t + d_2 t^2 + d_3 t^3}\right) \tag{4.8}$$

and

$$t = \sqrt{ln\left(\frac{1}{(H(x))^2}\right)} \tag{4.9}$$

$$t = \sqrt{ln\left(\frac{1}{(1 - H(x))^2}\right)} \tag{4.10}$$

Eq. (4.7) and Eq. (4.9) are used for $0 < H(x) < 0.5$ and Eq. (4.8) and Eq. (4.10) are used for $0.5 < H(x) < 1$. $c_0 = 2.515517$, $c_1 = 0.802853$, $c_2 = 0.010328$, $d_1 = 1.432788$, $d_2 = 0.189269$, and $d_3 = 0.001308$.

Table 4.1 Classification of drought based on SPI and SPEI indices.

Index	Classification	Probability
> 2	extremely wet	2.3
1.5 to 1.99	very wet	4.4
1 to 1.49	moderate wet	9.2
0 to 0.99	mildly wet	34.1
0 to -0.99	mild drought	34.1
-1 to -1.49	moderate drought	9.2
-1.5 to -1.99	severe drought	4.4
-2 <	extreme drought	2.3

4.2.3 The SPEI drought index

The SPEI method is originally based on the SPI procedure using monthly precipitation and temperature data and it uses a simple procedure to estimate evapo-transpiration using the Thornthwaite method (Thornthwaite 1948). Regarding to the choice of evapo-transpiration method, Sheffield et al. (2012) demonstrated that replacing the Thornthwaite method with the Penman-Monteith method leads to remarkably different results, in particular concerning the relation between global warming for the last 40 years. In this study, we use the Thornwaite method due to climatological data scarcity for Penman-Monteith analysis. A typical drought classification scheme based on the SPI and SPEI indices is presented in Table 4.1. The SPEI computation also requires a long-term monthly precipitation record with a measurement record of minimum 30 years.

In SPEI, the monthly difference between the precipitation (P) and evapo-transpiration (PET) for the month i is calculated as:

$$D_i = P_i - PET_i \tag{4.11}$$

L-moment ratio diagrams are used to calculate the time distribution difference, allowing a comparison of the empirical frequency distribution of D computed at different time scales (Hosking 1990). In Indonesia, the L-moment ratio is generally following the GEV (Generalized Extreme Value) distribution. For another location, the L-moment ratios (L skewness, τ_3 and L kurtosis, τ_4) can be used to determine the fitted distribution.

$$\tau_3 = \frac{\lambda_3}{\lambda_2}, \tau_4 = \frac{\lambda_4}{\lambda_2} \tag{4.12}$$

where λ_2, λ_3, and λ_4 are the L-moments of the D series, obtained from probability-weighted moments (PWMs, w symbol) using the formulas:

$$\lambda_1 = w_0 \tag{4.13}$$

$$\lambda_2 = w_0 - 2w_1 \tag{4.14}$$

$$\lambda_3 = w_0 - 6w_1 + 6w_2 \tag{4.15}$$

$$\lambda_4 = w_0 - 12w_1 + 30w_2 - 20w_3 \tag{4.16}$$

The PWMs of order s are calculated as

$$w_s = \frac{1}{N} \sum_{i=1}^{n} (1 - F_i)^s D_i \tag{4.17}$$

where F_i is a frequency estimator developed by Hosking (1990):

$$F_i = \frac{i - 0.35}{N} \tag{4.18}$$

where i is the observation range in increasing order and N is the number of observation points.

A three-parameter log-logistic distribution for standardizing the D series to calculate the SPEI values has been chosen following Vicente-Serrano et al. (2009). Using this distribution, the probability density function is expressed as:

$$f(x) = \frac{\beta}{\alpha} \left(\frac{x - y}{\alpha} \right)^{\beta-1} \left[1 + \left(\frac{x - y}{\alpha} \right)^{\beta} \right]^{-2} \tag{4.19}$$

where α, β, and γ are the scale, shape and origin parameters, respectively for D values in the range $(\gamma < D < \infty)$. In SPEI, these parameters can be obtained following the L-moment procedure:

$$\beta = \frac{2w_1 - w_0}{6w_1 - w_0 - 6w_2} \tag{4.20}$$

$$\alpha = \frac{(w_0 - 2w_1)\beta}{\Gamma\left(1 + \frac{1}{\beta}\right) \Gamma\left(1 - \frac{1}{\beta}\right)} \tag{4.21}$$

$$\gamma = w_0 - \alpha\Gamma\left(\frac{1 + 1}{\beta}\right) \Gamma\left(\frac{1 - 1}{\beta}\right) \tag{4.22}$$

where $\Gamma(\beta)$ is the gamma function of β.

According to the log-logistic distribution, the probability distribution function of the D series is given by

$$F(x) = \left[1 + \left(\frac{\alpha}{x - y} \right)^{\beta} \right]^{-1} \tag{4.23}$$

Finally, SPEI values are calculated using the standardized values of $F(x)$, following the classical approximation of Abramowitz and Stegun (1965):

$$SPEI = W - \frac{c_0 + c_1 W + c_2 W^2}{1 + d_1 W + d_2 W^2 + d_3 W^3} \tag{4.24}$$
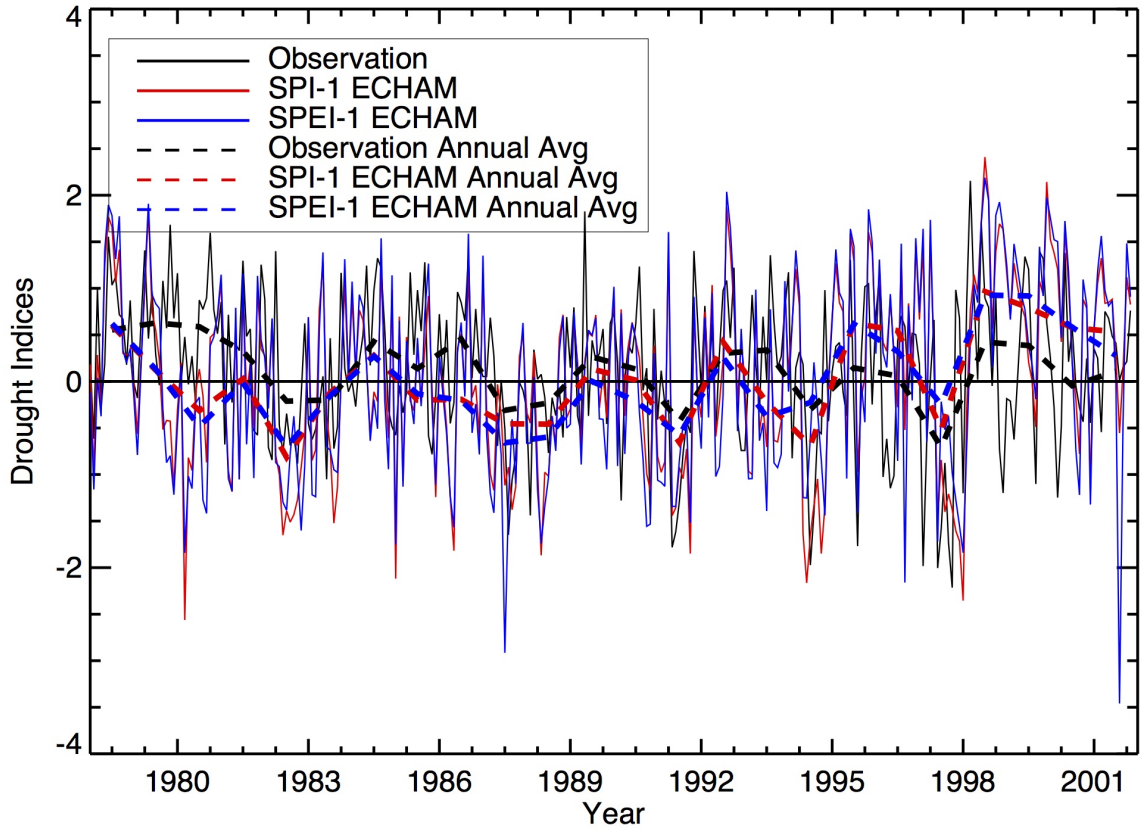
with,

Figure 4.2 Drought indices analysis from observation and ECHAM.

$$W = \sqrt{-2ln(P)} \quad for P \leq 0.5 \tag{4.25}$$

P is the probability of exceeding a determined D value, $P = 1 - F(x)$. Equation 4.25 is valid for P $\leq$ 0.5, and for P > 0.5, P is replaced by $1 - P$ and the sign of resultant SPEI is reversed. The constants are $c_0 = 2.515517$, $c_1 = 0.802853$, $c_2 = 0.010328$, $d_1 = 1.432788$, $d_2 = 0.189269$, and $d_3 = 0.001308$. Detailed information on the SPEI method can be found in Vicente-Serrano et al. (2009) and Sutanto and Adidarma (2015).

4.3   Results and discussion

4.3.1   Drought analysis

The SPI and SPEI drought indices over Indonesia are calculated using the model results and in-situ observations for validation (Fig. 4.2). The simulation period covers from 1978 to 2001 in order to have the same period between ECHAM and the observations. There is no observation data before 1978. SPEI analysis from observations is not conducted due to the lack of continuous temperature data.

The drought analysis from the GCM agrees well with the one from observations, although the model slightly overestimates the observations in one year (e.g., year 2000),
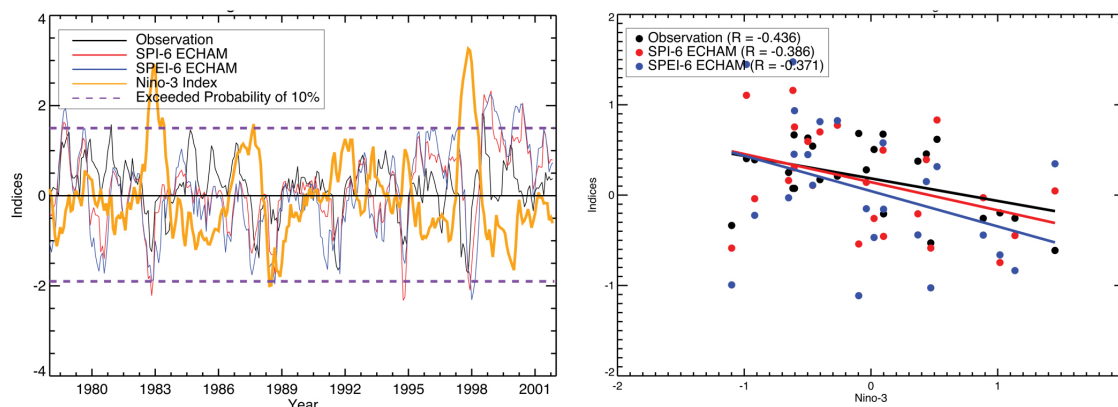
Figure 4.3 SPI-6, SPEI-6 and the Niño-3 index plot (left), and a correlation of annual average Niño-3 Index and the annual drought indices from observations and ECHAM (right).

and underestimates in another year (e.g., 1980). However, overall, the ECHAM model can reproduce drought signatures (frequency, severity, etc) from the observations. The results from SPI and SPEI analysis in Indonesia region are similar. This is due to the small temperature variability in Indonesia that is used for computing the additional evapo-transpiration in SPEI. The SPEI index, therefore, produces quite a different result compared to the SPI index if there is an extreme temperature deviation. For example, the cold temperature in year 1994 lowers the SPEI value relative to SPI.

4.3.2 Correlation between drought and ENSO

Figure 4.3 left shows the occurrences of dry and wet conditions during El Niño and La Niña with respect to the Niño-3 index. For this plot, SPI-6 and SPEI-6 are calculated to match the drought results with the duration of ENSO events from the point of increase to the peak ($\pm$ 6 months). Overall, the drought indices are anti correlated to the Niño-3 index showing that a positive Niño-3 index is associated to drought conditions, and it appears as a negative value in the drought indices. This anti correlation is more visible during strong ENSO events such as the 1982-1983 and 1997-1998 El Niños. Both well-known El Niño years produced droughts with exceeding probability of more than 10 % based on the Gumbel distribution. However, for the year of 1988 during La Niña, both the model and observations show a negative signal, indicating a drought condition.

To check the consistency of drought related to ENSO, data from a number of paddy field areas affected by droughts was collected from 1989 to 2001 in Central Java. There is no data in 1988, thus we cannot validate the drought in this year. Based on the data, the highest number of paddy fields affected by droughts occurred in 1991 and 1994, with affected areas of 18,928 ha and 19,817 ha, respectively (Adidarma et al. 2006). The Niño-3 index during the extreme droughts in these years only shows an index value of $\pm$ 1, while the SPEI values show severe droughts for both years. Surprisingly, the SPI value in the year 1994 shows an extreme drought with an index value of more than 2, in good agreement with the fact that the largest area of paddy field affected by drought was

occurred in 1994. A large precipitation deficit triggers low SPI value, since the SPI index is calculated based on precipitation data. In contrast, SPEI index indicates severe drought because the evapo-transpiration flux was also low (low temperature) in 1994. The severe drought in year 1994 calculated using SPEI and the extreme drought calculated using SPI from the ECHAM model outputs have been confirmed by the drought analysis from the observations (Adidarma et al. 2006). Recently, Sutanto and Adidarma (2015) show that the extreme drought occurred in 1994 has a SPEI value lower than -2.

For a better overview of the relationship between droughts and ENSO, the drought indices are plotted against the Niño-3 index (Fig. 4.3 right). The results show that the observation has a higher correlation coefficient (R = 0.436) than ECHAM (R = 0.386 and 0.371 for SPI and SPEI, respectively). Generally, there is no strong correlation between the strength of ENSO and the droughts denoted by the drought indices in Indonesia. The El Niño and La Niña events are not always followed by drought or flooding events in Indonesia, respectively.

4.3.3 Correlation between drought and water isotopologue

The correlation between SPI and the Niño-3 index with δD_v, in relation with the isotope amount effect and ENSO events, is presented in Figure 4.4. A strong anti-correlation between δD_v and SPI due to the isotope amount effect is visible in the annual data (R = -0.926). The anti correlation signal between SPI and δD_v is caused by the significant isotope amount effect, since in convective events the precipitation amount is inversely related to the isotopic composition of the rain water (Dansgaard 1964). The lower SPI values (dry) and the enriched δD_v values are dominated by El Niño events, and it is conversely for La Niña.

The correlation between the Niño-3 index and δD_v becomes slightly weakened (R = 0.738) compared to the correlation between SPI and δD_v. In addition, there is a positive correlation between Niño-3 and δD_v since positive values of Niño-3 mean drought or dry conditions. The weakened correlation of Niño-3 and δD_v might be caused by the time lag of dry/wet condition. One should note that the Niño-3 index is calculated based on the temperature anomaly in the Central-East Pacific Ocean, whereas the location of the study is over Indonesia region (West Pacific). In addition, Indonesia is located between two different climatic conditions, Indian Ocean and Pacific Ocean.

4.3.4 Correlation between ENSO with drought and δD

The correlations between ENSO denoted by the Niño-3 index with SPI and δD_v from ECHAM are presented (Fig. 4.5). The simulation of Niño-3 and δD_v results in an ENSO pattern, with a strong correlation in the region of Indonesia on one hand, and a strong anti correlation in the Eastern-Central Pacific Ocean on the other hand, as a result of the isotope amount effect (Fig. 4.5 left). It is vice versa for the correlation of Niño-3 and SPI (Fig. 4.5. right). During high ENSO, the Indonesia region is dry and the Pacific Ocean is wet. As a consequence, the δD_v values in Indonesia are enriched due to the dry conditions and the δD_v values in the Pacific Ocean are depleted due to the wet conditions.
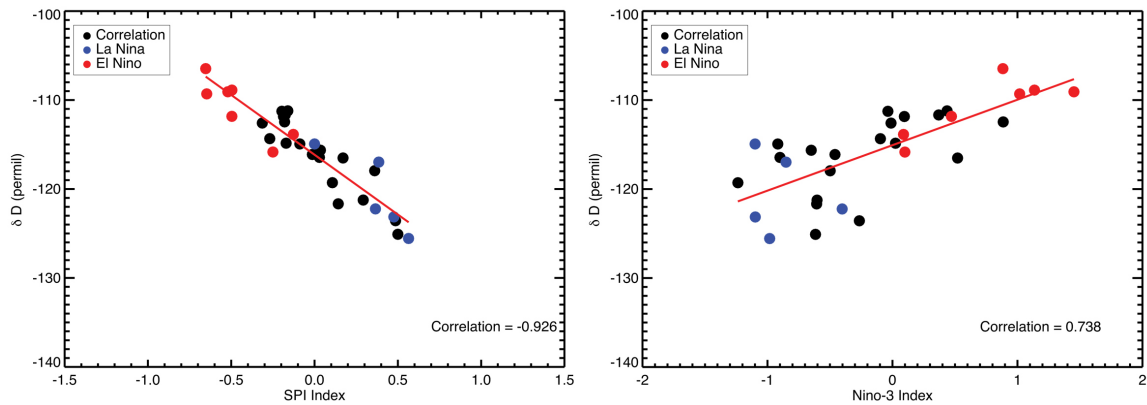
Figure 4.4 The correlation between SPI-1 and δD_v (left), and the correlation between the Niño-3 index and δD_v (right) in Indonesia (averaged grids from 5 °N to 10 °S, 100 °E to 135 °E).
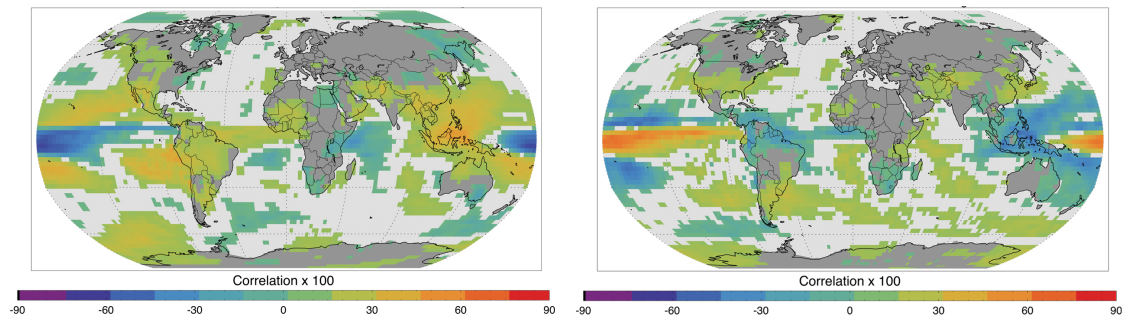

Figure 4.5 A correlation of the Niño-3 index and δD_v (left) and the Niño-3 index and SPI (right) from ECHAM at 1000 hPa nudged 1971-2001. A student's t-test statistical analysis is applied with significance level of 10 %. The correlation is multiplied by 100.

4.4 Conclusions

The results of the droughts analysis using the ECHAM model are realistic. The SPI drought index can be used as a good agricultural drought indicator in Indonesia since the dominant factor for drought in Indonesia is precipitation. The highest number of paddy field affected by drought in the year 1994 confirms the severe drought incident calculated using SPI, with the probability of occurrences higher than 10 %. There is no strong correlation between the strength of ENSO, denoted by the Niño-3 index, and the droughts, denoted by drought indices in Indonesia.

Stable water isotopologue, on the other hand, is a good climatic indicator for drought and flooding events compared to the Niño-3 index. The correlation between SPI and water isotopologue is remarkably good (R = -0.926), and the correlation between the Niño-3 index and water isotopologue is quite good (R = 0.738). Global correlation between SPI drought index and δD_v shows that there is a strong anti correlation in Indonesia and a correlation in the eastern Pacific Ocean. In contrast, the correlation between the Niño-3

Index and δD_v shows an opposite result, which is in agreement with the anti-correlation of ENSO and drought indices. The anti correlation of drought indices and δD_v points to the isotope amount effect as a dominant factor for the regional isotope signature not only on a seasonal but also on an inter-annual scale.

5 Atmospheric processes during ENSO events

"El Niño is a good example to illustrate that there is indeed predictability in the midst of chaos"
J. Shukla

Abstract

ENSO has profound effects on the global water cycle, which can be examined at the process level by investigating the associated water isotopologues. Many isotope-based studies are aimed at understanding ENSO variability in the tropics, however focusing principally on near-surface processes and isotopologue signals. The goal of the present study is to investigate the atmospheric processes governing the changes in the isotopic composition of water vapor both near the surface and at mid troposphere in the Pacific region during ENSO events, using a combination of remote sensing data and model simulations. For the lower atmosphere (e.g., 1000 hPa), the study shows that rainout processes, less rain re-evaporation of falling droplets, and increase of convective updrafts and diffusive exchange within the convective systems, contribute to "the isotope amount effect" and isotopically deplete the water vapor during wet conditions, in agreement with previous studies. However, the result finds that the ENSO associated isotopic signal in the mid troposphere (e.g., 500 hPa) diverges from the near-surface response. Analysis suggests that transport of enriched water vapor from lower atmospheric layers through convective updrafts controls the enrichment of mid tropospheric water vapor over the Pacific Ocean. In the observations, a strong positive correlation between the increase of convective precipitation and the isotopic composition of water vapor clearly points to such a mechanism (R of 0.7-0.8 in the Central Pacific and 0.5-0.6 in the West Pacific). Model results confirm this mechanisms though producing slightly lower correlation values, with R values of 0.6 in the Central Pacific and 0.5 in the West Pacific. However, the distinction between convective and stratiform precipitation remains a result of model dependent parameterization. This study suggests that two issues should be investigated in more detail in further studies: (1) the equilibrium and dis-equilibrium between rain droplets and surrounding vapor for convective and stratiform precipitation and (2) different convection schemes in the different isotopic GCMs, describing the triggering of convection and uplift of lower layer air to higher layers. Ideally such a comparison of different isotopic GCMs can provide an interesting benchmark test for the performance of the different convection schemes during ENSO, and to disentangle the importance of the different processes contributing to the amount effect.

5.1 Introduction

ENSO is globally the largest source of inter-annual climate variability. It is a quasi-periodic climate oscillation between two states of the tropical Pacific characterized as La Niña (cold phase) and El Niño (warm phase). ENSO triggers a number of atmospheric tele-connection patterns (Gershunov and Barnett 1998; Power et al. 1999; Trenberth and Caron 2000), which have a major impact on associated precipitation patterns. In general, El Niño is associated with dryer than normal conditions over many tropical continental areas such as the Brazilian Nordeste or Indonesia and wetter than normal condition in the northern extra tropics and over the Central Pacific. La Niña conditions are in particular marked by stronger than normal rainfall over the area of the West Pacific warm pool. The interactions between sea surface temperatures, evaporation and wind anomalies, changes in humidity gradients and convective activity contribute to the complexity of the system (Latif et al. 1998; Trenberth et al. 1998).

In many studies, water isotope signals have been used to better understand the relation between ENSO and rainfall anomalies, since various fractionation processes such as condensation and evaporation leave a characteristic imprint on the isotopic composition of rainwater and the corresponding water vapor (Ichiyanagi and Yamanaka 2005; Vuille and Werner 2005; Moerman et al. 2013). Condensation and evaporation lead to an isotopic enrichment of the liquid (solid) phase relative to the vapor phase. Thus, the isotopic composition of both water vapor and precipitation gives valuable information on the condensation history of a water vapor mass in the atmosphere. This provides us with useful information to disentangle the individual processes controlling the regional and global water cycle (Lee et al. 2012).

Most water isotopologue studies in the tropics, analyzing seasonal or spatial water isotopologue signals, demonstrate a negative correlation between the δ value of precipitation and local rainfall, which is called the amount effect (Dansgaard 1964). The uses of this modern analogue is to reconstruct local and regional rainfall in the past on times scales from decades to thousands of years based on water isotopologue records, preserved in different geological archives such as ice core, tree ring cellulose or calcium carbonate of speleothems (Becker et al. 1991; Jouzel et al. 1997; Vimeux et al. 2005; Jo et al. 2014; Lee et al. 2012). Recently, some studies have been carried out to understand in more detail the individual processes contributing to the amount effect. Most of these studies either use Atmospheric Global Circulation Models (AGCMs) equipped with water isotope modules and only few studies use water isotopologue signals from satellite records to analyze atmospheric processes affecting the isotope amount effect (Worden et al. 2007; Brown et al. 2008; Risi et al. 2010; Moore et al. 2014) or in a combination with more classical records measuring the water isotopologues in the meteoric water (for example the global network of isotopes in precipitation GNIP; Conroy et al. 2013; Moerman et al. 2013; Lekshmy et al. 2014). In the tropics, such studies principally focused on the analysis of the various monsoon systems or short-term variability as the Madden-Julian Oscillation (MJO; Hoffmann and Heimann 1997; Vuille and Werner 2005; Landais et al. 2010; Risi et al. 2010; Kurita et al. 2011; Lee et al. 2012).

This study is the first study, which scrutinizes the ENSO variability at lower and middle troposphere using water isotopologues measurement from satellites. Here, two different satellite data sets, the TES and the SCIAMACHY, and data of isotopes in precipitation from the GNIP, the International Atomic Energy Agency (IAEA) are used, and these observations are compared with simulations of the ECHAM4 AGCM fitted with a water isotope module. The study concentrates on the core region of ENSO variability, the tropical Pacific, analyzing changes of the isotopic composition of water vapor at lower and middle troposphere and relate these changes to atmospheric ENSO dynamics and cloud physics. Chapter 5.2 describes the general overview on the data and precipitation data used in the study. Chapter 5.3 compares the strength of ENSO with the water isotopologue signals and reports a characteristic near surface contrast between the West and Central Pacific and an inverse pattern at higher altitudes. Summary and discussion on the possible mechanisms leading to this pattern are presented in detail in chapter 5.4. Chapter 5.5 concludes all the findings and shares some perspectives for further study.

5.2 Data and instruments

5.2.1 General overview on the data

The atmospheric data sets used here stem from two satellite based remote sensing systems, TES (Worden et al. 2006, 2012) and SCIAMACHY (Frankenberg et al. 2009; Scheepmaker et al. 2013). They provide us with both atmospheric water vapor mixing ratios and the corresponding Deuterium content (i.e., the δD value). The δD values in precipitation are taken from the IAEA/GNIP global network, which has sampled rainwater and measured its isotopic composition on a monthly basis for more that 50 years (Aggarwal et al. 2007; Rozanski et al. 1993; Schotterer et al. 1996). Furthermore, two different precipitation data sets, the ERA-interim re-analysis from the European Center for Medium-Range Weather Forecasts (ECMWF; Betts and Jakob 2002; Bechtold et al. 2004; Dee et al. 2011) and the satellite product Tropical Rainfall Measuring Mission (TRMM; Schumacher and Houze JR 2003; Schumacher et al. 2004; Huffman et al. 2007) are used. The former is a blended product of observations assimilated into model simulations to obtain a physically consistent data set. These observations are compared with simulations of the ECHAM global circulation model. In order to mimic as closely as possible the climatological situation (Niño/Niña, Arctic Oscillation, etc.) and typical associated weather patterns the model was nudged with the observed wind fields. See chapter 1.5 for detailed information about the satellites and model data. In this study, we use the model outputs without applying collocation and convolution methods with the TES data sets. We also note that the different climatological periods are used in the analyses, e.g., we use TES data from 2004-2011, SCIAMACHY data from 2003-2007, and ECHAM data from 1971 to 2001.

5.2.2 Precipitation data

Two independent data sets of precipitation, The ERA-interim reanalysis data of the ECMWF and the TRMM radar data set, are used. The ERA-interim reanalysis model is designed to assimilate a huge amount of observational data (nearly 10^7 data per day

both from surface observations and satellite measurements; Dee et al. 2011) into the atmospheric model. Nevertheless, rainfall in the tropics is a known weakness of all re-analysis products (Uppala et al. 2005; Dee et al. 2011) because of the difficulties in the assimilation of humidity information and poor representation of the global transport of moisture in the atmosphere.

The TRMM satellite operates at an altitude of 350 km with a swath width of 215 km and a horizontal footprint of 4.3 km at nadir-viewing mode. The orbital domain of the TRMM satellite extends from $35\,°N$ to $35\,°S$. The TRMM precipitation radar operates in the K_u band (2.17 cm wavelength) with a sensitivity of 17 dBZ, corresponding to a precipitation rate of approximately 0.4 mm h^{-1} and vertical resolution of 250 m (Schumacher and Houze JR 2003; Schumacher et al. 2004). The precipitation radar also classifies the precipitation into convective and stratiform precipitation elements in the TRMM product. Detailed information about the TRMM satellite can be found in Kummerow et al. (1998). Convective precipitation data from both ERA-interim and TRMM in the years 2004-2011 are used in our study in order to compare it with TES measurements.

The isotopic composition of precipitation is obtained from IAEA. IAEA, in cooperation with the World Meteorological Organization (WMO), has run the Global Network of Isotopes in Precipitation (GNIP) since 1961. Monthly precipitation samples have been collected from over hundreds meteorological stations in more than 125 countries for δD and δ^{18}O analysis (selected stations also sample for Tritium). For this study, we selected the stations in the Central Pacific and West Pacific, which at least have one complete year of isotope observation during an ENSO event. Those stations are Canton Island, Manila, Diliman Quezon, Bonga, and Inang Maharang.

5.3 Results

5.3.1 Correlation of the Niño-3 index with global δD$_V$

In a first step, whether the ECHAM model shows a realistic response of its global water cycle to ENSO variability is tested. The pointwise correlation between ENSO (the Niño-3 index) and precipitation (Fig. 5.1) is computed. The correlation is calculated with a low significance level of 10 % using a student's t-test. The blank spots in Figure 5.1 are the correlations that did not pass the student's t-test analysis. The model reproduces features such as the drier conditions over Indonesia, Northern Australia and the Brazilian Noreste. Wetter than normal conditions are simulated in particular over the Central Pacific and on the Californian coast, in good agreement with known ENSO associated precipitation anomalies (Ropelewski and Halpert 1987). Without going into details of the quality of the simulated relation between the water cycle and ENSO, we conclude that the models large-scale response to ENSO is sufficiently realistic to warrant an investigation of the water isotopologue signals. In particular the weakening of the West Pacific branch of the Hadley-Walker circulation and the strengthening of convective activity over the Central Pacific during El Niño events are robust features, which are found also in observations (Curtis and Adler 2000; Dai and Wigley 2000).
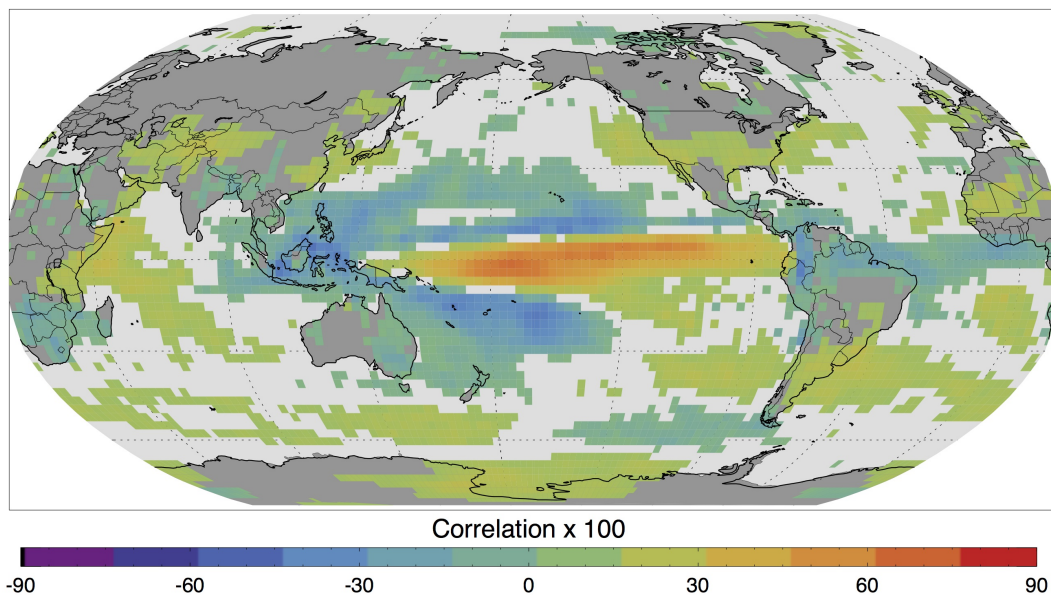
Figure 5.1 Correlation of the Niño-3 index and Precipitation amount at each grid point from ECHAM.

To detect a possible correlation between ENSO and the isotopic composition of water vapor, either in the satellite data or in the ECHAM simulations, the computation for each grid point a temporal correlation of the Niño-3 index (corresponding to the temperature anomaly over a large area in the tropical Central Pacific) and δD of the local water vapor is performed. The geographical distribution of the correlations is shown in Figure 5.2. In the ECHAM simulations, there is a clear correlation/anti-correlation pattern spread over the entire Central Pacific both in near-surface layers and in the middle troposphere. At 500 hPa, this pattern is confirmed by the TES satellite data although the signal is noisier. At 1000 hPa, TES cannot produce the correlation pattern due to its low sensitivity close to the surface. Most interestingly, the model shows that the correlation pattern at the surface is inverted compared to the 500 hPa levels. Regions, which show a positive (negative) correlation at the surface between Niño-3 and the water isotopologue, appear to be anti-correlated (correlated) at higher altitudes.

The near-surface pattern is in line with what one may expect from the amount effect in the tropics, which shows an anti-correlation between the precipitation amount and the isotopic composition of the rainfall. This anti-correlation was empirically demonstrated in several studies both on the spatial scale and on a seasonal timescale analyzing GNIP/IAEA data (Dansgaard 1964; Rozanski et al. 1993; Araguás-Araguás et al. 1998). During an El Niño event, convection and rainfall intensity are weaker over the Western Pacific Warm Pool (WPWP) and stronger over large parts of the warmer than normal surfaces of the Central tropical ocean (Ropelewski and Halpert 1987; Curtis and Adler 2000; Dai and Wigley 2000). This leading impact of ENSO variability on precipitation amount is also reproduced by the ECHAM model (see Fig. 5.1). Therefore the near-surface correlation pattern (Fig. 5.2c) is what it is expected from the amount effect: over the Western
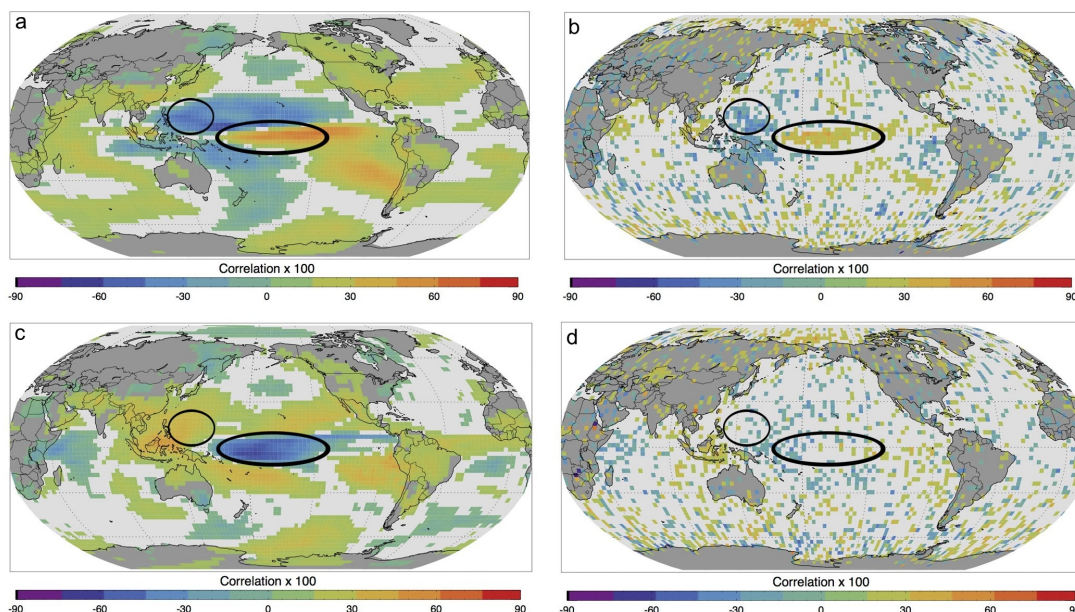
Figure 5.2 Correlation of Niño-3 index and δD_V at each grid point from ECHAM at 500 hPa (a), TES at 500 hPa (b), ECHAM at 1000 hPa (c), and TES at 1000 hPa (d).

Pacific warm pool precipitation is reduced during an El Niño event, and water vapor at near-surface layers is therefore more enriched than normal. Conversely, over the Central Pacific, the increase in precipitation leads to lower δD values there.

In the mid troposphere (500 hPa), however, an opposite correlation pattern is found in the ECHAM model. This pattern is convincingly supported by the TES observations, which are more sensitive to free troposphere water vapor than to water vapor close to the surface. At this level, water vapor is isotopically more depleted than normal over the WPWP area during an El Niño event (negative correlation) and more enriched than normal over the Central Pacific (positive correlation).

Figure 5.3 shows a longitudinal cross section of the correlation/anti-correlation pattern over the region of interest, allowing a more quantitative comparison between model results and observations. Though such a comparison is difficult at lower atmospheric layers since the sensitivity of the TES data is strongly reduced, there is a good correspondence between model and observations both close to the surface and at the 500 hPa level. Averaged over a tropical band from 15 °N to 15 °S, positive correlations between ENSO and the water isotopologues from 90 °E until 150 °E in near-surface layers is observed. From 150 °E to about 120 °W, there are negative correlations. At 500 hPa, negative correlation dominates in the Western Pacific (100 °E to about 180 °E) and the correlation changes sign near the date line to positive correlations (180 °W to 90 °W) in the Eastern Pacific, in the model results and in the observations. It should be noted that this pattern does not show up in the earlier TES version 4 data, confirming former results that indicate a
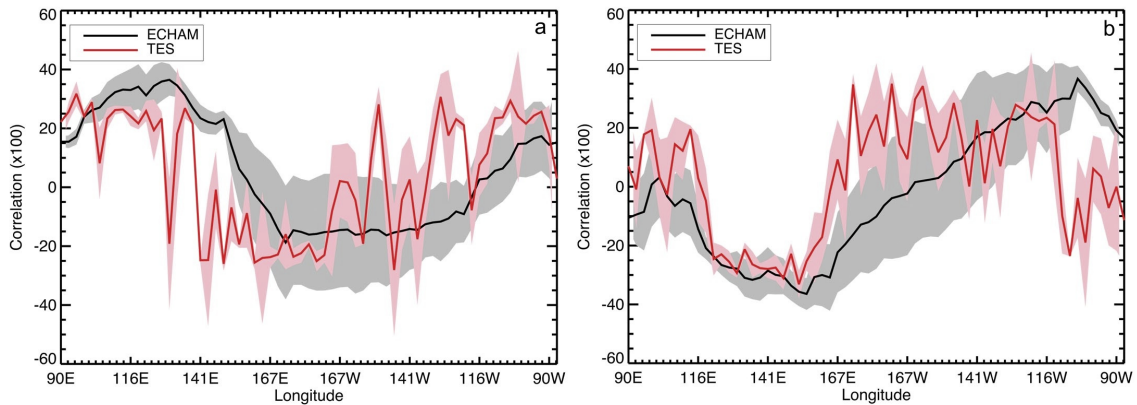
Figure 5.3 Zonal plot of correlation between the Niño-3 index and δD_V from $90\,°E$ to $90\,°W$ from ECHAM and TES at 1000 hPa (a) and at 500 hPa (b). The values are averaged from $15\,°N$ to $15\,°S$. Red and grey shade areas are error bars calculated using one sigma standard deviation from averaged points.

clear improvement of the water isotope product of the TES version 5 dataset (Sutanto et al. 2015).

5.3.2 Correlation of the Niño-3 index and global δD_V in Central Pacific and West Pacific

For a more detailed analysis of the identified ENSO-related isotope anomalies and the mechanisms controlling them, the analysis focuses in the following on two locations that are strongly affected by ENSO, the West Pacific warm pool ($130\,°E$ -$145\,°E$ and $7.5\,°N$-$7.5\,°S$) and the Central Pacific ($180\,°W$-$165\,°W$, and $1\,°N$-$5\,°S$). These two regions are situated in the centers of the above described correlation/anti-correlation patterns and correspond also to the two different climatic regimes during an El Niño event, i.e., a dryer than normal Western Pacific and a wetter than normal Central Pacific.

Figure 5.4 shows 30 years (1971 to 2001) of modeled monthly anomalies of the Niño-3 index vs δD_V (both at the surface and at 500 hPa) averaged over the two regions described above. The anomalies in three climatic regimes, i.e., normal conditions, El Niño conditions and La Niña conditions are separated. "Normal" here is defined as a range of the Niño-3 index values between -0.5 and +0.5 (orange); El Niño events correspond to the Niño-3 index values above 0.5 (red) and La Niña events to the Niño-3 index values below -0.5 (blue).

Close to the surface there is no clear distinction in δD_V between the "La Niña" and the "normal" regime (blue and orange points), both in the Western and the Central Pacific. Also the spread of the corresponding δD_V values is about the same. The correlation/anti-correlation pattern at the surface is mostly driven by the El Niño events. In the Central Pacific, the δD_V values also show a much larger variability during the El Niño period. As expected from Figures 5.2 and 5.3 there is a negative (anti-) correlation in the Central
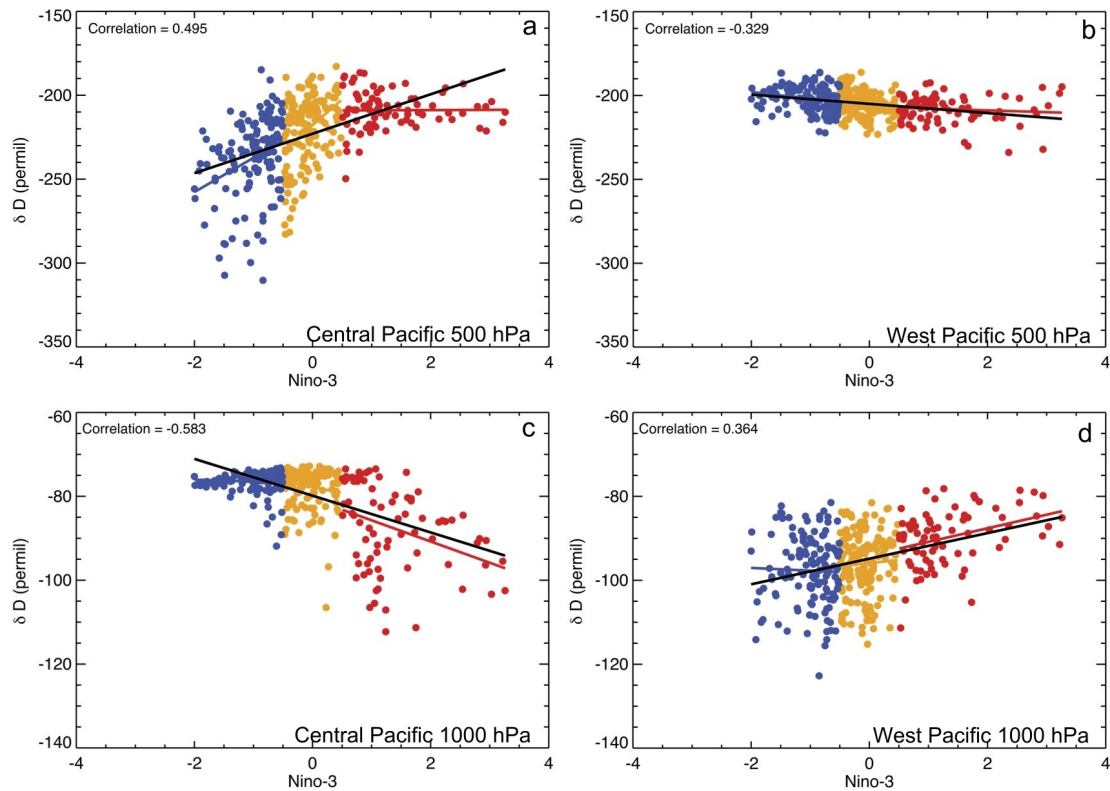
Figure 5.4   Correlation of the Niño-3 index and δD_V at 500 hPa in the Central Pacific (a), in the West Pacific (b) and at 1000 hPa in the Central Pacific (c), in the West Pacific (d) as simulated by the ECHAM model. The blue lines correspond to La Nia, the red lines correspond to El Nio, the yellow lines correspond to normal condition and the black lines correspond to all data sets. The correlation coefficients in the figure represent the overall correlation (black lines).

Pacific (R = -0.58) and a positive correlation in the Western Pacific (R = 0.36; Fig. 5.4c and d).

At high altitudes (500 hPa, see Figures 5.4a and b), the correlation is noisier than the respective relation close to the surface and it is not driven principally by the El Niño events in the simulated 30 years record, as it was the case for lower layers. In the Central Pacific at 500 hPa, for instance, the relation between the water isotopologues and the Niño-3 index during El Niño events is completely flat (red curve in Figure 5.4a). Therefore, not only one has to explain inverse relationships between the water isotopologues and the ENSO affected intensity of convection, circulation and rainfall at lower and higher levels, but also a certain asymmetry between La Niña/El Niño events and their respective impact on the water isotopologues.

5.3.3 Evaporation and condensation

The associated anomalously warm and cold SST during El Niño and La Niña for long periods in the tropical pacific change the isotopic composition of water vapor. The phase changes during evaporation and condensation are linked with isotope fractionation processes and mark the isotopic composition of water in an air mass with its "fractionation history", marked by one or several cycles of evaporation, transport, condensation, re-evaporation, etc. A Rayleigh distillation diagram (such as in Fig. 5.5) can be used to characterize an air mass by its specific humidity, q, and its water isotopic composition. Following Worden et al. (2007); Noone (2012), here two extreme cases of air mass histories are specified. The black solid line describes the δD_V-q composition of an air mass that undergoes a Rayleigh distillation. Starting from isotopic equilibrium with the ocean water (δD = -79 ‰), an air mass is cooled down and all forming condensate is immediately removed. This rainout leads to a strong isotopic depletion of the remaining air mass (black curve in Fig. 5.5). A mixing evaporation line (orange curve) is defined by mixing the evaporative flux and its comparably enriched water isotopic composition with a dry depleted air mass originating at higher altitudes (Worden et al. 2007; Brown et al. 2008; Lee et al. 2011).

When plotting the near surface and high-altitude measurements and model results in such a diagram (δD_V vs q), a number of interesting features with regard to ENSO variability can be identified.

1) Under normal (orange symbols) and La Niña conditions (dry, blue symbols), surface evaporation predominates at the Central Pacific and consequently the model results (Fig. 5.5a, at 1000 hPa) indicate that the water vapor is close to isotopic equilibrium with the ocean water, which means that the surface water reservoir originates nearly entirely from ocean evaporation. During El Niño events, the isotopic composition of water vapor at the Central Pacific is lower than normal since it is under a stronger influence of moisture convergence (Lee et al. 2007a; Moore et al. 2014) and convective rain (red dots in Fig. 5.5a; Risi et al. 2008; Kurita 2013; Lekshmy et al. 2014). The convergence vapor imported from the subtropics, which has lighter isotopologue, lowers the isotopic composition of water vapor in the tropics and it becomes more important as convection strengthens (Kurita 2013; Moore et al. 2014). In addition, the vapor is tagged by isotopic fractionation processes associated with convection and accompanying condensation processes is displayed onto the boundary layer vapor via the falling raindrops. Re-evaporation of falling raindrops and isotopic equilibration of the droplets below the cloud base with the surrounding water vapor leads to a clear shift of the isotopic composition of the surface-near vapor towards the condensation line. Thus the vapor at near-surface layer is influenced by the convergence of vapor and by the condensation process from higher altitudes through equilibration of rain droplets with surrounding vapor in a wetter condition and not by the local condensation.

2) The West Pacific warm pool is marked by less variability (small range of humidity variations), which is probably due to the smaller SST variations (Fig. 5.5b). The region is also wetter than the Central Pacific both close to the surface and in the middle troposphere. In the West Pacific region, El Niño states are representative of dryer than Normal/La Niña conditions. Consequently, the vapor is closer to isotopic equilibrium with

the ocean during El Niño conditions and more influenced by condensation from the isotopic exchange of falling rain droplets with surrounding vapor during the wetter La Niña conditions (Fig. 5.5b).

3) At 500 hPa, the model results indicate in general wetter air and isotopically more enriched water vapor in the West Pacific than in the Central Pacific (Fig. 5.5a and b). This is also clearly confirmed by the TES observations indicating specific humidity between 3-5 g/kg in the West Pacific and between 1-3 g/kg in the Central Pacific (Fig. 5.5c and d). Also, the vapor is about 50 ‰ more enriched in the West Pacific. Both features corroborate the idea that the mid troposphere over the WPWP is closer connected to surface humidity both in terms of the actual specific humidity values and the stronger enrichment of the vapor. This property is probably due to a more intense and regular convective activity over the WPWP region.

4) Central Pacific TES data are constrained by the pure Rayleigh distillation. On the contrary, high altitude data over the WPWP are generally more moist and enriched than the Central Pacific data. The intense convection over the WPWP is probably responsible for this feature. There are a number of possible processes suggested to explain "non Rayleigh distillation" δD_V-q values at high altitudes. Most of them are associated with convective activity such as intense condensation during the ascent of the air parcels, which lower δD (Risi et al. 2008), uplift and evaporation of ice crystals and/or detrainment/entrainment of air within convective towers, which moisten and enrich δD (Smith et al. 2006; Moyer et al. 1996). The ECHAM model does not reproduce this non-Rayleigh distillation influence as it is seen in the TES data where the isotopic composition of water vapor is relatively more depleted than the Rayleigh distillation curve. The simulated vapor data from the model are largely situated in between the mixing evaporation/condensation lines for both over the Central Pacific and over the WPWP. The deviations from the Rayleigh-like behavior can arise from mixing between different air masses, detrainment of condensate, or from rainfall evaporation (Risi et al. 2012b). These processes may not be simulated well in the ECHAM model and lead to the δD bias at high altitudes. The possible role of convection will be discussed in more detail in chapter 5.3.5.

Though simulated WPWP high altitude data from ECHAM are not in good agreement with TES data when comparing absolute values of q and δD_V, the simulated isotopic response to ENSO variability in both regions, WPWP and Central Pacific, corresponds quite well to the TES observations. Water vapor over the Central Pacific is shifted from dryer and more depleted values during La Niña to wetter and more enriched values during El Niño with neutral ENSO conditions being situated in between (Fig. 5.5c). Over the WPWP, Figure 5.5d shows nearly the contrary. El Niño events appear more depleted, though only slightly wetter. Model results and TES observations only agree in this isotopic reaction to ENSO. For humidity, however, the model results and TES disagree, with more humid from the model and drier from the observation during La Niña. Interestingly, over the Central Pacific, ENSO provokes a clear response of the specific humidity q and δD_V, whereas over the WPWP, we mainly identify a reaction of the isotopic composition of δD_V and virtually only small changes in q. The reason is that the WPWP is a well-known area with persistent convection and thus the ENSO only increases/reduces the convective activities during La Niña/El Niño. In general there is a specific ENSO pattern at high
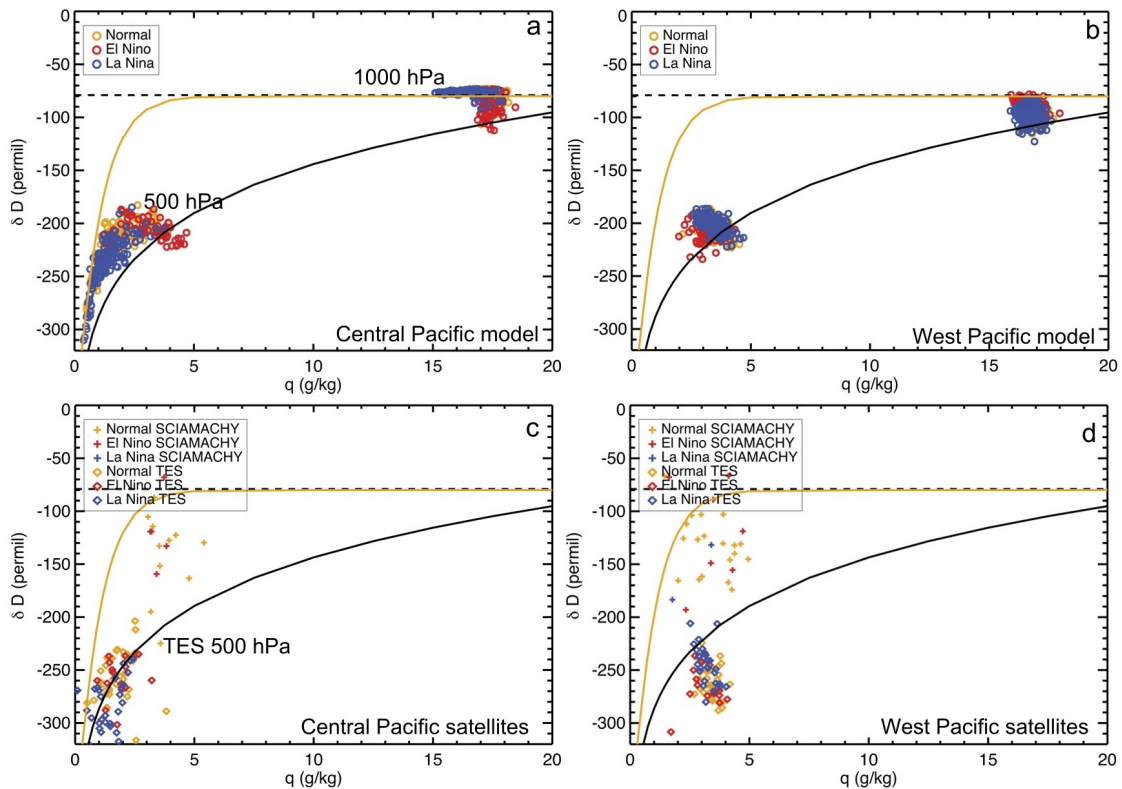
Figure 5.5 δD_V as a function of specific humidity (q) from the ECHAM model in the Central Pacific (a) and in the West Pacific (b); δD_V as a function of specific humidity (q) from observations in the Central Pacific (c) and in the West Pacific (d). The black lines correspond to a Rayleigh model and the orange lines correspond to a mixing evaporation model.

altitudes which is not trivial to explain in terms of known isotope effects (e.g., amount effect as described by an inverse relation with the amount of precipitation) and whose signature might serve in the future to evaluate simulated ENSO responses of the water cycle.

Figure 5.5c and d show also SCIAMACHY total column data. Unfortunately, the SCIAMACHY data do not appear to be very realistic. For total column data the δD_V and q are much too depleted and much too dry, respectively. This is caused by the fact that SCIAMACHY only measures HDO and H_2O above low-level clouds over the ocean (since the ocean surface itself is too dark in the short-wave infrared). Also, during SCIAMACHY measurements from years 2003-2007 there was no strong ENSO event, neither El Niño nor La Niña. This probably also contributes to the difficulty to distinguish any clear ENSO associated pattern in the SCIAMACHY data. Note, the ENSO signature similar to the figure 5.2 cannot be produced.

5.3.4 The isotope amount effect

Above, the hypothesis that near-surface layers are "isotopically" under the influence of re-evaporation and of re-equilibration with falling raindrops is formulated. The first flux is a net flux from the raindrops into the surrounding atmosphere. The second process is the result of gross fluxes after rain evaporation, which could affect the Planetary Boundary Layer (PBL) isotopically. Both processes possibly contribute to the amount effect-like response of the water isotopologues in near-surface vapor to ENSO variability. Wetter (dryer) conditions lead to more (less) depleted water vapor. Note that these processes (re-evaporation and re-equilibration) were already mentioned in the first publication on interpreting water isotopic signals as possible processes contributing to the amount effect in rainwater (Dansgaard 1964). More (less) rainfall, so goes the argument, humidifies the boundary layer and leads to less (more) re-evaporation and therefore less fractionation, which would then deplete (enrich) the corresponding rainfall. The rain re-evaporation and diffusive exchange between rain and vapor explain why the boundary layer water vapor reacts in the same way as precipitation (Lee and Fung 2007; Risi et al. 2008; Tremoy et al. 2014). Formulated this way, the mechanism served to explain the amount effect in tropical/sub-tropical precipitation and water vapor.

To check the relevance of the proposed isotopic exchange processes between rainfall and boundary layer water vapor, Figure 5.6 presents the time evolution (1971-2001) of both the water isotopic composition of vapor and corresponding precipitation for two target regions in the model. Unfortunately, only model results are available to do such an analysis. A sufficiently dense network of rain sampling stations combined with isotopic analysis (such as GNIP; Aggarwal et al. 2007) does not exist in the tropical Pacific.

The comparison of the Niño-3 index with the isotopic composition of near-surface water vapor and the corresponding dis-equilibrium between precipitation and the respective vapor in the model is performed. In perfect equilibrium between rain and vapor the following relation holds (Gat 1996):

$$R_P = \alpha \cdot R_V \tag{5.1}$$

with R_P and R_V being the isotope ratio HDO/H$_2$O ($\sim$0.5xHDO/HHO) for rain and vapor, respectively, and α is the equilibrium fractionation factor, which is only controlled by temperature (Majoube 1971b). Consequently, the isotopic dis-equilibrium is defined as:

$$\delta D_{dis} = \delta D_P - (\alpha \cdot \delta D_V + \varepsilon) \tag{5.2}$$

$$\varepsilon = (\alpha - 1) \cdot 1000 \tag{5.3}$$

In perfect equilibrium the difference R_P - $\alpha \cdot R_V$ is zero, thus indicating that the liquid and the vapor had enough time to reach an isotopic equilibrium that is only controlled by the surrounding air temperature. Temperature is supposed to be constant during the time of the isotopic exchange processes. Obviously, this will hardly be the case for falling raindrops. Equilibrium then depends on, among other factors, the respective droplet size, fall velocity and the surrounding relative humidity (Stewart 1975).
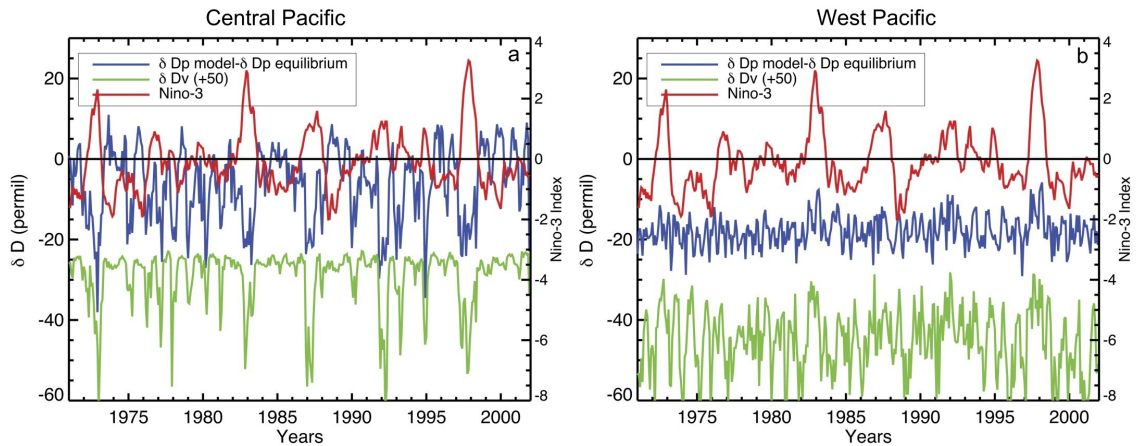
Figure 5.6 Monthly plot of δD_P from ECHAM and δD_P equilibrium differences in Central Pacific (a) and West Pacific (b) at 1000 hPa. 50 ‰ has been added in δD_V for plotting purposes.

Figure 5.6a (Central Pacific) shows strong negative excursions of δD_V that systematically coincide with El Niño events. However, most of the smaller scale variability of δD_V does not seem to be influenced by ENSO. Many processes may influence the δD_V during normal condition such as mixing, moisture convergence, rain evaporation, and surface evaporation. The control of ENSO on δD_V is mainly taking place during the 3-5 major Niño events (1972, 1982, 1987,1992, 1997). The water isotopologues respond to rising tropical SSTs (Niño-3 index). However, a different intensity of the Niño event (at least based on the Niño-3 index used here) does not provoke similarly different excursions of the water isotopologue. The response of δD_V is not linear and this holds both for the variations between El Niño and La Niña events and even between the different El Niño events.

In both regions, the mean value of the isotopic dis-equilibrium is negative implying incomplete equilibration with the surrounding boundary layer water vapor. This is to be expected, since the model's parameterization only allows partial equilibration of falling raindrops (nearly complete equilibration for small droplets i.e., formed in stratiform precipitation and only ∼50 % equilibration for big droplets i.e., formed in convective systems). This model result is in agreement with other model-based studies (Lee and Fung 2007; Risi et al. 2008).

In the Central Pacific, major El Niño events are associated with strong negative excursions of the isotopic dis-equilibrium (blue line, Fig. 5.6a). Together with the negative excursions of the PBL water vapor (green line, Fig. 5.6a), this leads to the following scenario:

1) When raindrops fall into a wet boundary layer, there is less isotopic exchange between the raindrops and the surrounding vapor, keeping the raindrops out of equilibrium with the vapor. The raindrops pass the PBL without being effectively enriched by fractionating re-evaporation since relative humidity increases considerably under El Niño

conditions. In addition, the falling rain droplets transfer depleted cloud conditions to the PBL.

2) Furthermore, there is a shift of precipitation from stratiform cloud systems to convectively formed precipitation when changing from neutral or La Niña conditions to El Niño conditions (see also chapter 5.3.5). This is shown in figure 5.5a where the humidity becomes wetter during El Niño events for both at near-surface and higher altitudes. Convectively formed precipitation is typically composed of larger and therefore faster falling raindrops. In the ECHAM model it is parameterized as only partly (i.e., 50 %) reaching full isotopic equilibrium. Thus the predominance of convective precipitation leads to less equilibration with the surrounding layer.

In summary, both mechanisms, i.e., a more humid atmosphere suppressing fractionating re-evaporation and a shift to more dominating convective precipitation, lead to less isotopic equilibration of the simulated rainfall.

In contrast to the Central Pacific, the West Pacific warm pool region shows a slightly different pattern. The δD_{P-eq} values are always negative meaning that there the precipitation is never in isotopic equilibrium with the surrounding vapor. This is in agreement with our reasoning above. Over the WPWP, precipitation is clearly dominated by convective processes and thus out of equilibrium with the vapor, which leads to more depleted rain relative to the PBL vapor. During El Niño events this dis-equilibrium is slightly reduced (blue curve, Fig. 5.6b). The arguments presented above regarding the relation between wetter than normal conditions and more convectively formed precipitation in the Central Pacific apply to the WPWP, but with an opposite sign. One reason for the relatively weak signal in the dis-equilibrium time series during El Niño events might be that the shift towards less convectively formed precipitation (leading to potentially more isotopic equilibration) is less clear in this region.

One should keep in mind that the respective isotope exchange and raindrop evaporation processes discussed above are the result of a model simulation. The respective processes are highly parameterized and idealized and the choice of the involved parameters is hardly constrained by direct observations.

5.3.5 Convective updrafts

In section 5.3.4 it is argued that changes from stratiform to convective precipitation could contribute to the simulated variability of the isotopic dis-equilibrium between rainfall and water vapor. Already in several former studies (Gedzelman and Arnold 1994; Kurita et al. 2011) it was shown that convective precipitation produces higher δD_P than stratiform precipitation. In addition, Kurita et al. (2011) showed that convection would enrich the isotopic composition of water vapor at altitudes above 600 hPa. Following the hypothesis from the former studies that the convection will produce higher δD in precipitation and vapor at higher altitudes, the simulated shifts of convective precipitation are analyzed and compared with the water isotopologues at 500 hPa. Again one should keep in mind that such a clear distinction between stratiform and convective precipitation is a result of climate model design, which does not exist in nature.
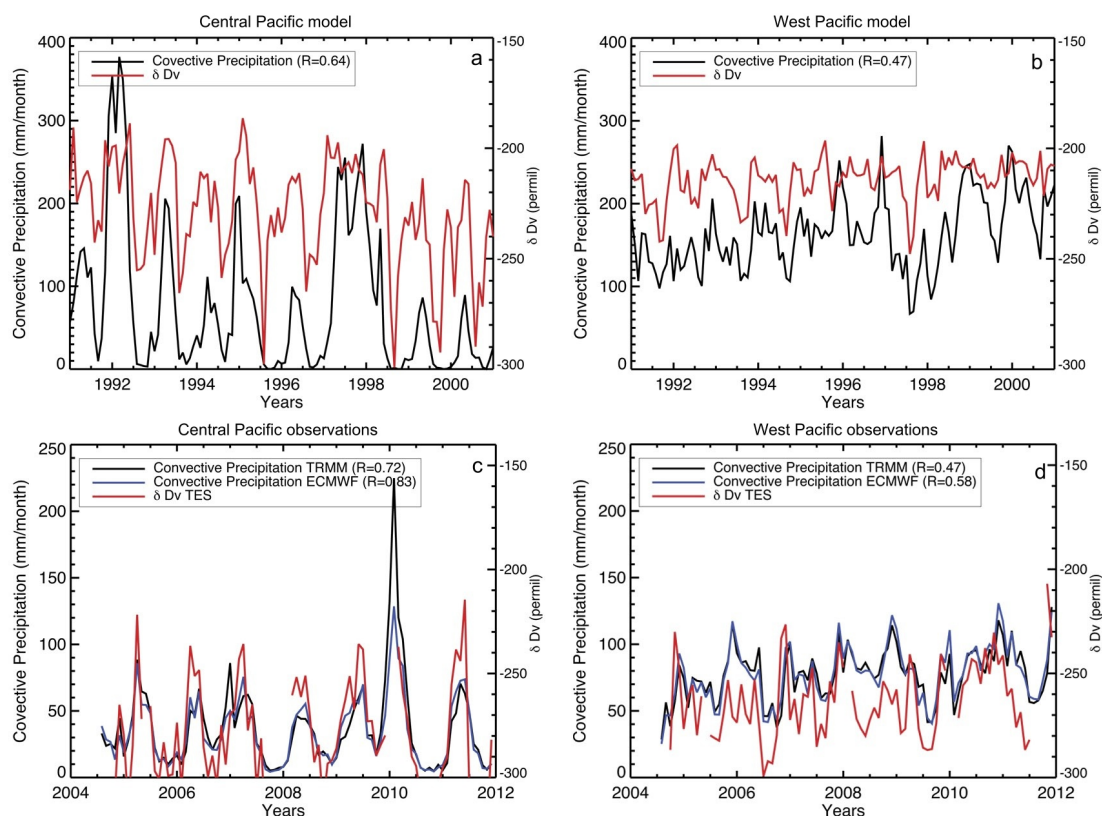
Figure 5.7 Relationship of δD_V at 500 hPa and the amount of convective precipitation from ECHAM in the Central Pacific (averaged from 165°W-150°W and 5°N-5°S, a) and in the West Pacific (averaged from 110°E-135°E and 10°N-10°S, b); TES δD_V at 500 hPa and the amount of convective precipitation from ECMWF and TRMM in the Central Pacific (c) and in the West Pacific (d).

Figures 5.7a and b demonstrate the influence of convection on δD_V at 500 hPa in the two regions from the model. Over the Central Pacific the correlation of convection intensity and the water isotopologues is high (R = 0.64, Fig. 5.7a) whereas over the WPWP it is weaker (R = 0.47, Fig. 5.7b). More (less) convection is associated with less (more) depleted water vapor. Though the time series of both precipitation and the water isotopologues are dominated by the seasonal passage of the ITCZ over the regions of study, many intra-seasonal variations are also in apparent synchronization.

A possible explanation for this simulated feature involves the uplift of marine boundary layer vapor. In the tropics, convection picks up vapor at lower altitudes, even from the marine boundary layer, and lifts it up to typically heights of 10-12 km. In the sub-saturated regions outside the updrafts, the convective tower release vapor with δD characteristics similar to near surface layers, leading to an efficient enrichment process of the mid-troposphere (Smith et al. 2006).

Since the distinction between stratiform and convective precipitation partly depends on model design and parameterization, the corresponding comparison between convective precipitation and the water isotopologues using observations is difficult. In Figure 5.7c

and d, two different observational data sets of precipitation are shown together with the TES δD_V data centered at 500 hPa. Obviously, there is a good correspondence between convective precipitation and δD_V above the Central Pacific and the correlation is weaker over the WPWP. Not only the seasonal cycle, but also second order variations of convective precipitation and δD_V vary, leading to a correlation of R = 0.83 and 0.72 in the Central Pacific and R = 0.58 and 0.47 over the WPWP using ECMWF and TRMM, respectively. One shall note that TES cannot retrieve δD_V signal in the presence of deep convection or the data are biased high to higher altitudes (e.g., no measurements during high precipitation year 2010) and that a correct representation of tropical precipitation is a persistent problem for models. The ERA Interim reanalysis data are obtained by assimilating observational data (surface observations but also radiosonde and satellite data) into the weather forecast models of the ECMWF. The distinction between convective and stratiform precipitation remains a result of model dependent parameterization also in case of the re-analysis data.

The correlation between stratiform precipitation and δD_V above the Central Pacific and the West Pacific is also calculated (Figure not shown). Although, there is also a correlation between stratiform precipitation and δD_V, the correlation values (R) from all datasets in general are weaker than for convective precipitation. Moreover, convective precipitation has higher contribution to the total precipitation amount than stratiform precipitation and this is also applicable for ENSO case.

5.4   Summary and discussion

This study has investigated the impact of ENSO on the tropical water cycle and the corresponding water isotopologue signatures. To that end, satellite data and model results have been used providing simultaneous information on both the atmospheric vapor and its isotopic composition. Within the tropics, two key regions were identified where δD_V reacts particularly sensitive to ENSO and systematically with opposite signs: the Central Pacific and the region of the West Pacific Warm Pool. Figure 5.8 summarizes these findings comparing the water isotopologue signals near the surface and in the middle atmosphere during ENSO neutral, El Niño, and La Niña conditions. Figure 5.8a and b show two different sets of observational data (remote sensing data and GNIP surface observations), and model results over our two study regions. The regional mean δD_V is shown at 500 hPa (both for ECHAM model results and TES data) and at near-surface layers (only ECHAM results due to the poor quality of TES data near the surface). This allows visualizing the isotopic gradients between the lower and the middle atmosphere and their changes under varying ENSO conditions. Furthermore, the isotopic composition of precipitation (ECHAM and GNIP data) is added. The difference between the isotopic signals of precipitation and of near-surface water vapor is indicated by the length of the colored bars, which are each associated to a different ENSO state (always with the above introduced distinction of El Niño, La Niña and Neutral states).

Over the Central Pacific, El Niño conditions correspond to an anomalously warm and wet atmosphere with more intense convection and correspondingly more precipitation (see
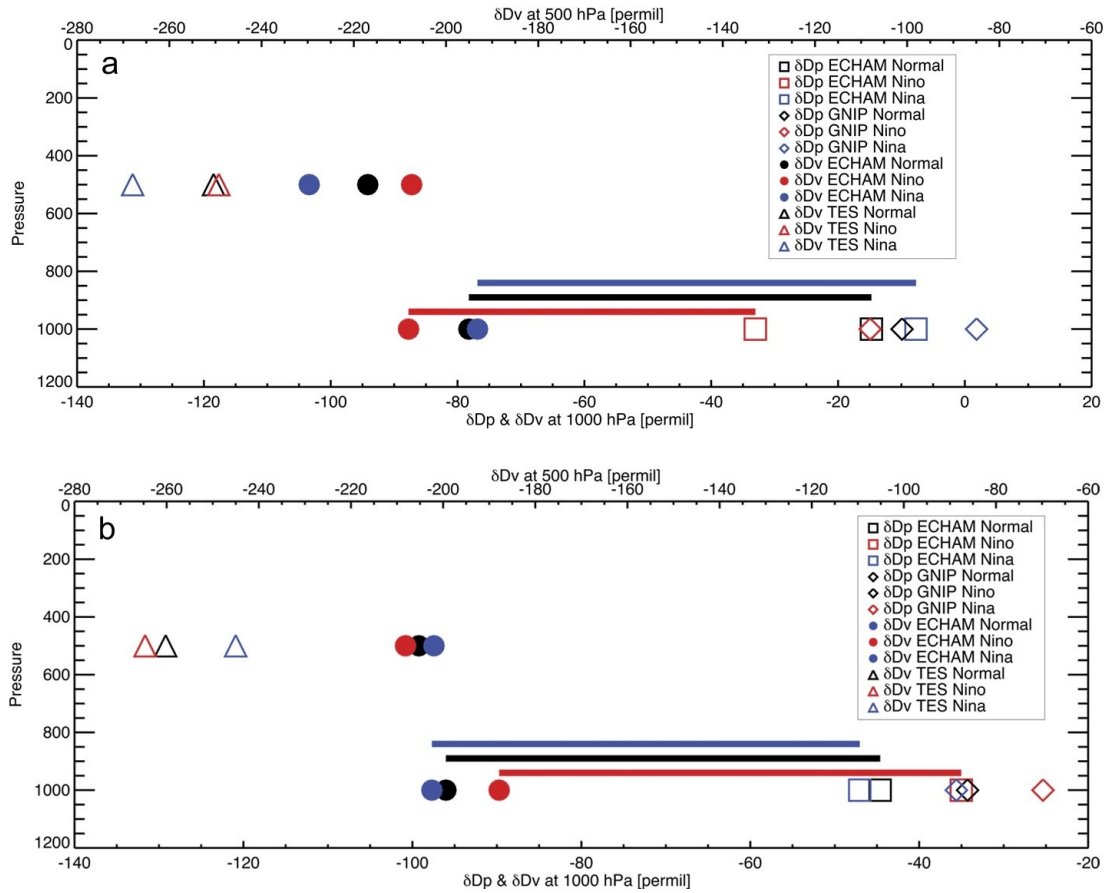
Figure 5.8 Average δD_P and δD_V during La Niña, normal, and El Niño condition from ECHAM, TES, and GNIP database at Central Pacific (a) and West Pacific (b). Lines show the differences between normal condition (black), El Niño (red), and La Niña (blue) from ECHAM as a benchmark.

Fig. 5.1). The combination of these changes results in a reduced vertical isotopic gradient during El Niño events. Both atmospheric levels, near-surface layers and the middle troposphere (500 hPa), contribute to this reduced gradient. The near-surface layers become more depleted and the middle troposphere becomes more enriched than during ENSO neutral conditions. During La Niña the atmosphere reacts oppositely with more depleted δD_V in the middle troposphere. Near-surface levels remain nearly unchanged compared to ENSO neutral conditions. Nevertheless the consequence of La Niña conditions is an increased isotopic gradient. Over the WPWP (Fig. 5.8b) one recognizes an inverse response, i.e., the vertical gradients of the water isotopologues are reacting in an opposite sense compared to the Central Pacific. Though the shift to a steeper isotopic gradient under El Niño conditions and to a less steep gradient during La Niña is not so clear as at the Central Pacific (Fig. 5.8b), it is evident that the WPWP region reacts inversely to the Central Pacific.

The variable dynamics of δD_V in the atmospheric column is accompanied by associated changes in the isotopic equilibrium between precipitation and near-surface water vapor. In Figure 5.8, the length of the three colored bars gives a qualitative measure of the isotopic difference between the falling raindrops and surrounding vapor during the three ENSO phases. The bars connect the ECHAM modeled isotopic values of the near-surface vapor ($\delta D_{vap-surface}$) and precipitation (δD_P). Over the Central Pacific the distance between both values is shortest during El Niño and largest during La Niña. As was explained in detail in chapter 5.3.4, these changes correspond to negative excursions from the isotopic equilibrium during El Niño and to near equilibrium situations during La Niña. Again the inverse situation over the WPWP area is found. There, the distance between $\delta D_{vap-surface}$ is largest during El Niño (approaching equilibrium) and smallest during La Niña. It is not possible to fully confirm these model results by observations since there is no access to reliable information on the isotopic composition of near-surface water vapor over the respective areas. However, at least all available GNIP δD_P data correspond to the variations of the modeled precipitation δD values in our study areas, i.e., a response corresponding to the isotope amount effect. El Niño, La Niña, and neutral conditions are associated to wet, dry and intermediate situations over the Central Pacific and the associated precipitation is isotopically most depleted, less depleted and intermediate in the GNIP observations similar to the ECHAM model results. The contrary holds for the WPWP area where again the GNIP data confirm the ECHAM model results.

Although there are many processes that may influence the isotopic composition of water vapor during ENSO events such as moisture convergence, large-scale advection and subsidence, the response of the water isotopologues to ENSO conditions in different parts of the Pacific/Indian Ocean is plausible caused by the associated changes in convective activity and convectively formed precipitation. Convection picks up water vapor in near-surface layers, which is isotopically enriched relative to water in the middle troposphere. Within the convective updrafts this comparably enriched vapor is lifted up to higher levels undergoing continuous condensation and isotopic depletion of the corresponding vapor. A further process often linked to convective activity is the possible uplift of condensate (possibly in form of ice crystals) and the re-evaporation of this comparably enriched condensate. The latter process was often discussed as one of the leading mechanism humidifying the upper troposphere (Moyer et al. 1996; Smith et al. 2006; Lee et al. 2011) and might also contribute to the anti-correlation between ENSO and δD_V at mid altitudes. In summary, more intense convection means less depleted vapor in the middle troposphere since it connects lower atmospheric layers more effectively with higher layers. The inverse is true for situations with less intense convection as for the WPWP during El Niño events.

An increase in convective precipitation also affects the isotopic composition of near-surface vapor and the corresponding precipitation. Convective precipitation is typically formed by larger raindrops with greater fall velocities than smaller droplets, the later being more typical for rain formation within stratiform clouds. Both size and fall velocity do not favor isotopic equilibrium between raindrops and surrounding vapor (Stewart 1975). The shorter the time a raindrop is in contact with the corresponding water vapor, the more incomplete is the isotopic equilibrium between both. Also a comparably wet atmosphere below the cloud base reduces the evaporative flux from the raindrops. The combination of

these factors typical for El Niño condition in the Central Pacific, i.e., larger rain drops, large fall velocities of the raindrops and a wetter atmosphere below the cloud base suppress the isotopic exchange between the raindrops and the atmosphere and lead to a larger isotopic dis-equilibrium. This is exactly what the ECHAM model simulates and what is qualitatively in agreement with the available data (see chapter 5.3.4). The latter mechanisms have been mentioned repeatedly as contributing to the classical isotope amount effect (Dansgaard 1964; Rozanski et al. 1993; Araguás-Araguás et al. 1998; Bony et al. 2008; Risi et al. 2008). Here this study has shown that, at least in the ECHAM model (and in qualitative agreement with observations), the amount effect and the rain-vapor equilibrium processes are strongly linked to the intensity of convective precipitation.

5.5   Conclusions and perspective

The study demonstrated that the ECHAM model is able to reproduce observed changes of the isotopic composition of water vapor and precipitation associated to ENSO, both in near-surface atmospheric layers and in the middle atmosphere. Two locations that are particularly influenced by ENSO and represent different climatic conditions, the Central Pacific and the West Pacific warm pool area are identified. The ECHAM model reproduces the variable relationships between ENSO indices and δD_V at different height levels and variable degrees of isotopic equilibrium between $\delta D_{vap-surface}$ and δD_P and its relation with ENSO. The analysis also demonstrates that the leading process controlling these variable relationships between the δD_V and different climate quantities in the ECHAM model is the simulated convective activity. The importance of convection is also in qualitative agreement with observations.

However, does the model do the right thing for the right reason? This persistent question of all climate modeling is important in particular with regard to the use of the water isotopologues. Equilibrium fractionation processes are established from laboratory experiments. However, most non-equilibrium processes are parameterized within the hydrological cycle of the GCMs in a simplistic way. Even the exact functioning of ocean surface evaporation and the dependence of the isotopic fractionation during evaporation on wind conditions and ocean surface properties is still unclear (Schmidt et al. 2005; Bony et al. 2008; Risi et al. 2008). This analysis suggests that two issues should be investigated in more detail in further studies.

1) The equilibrium between rain droplets and surrounding vapor is introduced into the ECHAM model as into most existing isotopic GCMs in a simplistic way. Raindrops from stratiform clouds are prescribed being in near equilibrium with the vapor ($\sim$95 % equilibrium) whereas convective rain is prescribed being only partly in equilibrium ($\sim$50 %). This parameterization is certainly reasonable based on observations of typically different raindrop sizes. However, nature does not know such a clear distinction between stratiform and convective rain as it is used in most climate models. A mechanistic representation of isotopic equilibrium processes for falling raindrops needs a realistic representation of raindrop size spectra in climate models, something which is not yet available. It would also need additional laboratory experiments since existing parameterizations of below cloud isotopic

processes (evaporation of raindrops into a relatively humid atmosphere) is based on few experiments performed in the 1970s (Stewart 1975) and needs certainly a broader experimental base. Here, the found robustness of the varying isotopic dis-equilibrium between $\delta D_{vap-surface}$ and δD_P should be studied in more detail in future sensitivity experiments such as in Jouzel et al. (1991). Furthermore, a broader observational basis is needed in particular for δD_V above the ocean surface, preferentially by remote sensing techniques to provide a large spatial coverage or by in-situ ship measurements.

2) This study associated the anti-correlation of δD_V at 500 hPa and ENSO to the uplift of comparably enriched surface vapor within convective systems. This result needs also a more detailed analysis preferentially using multi model ensemble runs. Different parameterization schemes describing the triggering of convection and the uplift of lower layer air to higher layers might differ with regard to the simulated water isotopologue signal during ENSO. Ideally such a comparison of different isotopic GCMs could provide us with an interesting benchmark test for the performance of the different convection schemes during ENSO.

The leading mechanisms controlling the anti-correlation between water isotopologues and precipitation in the tropics/sub-tropics (i.e., the amount effect) are disputed since the first description of the amount effect in the 1960s (Dansgaard 1964). Recent studies show that evaporation of falling raindrops into the atmosphere under the cloud base is an important source of humidity for the boundary layer (Sud and Walker 1993; Worden et al. 2007). Less precipitation, therefore, means that the evaporative flux from the ocean becomes a more important humidity source compared to the evaporation from raindrops formed in convective events. This flux is considerably more enriched. On the other hand, in the tropics, more rainfall means more intense uplift within the tall convective towers. Such a vertical rainout effect leads to condensation at colder cloud top temperatures and produces more fractionation at the end of the Rayleigh distillation process. Both circumstances lead to more depleted precipitation and, finally, by less re-evaporation of raindrops and isotopic exchange to more depleted water vapor in the boundary layers (Lee and Fung 2007; Risi et al. 2008; Moore et al. 2014). Despite these important recent contributions, the importance of the different processes contributing to the isotope amount effect is still under debate. Here, the role of evaporation and isotopic re-equilibration of falling raindrops below the cloud base is pointed out. Again a multi-model sensitivity study might be able to disentangle the importance of the different processes. The latter is particularly important in order to obtain a solid basis for the interpretation of the many existing and upcoming paleo isotope records from the tropics of which interpretation is notoriously complicated (LeGrande and Schmidt 2011).

In this study we do not discuss the influence of moisture convergence to δD in precipitation and vapor during ENSO in detail. Lee et al. (2007a); Moore et al. (2014) discuss the importance of moisture convergence to understand the amount effect processes in the lower troposphere. A comparison between the strength of moisture convergence and the isotopic composition of water during ENSO events is suggested in further study.

The finding shows that the isotopic composition of water vapor measured by satellites can be used to study the ENSO variability and its impact at low and high altitudes. It is now generally believed that the key processes controlling the spread in simulated climate

sensitivity of the existing climate models are situated in the tropics/subtropics and are linked principally to cloud processes and their coupling to the atmospheric dynamics as represented by the different models (Sherwood et al. 2014). A possible application of studies like the one presented here is to develop a diagnostic tool based on the water isotopologues to evaluate the different cloud processes simulated by GCMs (Stevens and Bony 2013).

6 Spread in lower tropospheric mixing, climate sensitivity, and isotopic gradient

"The most reliable way to forecast the future is to try to understand the present"
John Naisbitt

Abstract

State-of-the-art climate models simulate a wide spread among their respective equilibrium climate sensitivity (ECS about 1.5-4.5 °C). Several studies have demonstrated that there is a link between lower tropospheric mixing, low-level cloud feedbacks and the respective modeled climate sensitivity. Here the isotopic composition of water vapor is used to study small-scale convective mixing and the inter-model spread of ECS. This study investigates whether the strength of lower tropospheric mixing leaves an imprint on the observed and modeled δD gradients using 10 different isotope-enabled GCMs and compares the model results with TES observations. The results confirm that regions with intense mixing and strong convection are marked by a flatter isotopic gradient. However, a model intercomparison does not show a similar relation: models simulating steeper or flatter isotopic gradients are not necessarily marked by weaker or stronger mixing (or smaller/larger ECS). A possible main reason for the lack of such a straightforward relation may be that the different "isotopic" GCMs vary too much in the parameterization of important hydrological processes and even in the parameterization of the water isotope fractionation processes themselves. Therefore, the simulated gradients in the atmosphere potentially are controlled by processes other than vertical mixing. The subtraction of a part of the variability due to the isotopic composition of precipitation computed by each model confirms our hypothesis. It is suggested that model sensitivity studies are needed to identify the leading processes controlling the isotopic gradient and to isolate properly the impact of the mixing processes.

6.1 Introduction

The Equilibrium Climate Sensitivity (ECS) is commonly used to measure the Earth's temperature response to a change in external forcing, e.g., a change of the concentration of atmospheric greenhouse gases (GHGs such as CO_2, CH_4, N_2O) or of the intensity of solar radiation (solar constant). Global Circulation Models (GCMs) submitted to the Coupled Model Inter-comparison Project phase 5 (CMIP5) exhibit a wide range of ECS, roughly 1.5-4.5 °C warming for a doubling of CO_2 concentrations relative to preindustrial

levels (Andrews et al. 2012; Sherwood et al. 2014). Obviously this uncertainty is very relevant when estimating the possible consequences of a projected future rise of GHG concentrations. Several studies have demonstrated that the main mechanism responsible for the large spread in simulated ECS is the cloud feedback, i.e., the aggravating or mitigating effects of cloud coverage and its influence on the Earths radiative balance (Cess et al. 1990; Soden and Held 2006; Dufresne and Bony 2008).

The cloud feedback depends also crucially on where the respective clouds are formed or disappear. An increase of low-level clouds, which have a strong albedo effect, provokes a cooling effect. To the contrary, mid- and high-level clouds have strong long wave absorption and re-radiation properties, which is why they act similar to greenhouse gases. An increase of this type of clouds leads to an additional warming (Webb et al. 2006; Zelinka et al. 2012). However, it is a complicated problem whether there will be more or less clouds at a certain height in a warming environment due to increasing GHG concentrations. It's solution needs a thorough understanding of the dynamic-thermodynamic coupling of a warming atmosphere, changing air movements and cloud formation (Stevens and Bony 2013). Models give quite different answers to this highly non-linear problem and it is one of the key problems of climate sciences to identify which models have a more realistical representation of the cloud feedback. The most important contributor to the wide spread of the simulated cloud feedbacks presumably is tropical/subtropical low-level clouds (Bony et al. 2004; Bony and Dufresne 2005; Zhao 2014).

As climate warms, the evaporation from the oceans and the liquid water lapse rate will increase by about 1-3 % K^{-1} depending on different estimates (Wentz et al. 2007; Rieck et al. 2012). The additional vapor might increase low-level cloud covers leading to a negative feedback. On the other hand, a possible intensified mixing with free tropospheric air due to the increase of boundary layer depth in the warm climates will dry the atmospheric boundary layer, leading to a decrease of low-level clouds and therefore produces a positive feedback (Bony and Dufresne 2005). Humidifying or dehydrating the lower troposphere involves a large list of possible mechanisms, such as convective mixing between the free troposphere and the boundary layer, downdrafts associated to tropical convection, local compensating subsidence, and evaporation of falling rain. Sherwood et al. (2014) demonstrated that models with a relatively intense mixing over certain tropical areas better agree with observational estimates of Planetary Boundary Layer (PBL) to free troposphere mixing. Models with such an intense mixing under todays climate condition desiccate the PBL in a warming scenario and consequently tend to produce less low-level clouds in the tropics and therefore more intense warming (i.e., a higher ECS). This result was partly confirmed by other model inter-comparison studies showing that models with a more realistic hydrological cycle in the tropics under present conditions tend to have larger ECSs (Fasullo and Trenberth 2012; Su et al. 2014).

However, it is quite precarious to select just one specific simulated variable among hundreds of possible climate variables and use its correlation to ECS as the basis for constraining simulated ECS values. The problem of data mining between model quantities and ECS easily produces a number of false positives since in a highly non-linear system the interdependency of different parameters is very high (Peter Caldwell, talk at AGU 2013). Certainly one has good reason to focus for example on mechanisms that

humidify or desiccate the tropical PBL and influence low-level clouds, but further independent variables to test against are certainly desirable. Also, in the studies mentioned above (Sherwood et al. 2014; Su et al. 2014), the models were tested against highly derived quantities from re-analysis data. Re-analysis data are blended products of observations and model calculations, which bear of course a certain risk of circular reasoning. Ultimately, model quantities are tested against "observations" (e.g., small-scale mixing) partly produced by climate models themselves. This motivates to look for other directly observable parameters, which are simulated by climate models and which also relate to ECS.

Here, the use of the water isotopic composition (δD), which is a longtime existing proxy of the hydrological cycle (Dansgaard 1964), is proposed. The physics of fractionation of the water isotopologues is very well-known (Merlivat 1978). Due to their different partial pressure and diffusivities, the heavier water isotopologues, HD^{16}O and H$_2$^{18}O, separate during each phase change from the lighter and far more abundant one, H$_2$^{16}O. Therefore, the fractionation processes leave a characteristic imprint of the respective condensation, evaporation and transport history on the isotopic composition of both precipitation and water vapor. In particular, it is interesting whether the water isotopologues are sensitive to mixing processes and cloud formation in the tropical areas where the discussed cloud feedbacks presumably have the greatest effect. The study uses water isotopologue measurements from the Tropospheric Emission Spectrometer (TES) instrument onboard Aura (Worden et al. 2012) and the results from 10 isotope-enabled GCMs submitted to the Stable Water INtercomparison Group phase 2 (SWING2).

The study is organized as follows: data and methods used in the study are briefly discussed in chapter 6.2. Chapter 6.3.1 verifies that the subset of climate models used here showed similar relationships between ECS and vertical mixing as the full set of CMIP5 models. The focus here is on a simple index, S, of small-scale mixing. Analysis shows that this index is related to convective activity and that within one model it is spatially related to the water isotopologues (Chapter 6.3.2). Finally, it is examined whether a relationship between S, ECS, and δD holds when comparing different models and large geographical means of the respective quantities (Chapter 6.3.3). Chapter 6.4 discusses and concludes the findings.

6.2 Data and methods

Sherwood et al. (2014) introduced the lower tropospheric mixing index (LTMI) as a measure of the strength of shallow convective mixing, such as by cumulus clouds and large-scale shallow overturning over global ocean regions. The LTMI index consists of two mixing components: small-scale mixing (S) and large-scale mixing (D), where these components are not directly available in the CMIP3/5 GCM model outputs.

In our study, we only use the small-scale mixing index (S) focused over the West Pacific Warm Pool (WPWP, 75-165 °E and 10 °N-10 °S) as in Sherwood et al. (2014). The S index is a linear combination of the differences between temperature (T) and relative humidity (R) between 700 and 850 hPa, calculated as:

$$S = \left(\frac{\Delta R_{700-850}}{100\%} - \frac{\Delta T_{700-850}}{9K} \right) / 2 \qquad (6.1)$$

When mixing between the boundary layer and free troposphere is mainly through shallow convection, the free tropospheric air that is being mixed with the boundary layer is moist (due to shallow convective detrainment) and cool (due to its limited subsidence from shallow cloud tops to the boundary layer top). Therefore, $R_{700-850}$ is weakly negative and $T_{700-800}$ is strongly negative, so that S is large. In contrast, when mixing between the boundary layer and free troposphere is mainly through deep convection, the free tropospheric air that is being mixed with the boundary layer is dry and warm (due to its long subsidence from deep convective cloud tops to boundary layer top). Therefore, $R_{700-850}$ is more negative and $T_{700-800}$ is less negative, so that S is small (Sherwood et al. 2014).

The measurement of water vapor isotopologues (HDO/HHO) from TES onboard Aura satellite is used in the study (Worden et al. 2006, 2012). The S index is calculated using observational parameters from both the ERA-interim re-analysis from the ECMWF (Betts and Jakob 2002; Bechtold et al. 2004; Dee et al. 2011), and from the TES satellite. Two different convective precipitation datasets are obtained from ERA-interim and the TRMM (Schumacher and Houze JR 2003; Schumacher et al. 2004; Huffman et al. 2007). Although the ERA-interim product is re-analysis data, it is considered as an "observational" product since ERA-interim is a blended product of observations assimilated into model simulations to obtain a physically consistent dataset.

In the study, we also use several GCMs equipped with water isotope modules submitted to the SWING2 database. These models are ECHAM4, ECHAM5, LMDZ5A, LMDZ5B, IsoGSM, MUGCM, GissE, CAM2, HadAM, and MIROC. We use the model outputs without applying collocation and convolution methods with the TES dataset. The analysis results of convective mixing from the CMIP3 and CMIP5 GCMs are also presented for comparison with models from the SWING2 database. The ECS values of SWING2 models are taken from the parent GCMs submitted to CMIP project (i.e., LMDZ5A uses ECS value from IPSL-CM5A).

6.3   Results

6.3.1   Small-scale mixing and the equilibrium climate sensitivity from the SWING2 models

Using the full ensemble of CMIP5 climate models, the Sherwood et al. (2014) showed that the index S was quite well correlated to the models climate sensitivity. Here it is checked whether the subset of isotope physics enabled models (at least) fits into the general behavior of the full set, i.e., more intense mixing corresponds to higher ECS values.

In Figure 6.1, S is correlated with the models ECS values using the full set of CMIP5 models and the SWING2 model subset. The ECS values of MUGCM, HadAM, and IsoGSM are then interpolated from the correlation line because ECS values are not available from these parent models. The S index computed from TES data is situated within the ERA-
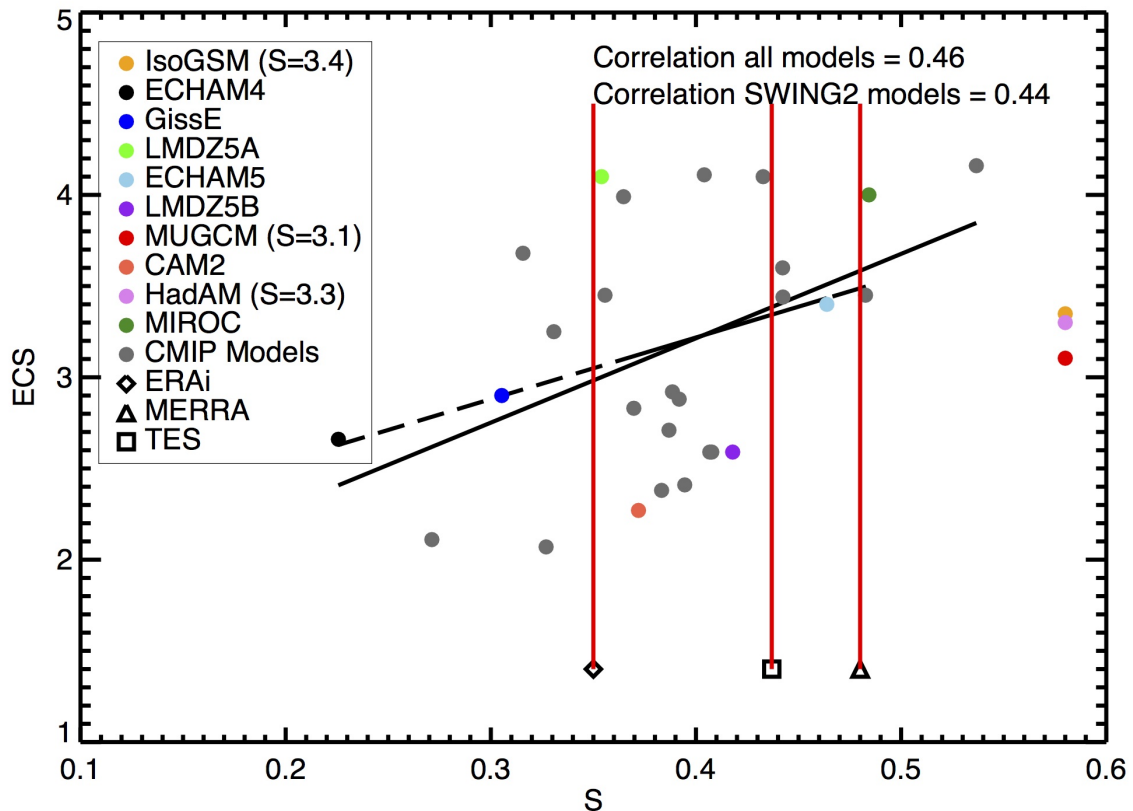
Figure 6.1 Correlation of S and ECS from the CMIP models, the SWING2 models, and the observations. The solid line is the correlation line for all models including SWING2 models and the dash line is the correlation line for the subset of SWING2 models. ECS values for IsoGSM, HadAM and MUGCM are interpolated from the correlation line (plotted on the right figure).

interim ECMWF and the Modern Era Retrospective-Analysis for Research and Applications (MERRA) satellite observation range, with value closer to MERRA than ERA values. The ECHAM4 and GissE models underestimate the S index compared to observations and the S index calculated by MIROC is slightly higher than MERRA. In general, the isotope-enabled models are consistent with the results from the CMIP models (R = 0.46) and also within the subset of isotope-enabled models itself (R = 0.44).

6.3.2 Relation of convection to S and water vapor isotopic gradient

Small-scale lower tropospheric mixing comprises the mixing mechanism between the boundary layer (approximately < 2 km) and the free troposphere, where convection, subsidence, and rain evaporation play a role (Sherwood et al. 2014). Here, it is tested whether S is indeed associated to convective activity. Fig 6.2a shows the spatial correlation of S and the amount of convective precipitation over the WPWP region from ECHAM and ECMWF. From both datasets, one can infer that stronger S values are related to more convective precipitation (R values of 0.76 and 0.47 for ECHAM and ECMWF, respec-
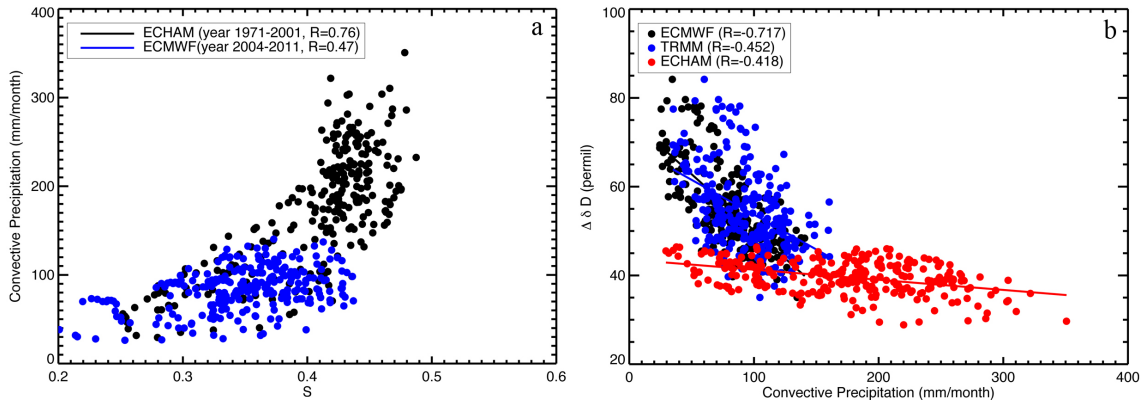
Figure 6.2 Spatial correlation of S and convective precipitation from ECHAM and ECMWF (a); correlation of convective precipitation and WV isotopic gradient ($\Delta\delta$D) from observations year 2004-2011 and the ECHAM model (b). For observations, TES $\Delta\delta$D is used.

tively). However the relation is quite noisy for the ERA-interim data and seems quite non-linear for the ECHAM climate model data. Such an analysis however does not allow to disentangle cause and effect. It is not clear whether larger S and therefore smoother humidity and steeper temperature gradients (see Eq. 6.1) trigger convective activity or if the latter produces steeper S gradients. ECHAM results show in particular much higher precipitation rates than ECMWF re-analysis data. However regional differences between re-analysis and model precipitation by a factor of more than 2 are often reported (Dai 2006). The simulated range (ECHAM4: 50-300 mm/month) of precipitation amount is about twice as large as the observed range (TRMM and ECMWF: 50-180 mm/month). The ECMWF re-analysis precipitation data agree well with TRMM observation, thus it gives confidence to ECMWF product.

Figure 6.2b investigates the impact of convection on the gradient (between 850 and 700 hPa) of water isotopologues in vapor ($\Delta\delta$D). It is known that the intensity of convection and convective precipitation amount has a local impact on the isotopic composition of precipitation via the isotope amount effect (Dansgaard 1964; Risi et al. 2008). However, the vertical gradient of δD is influenced by many factors and a priori assumptions. It is not clear if the gradient steepens or flattens during convectively active phases. The ECHAM model and the TRMM observation show similar negative correlation between $\Delta\delta$D and convective precipitation (TRMM uses δD from TES), with R values of -0.42 and -0.45 for ECHAM and TRMM, respectively. Apparently convective updrafts and convective mixing transport isotopically enriched WV from lower atmospheric layers near the ocean surface to higher altitudes (Gedzelman and Arnold 1994; Kurita et al. 2011; Sutanto et al., submitted to JGR Atmosphere). ECMWF re-analysis precipitation data are even better correlated with the observed (i.e., TES) isotope gradient (R = -0.72) than ECHAM and TRMM.

There is a spatial linear relation between the small-scale mixing index (S), convective intensity (i.e., convective precipitation), and the δD gradient in water vapor, at least in
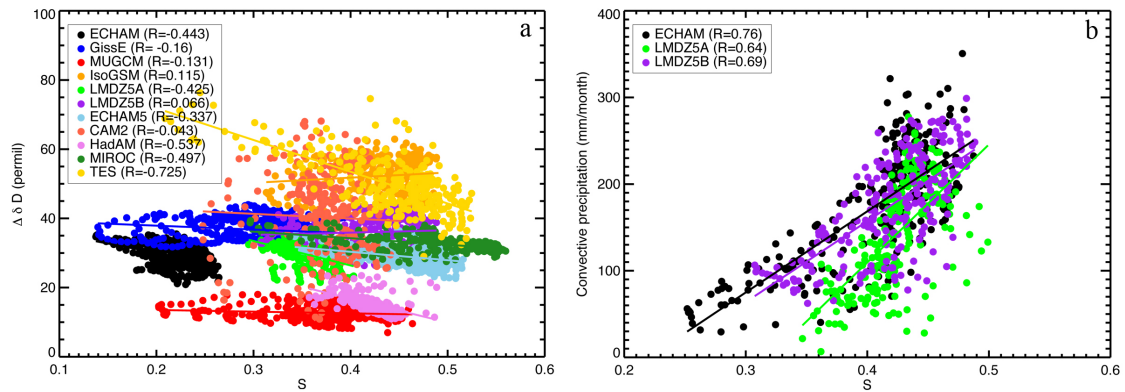
Figure 6.3 Spatial correlation of S and $\Delta\delta$D from isotope-enabled GCMs and TES (a); spatial correlation of S and convective precipitation from ECHAM, LMDZ5A and LMDZ5B (b).

the ECHAM model. Combining different observational and re-analysis datasets (TRMM, ECMWF) confirms this relationship. However, the robustness and the quantitative spread verification of these correlations among the available SWING2 models need to be carried out.

Figure 6.3a shows all correlations between S and $\Delta\delta$D, and between S and convective precipitation, from the ensemble of the SWING2 models and the TES observations. In general it confirms the hypothesis that S and $\Delta\delta$D relate to each other as expected. ECHAM4, GissE, MUGCM, LMDZ5A, ECHAM5, CAM2, HadAM, and MIROC simulate negative correlations, though the correlation is often quite small. Only ECHAM4, LMDZ5A, and HadAM produce relatively steep slopes (Table. 6.1) though these three models clearly underestimate the correlation coefficients and slopes compared to the TES data (R = -0.73 and δD slope = -91.79).

Figure 6.3b confirms that the spatial relation between the small scale mixing, S, and convection is relatively similar among different models. Convective precipitation is only available from three of the SWING2 models (LMDZ5A, LMDZ5B, and ECHAM4).

6.3.3 Intermodel comparison of simulated S, ECS, and $\Delta\delta$D

In section 6.3.2 the study hypothesis that small-scale mixing (S), convection, and $\Delta\delta$D are spatially related was confirmed. Areas with strong mixing tend to be marked by strong convective activity and finally by a reduced isotopologue gradient. However, the final aim of this analysis is a model intercomparison, which will relate a directly observable feature, the δD gradient averaged over a significant area, to the models ECS values. Are models with relatively low δD gradients indeed characterized by a comparably intense mixing (S) and by relatively large ECS values? The step between S and ECS was already demonstrated in Sherwood et al. (2014).

Figure 6.4a shows that there is in fact no correlation between regionally averaged S and $\Delta\delta$D. Here the model results are averaged over the WPWP region (75-165 °E and 10 °N-10 °S) similar to Sherwood et al. (2014). However, the respective averaging region

Table 6.1 Correlation slopes of S and $\Delta\delta$D from models and TES, and the correlation coefficient.

Models	Slope δD	Correlation (R)
ECHAM4	-53.65	-0.443
GissE	-11.21	-0.16
MUGCM	-4.88	-0.131
IsoGSM	14.93	0.115
LMDZ5A	-70.68	-0.425
LMDZ5B	6.73	0.066
ECHAM5	-24.23	-0.337
CAM2	-13.63	-0.043
HadAM	-68.83	-0.537
MIROC	-18.87	-0.497
TES	-91.79	-0.725
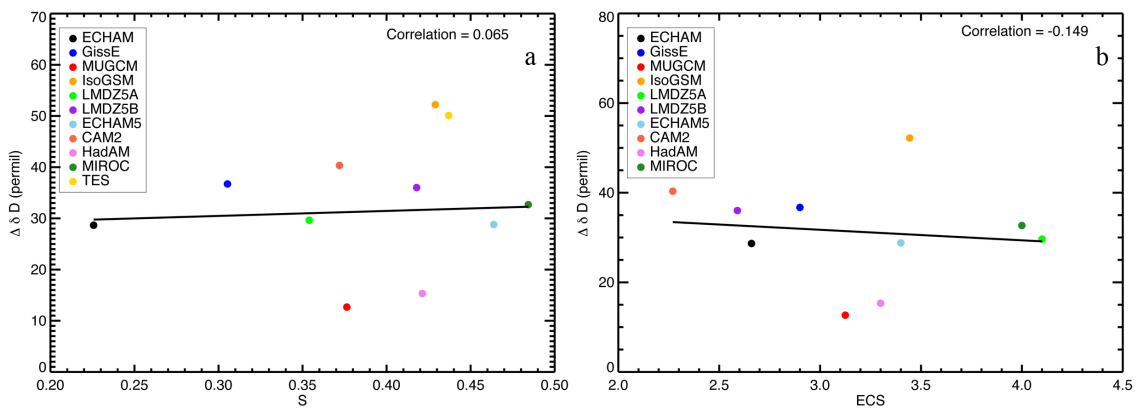
Figure 6.4 Correlation of S and $\Delta\delta$D (a) and correlation of ECS and $\Delta\delta$D (b) from the SWING2 models.

is modified without any impact on the relation between S and $\Delta\delta$D. The model spread is in general around 30-40 ‰ for the averaged $\Delta\delta$D values and around 0.22-0.48 for S values. Again, all models underestimate the $\Delta\delta$D value compared to TES, except the IsoGSM model.

Although there is no correlation between S and $\Delta\delta$D, a very weak (not significant) negative correlation between ECS and $\Delta\delta$D with an R value of -0.149 was found (Fig. 6.4b). In the following, the discussion on the possible causes of the failed relation between $\Delta\delta$D on one hand and model quantities such as convective mixing (S) and the models climate sensitivity on the other hand is presented.

6.4 Discussion and conclusions

This study has evaluated the relation between small-scale mixing, tropical convection and the δD gradient from several isotope-enabled GCMs, which are participating in the SWING2 project. On the observational side, the same relationships using the TES satellite data were analyzed.

The subset of the CMIP5 models used here represents a subset of the models used in Sherwood et al. (2014). Those SWING2 isotope-enabled models, which have an intense/less intense convective mixing S, are also marked by relatively high/low ECS. The results here added with the TES data as another observational point to relatively high ECS values of about $+3.3$ °C (see Fig. 6.1). However it must be noted that in Sherwood et al. (2014) a strong relation between mixing quantities and ECS was only evaluated when using a combined mixing index of small-scale (S) and large-scale mixing (D). Still it seems that TES results rather bolster conclusions pointing to intense mixing models as more reliable (Fasullo and Trenberth 2012; Su et al. 2014).

It is therefore a valid next step to test if this mixing and the associated convective activity affect the vertical gradient of the isotopic composition of water vapor. In fact this study was able to confirm that spatially the assumption is true: regions with intense mixing and strong convection are marked by a more uniform isotopologue profile. This holds also for the TES observational data, which even shows the highest correlation between S and $\Delta\delta$D. However, when we compare the different models with each other, the relation between the water isotopologues and convective mixing or ECS falls apart. What are the probable causes for this non-existing relation?

The modeled δD gradient are controlled by many more factors and processes than just the small-scale convective mixing. First, there is the actual fractionation physics, which is implemented in a similar but not exactly the same way in the different models. For example, a potentially important parameterization implemented in most climate models with considerably uncertain parameters is evaporation of raindrops below the cloud base and its isotopic equilibration with the surrounding vapor. The effectiveness of the isotopic exchange between raindrops and vapor depends on the fall velocity and thus on the size of raindrops. A full mechanistic description of this process is not available but will certainly involve knowledge of the drop size spectrum (Stewart 1975). Since convective rain is formed typically by larger raindrops than rain formed in stratiform cloud bands, most models decided on an ad hoc value which fraction of the falling raindrops equilibrates with the surrounding water vapor, approximately 90 % for stratiform rain and 50 % for convective rain. Sutanto et al. (submitted to JGR Atmosphere) argued that this process in fact affects the isotopic composition of vapor in the lowest layers of the troposphere in model and is partly responsible for the isotopic variations observed and simulated during El Niño events. It is therefore possible that the choice of the fractional equilibration (i.e., 50 % for convective rain or 90 % for stratiform rain) has some influence on the isotopologue gradient. Several other model properties probably have also significant influence on the water isotopologues and perturb the influence of convective mixing such as the typical cloud height, cloud types or the models lapse rate. All these processes have an influence on
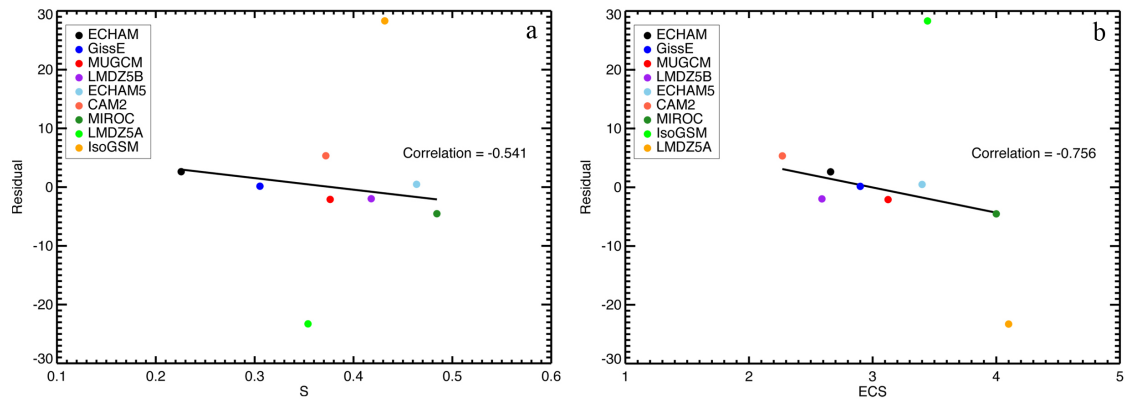
Figure 6.5   Correlation of S and residual (a) and of ECS and residual (b) from the SWING2 models. The correlation coefficients were derived from 7 models, excluding LMDZ5A and IsoGSM models.

the δD gradient. It would need very extensive sensitivity studies to evaluate the influence of each factor and to estimate their interdependencies.

Since the differences of the simulated δD gradients seem to be deeply buried in the models physics and parameter choices, this study tried a very simple approach to isolate the part that is affected by convective mixing. The linear regression of the different simulated gradients ($\Delta\delta$D) towards the isotopic composition of precipitation over the respective area was computed (δD$_P$). Isotopic composition of precipitation is probably much more directly influenced by cloud height, cloud temperatures or below cloud equilibration processes than the isotopologue gradient. The difference between $\Delta\delta$D and the regression line is called residual. By computing the residual of this regression (R = 0.97, figure is not shown), this study tried to subtract efficiently part of those processes, which largely control the δD gradients in different models and keep the influence of convective mixing. Obviously such an approach cannot be perfect. Even if δD$_P$ may be more influenced by cloud temperatures than the isotopologue gradient, the latter is not independent of these temperatures.

The residual of this calculation is shown in Fig 6.5a and b as function of the convective mixing and ECS, respectively. Both correlations are now clearly improved compared to Fig 6.4a and b. Convective mixing was not related at all to $\Delta\delta$D (Fig. 6.4a) and shows now, after correction by δD$_P$, a correlation of R = -0.54. There are two large model outliers (IsoGSM and LMDZ5A), which are excluded in the residual analysis. The number of model simulations used is obviously not sufficient to come to a robust conclusion. However, at least the relation between residual $\Delta\delta$D and S is now as expected: models with a more intense mixing tend to have less steep δD gradients. The same is true for the relation of $\Delta\delta$D to the models climate sensitivity. The relation changed by computing the residual from R = -0.15 (Fig. 6.4b) to R = -0.76 (Fig 6.5b). Models with less steep δD gradients (Residual $\Delta\delta$D) are characterized by higher climate sensitivity (ECS).

It is clear that this analysis is preliminary in many senses. The statistics of only 7 isotope-enabled models is poor and not conclusive (note: there is no δD$_P$ result for HadAM submitted to SWING2). Still, the subtraction of a part of the variability due

to the isotopic precipitation computed by each model seemed promising to eliminate the disturbing factors such as cloud physics and temperatures, which vary from each model to the other. The resulting residual correlation may depend less on the diverging model physics and depend more just on the models mixing processes. Model sensitivity studies could certainly help to clarify this point and to improve the respective statistics.

This study has shown that there is an interesting potential in studying the vertical distribution of δD in the troposphere. Though the latest version of the TES dataset (version 5) has clearly improved and provides reasonable values of the water isotopologues in lower tropospheric layers (Sutanto et al. 2015), the uncertainties are still too large to constrain quantitatively the different climate models. The use of the water isotopologues within GCMs has slowly and steadily increased over the last decades and the need for more precise data is increasing as well. The mixing between isotopically enriched water vapor from near-surface layers with water vapor at higher altitudes will isotopically enrich the water vapor at higher altitudes. It was speculated that the water isotopologue information at high altitudes could effectively constrain moistening processes at tropopause layers and even in the stratosphere (Smith et al. 2006; Moyer et al. 1996; Zhao 2014). However, a very important application may be to study the moistening and drying mechanisms in the planetary boundary layer and the concurring mixing processes with the free troposphere.

7 General conclusions and outlook

"In literature and in life we ultimately pursue, not conclusions, but beginnings"
Sam Tanenhaus

7.1 General conclusions

The transport of water vapor through the atmosphere plays a major role in the hydrological cycle and it is strongly coupled to phase changes associated with evaporation and condensation processes. Isotope fractionation associated with these phase-changes leaves a characteristic imprint on the isotopic composition of rainwater and the corresponding water vapor, which facilitates the use of water isotopologues as valuable tracers. The recent development of fast and robust optical in-situ measurement methods for water vapor isotopologues offers the possibility to study the isotope effects in the hydrological cycle in more detail. In addition, global-scale datasets of the isotopic composition (primarily δD) of atmospheric water vapor have become available from different remote-sensing instruments.

This study used global-scale measurement of δD from satellite-borne instruments and isotope-enabled general circulation models to gain new insight into the hydrological cycle, focusing on atmospheric processes and the land-surface interaction. Various important processes in the water cycle have been studied, namely the partitioning of the total land-surface flux into evaporation and transpiration using the associated isotope effects, the representation of global-scale isotope effects in datasets available from satellites and models, the relation between drought and water isotopologues associated with ENSO variability, the underlying atmospheric processes contributing to the isotope amount effect during ENSO, and the possibility to use vertical isotopic gradients to identify and quantify lower tropospheric mixing and its relation to climate sensitivity.

In the following, the main results from the individual chapters of the thesis are summarized related to the research questions that were posted in chapter 1 of the thesis.

- **How accurate is the isotope-based approach to determine the contribution of transpiration to total evaporation (Chapter 2)?**

There are a variety of methods to disentangle the evaporative flux over continental surfaces into a transpirative part and evaporation from bare soils, open liquid water, and snow covered surfaces. Although every method has its limitations and uncertainties, a number of comparison studies using the isotope-based method and hydrometric measurements using the same plants and under the same climatic conditions are consistent within the errors. The transpiration from vegetation clearly dominates over most surface types and in most climates (> 70 % during summer).

- **How good are the satellite data and an isotope-enabled global circulation model in representing the first-order isotope effects on the global scale (Chapter 3)?**

A comparison between model and satellites shows that the model reproduces geographical variability of δD in the tropics quite well although the sub-tropical δD maximum in the ECHAM model is significantly wider than for SCIAMACHY and TES V5. A number of established isotopologue effects as well as the movement of ITCZ are observed in the TES V5 product, SCIAMACHY and the ECHAM model, which confirms the improvement of TES V5 product over TES V4. A humidity bias correction and a posteriori analyses can be used to avoid the mid troposphere humidity bias that can arise when the satellites averaging kernels are applied to the model results.

- **Are changes in the isotopic composition of water useful climatic indicators for drought and flooding events (Chapter 4)?**

The magnitudes of drought and flooding analyzed using two drought indices correlate well with variations in the isotopic composition of water vapor over Indonesia. δD is a good climatic indicator for drought and flooding events and it outperforms the Niño-3 index. This finding has potential impact for the future use of water isotopologues as climate proxy in the region and as an independent climate indicator for this type of climatic extreme events.

- **What atmospheric processes control the isotopic composition of water vapor in the lower and middle troposphere during ENSO events in the Central and West Pacific regions (Chapter 5)?**

A three-dimensional large-scale pattern in in δD of water vapor was identified that extends throughout the tropical Pacific. The near-surface pattern corresponds to what is expected from the isotope amount effect: humid/dry conditions during ENSO events are associated with isotopically depleted/enriched precipitation and water vapor. Interestingly, an associated inverse pattern is observed in the mid-troposphere, both in the satellite observations and in the model results. Several mechanisms are suggested to explain this correlation/anti-correlation pattern: re-evaporation and isotopic equilibration of falling raindrops, uplift and more intense vertical mixing in convectively active regions are qualitatively in agreement with the δD patterns. Independent observations also confirm that these mechanisms vary as suggested over an ENSO cycle.

- **Does the strength of lower tropospheric mixing and climate sensitivity leave an imprint in isotopic composition of water vapor (Chapter 6)?**

Lower tropospheric mixing has been suggested as an important factor for determining equilibrium climate sensitivity in GCMs. It was investigated whether the strength of lower tropospheric mixing leaves an imprint in observed and modeled δD gradients using an ensemble of 10 different isotope-enabled GCMs. There is no clear correlation found

between models with more or less vertical mixing in the tropics and models with more or less steep δD gradients unless the possible processes that control the isotopic gradient are substracted via δD$_P$. A possible reason for the lack of such a straightforward relation might be that the different "isotope" GCMs vary too much in the parameterization of important of hydrological processes and even in the parameterization of the water isotope fractionation processes themselves. Therefore the simulated gradients in the atmosphere potentially are controlled by more model-dependent processes than vertical mixing.

7.2 Outlook

The availability of global-scale isotopologue measurements of atmospheric water vapor from satellite-borne optical instruments opens many opportunities to study various aspects of the hydrological cycle. This study has shown some of the great opportunities, but also some of the pitfalls in the application of such datasets. A promising development is the well-documented improvement of the TES V5 sensitivity compared to the previous version 4 dataset, which allows TES to capture important seasonally varying climate modes that control the hydrologic cycle in the tropics. Together with the isotope-enabled GCMs, this new dataset opens further opportunities to study other aspects of the water cycle in detail.

One important future application can be the assessment of the land-surface model parameterizations. Such models tend to produce a lower transpiration fraction compared to the isotope-based method and hydrometric measurements. An isotope-enabled land-surface modeling study opens an opportunity for the evaluation of the parameterization of land-surface models, by comparing the computed water isotopologue signals in the lower troposphere with remote sensing dataset or in-situ measurements. Future studies should perform this evaluation in order to provide a better understanding of the hydrological cycle in vegetated regions.

A second promising aspect that was highlighted in Chapter 5 is the evaluation of the (dis-) equilibrium between rain droplets and surrounding vapor for convective and stratiform precipitation. A mechanistic representation of isotopic equilibrium processes for falling raindrops needs a realistic representation of raindrop size spectra in climate models, something which is not yet available. Also, additional laboratory experiments on evaporation of raindrops into a relatively humid atmosphere below clouds are needed.

The work presented in chapter 6 is just the beginning of a thorough investigation of the use of isotopes to investigate mixing processes between the boundary layer and the free troposphere. Although the first result is negative, this should be investigated in more detail. The most challenging requirement to investigate the mixing processes is the vertical resolution of the observations. The satellite observations must provide isotope information in several vertical layers with high sensitivity near to the surface (e.g., TES version 5). SCIAMACHY and GOSAT, for examples, cannot be used to investigate the mixing processes in the lower troposphere since they measure total column δD.

It is now generally believed that the key processes controlling the spread in simulated climate sensitivity of the existing climate models are situated in the tropics/subtropics and are linked principally to feedbacks related to uncertainties in the distribution of middle

and lower tropospheric cloud processes and their coupling to the atmospheric dynamics as represented by the different models (Sherwood et al. 2014). Though low-level clouds cause an important feedback in the models, only some models in the CMIP3 and CMIP5 database simulate the observed decrease of low cloud cover as a result of warmer temperature, which indicate a positive feedback (Clement et al. 2009; Zelinka et al. 2013). In addition, a dry bias in the boundary layer and a large moist bias in the free troposphere are commonly found in the models, which have a great impact on the (mis-) interpretation of the strength of water vapor feedback mechanisms (Pierce et al. 2006; John and Soden 2007). Upward moisture transport by shallow cumulus clouds, subsidence, and evaporating rainfall contribute to lower tropospheric mixing and vary depending on the cloud parameterizations in the models. The TES V5 HDO profile measurements, which can now distinguish water isotopologue distributions from the middle and lower troposphere, provide potentially a powerful tool to study how mixing between and within atmospheric layers control cloud distributions.

Characterizing lower tropospheric mixing and its effect on cloud distribution in GCMs therefore are of critical importance for more confident future climate projections. Model sensitivity studies with different physical parameterizations and the uses of CFMIP (Cloud Feedback Model Intercomparison project) Observation Simulator Package (COSP; Bodas-Salcedo et al. 2011) provide a prospect for new techniques to parameterize cloud processes such as cloud entrainment, condensation and re-evaporation. The COSP simulator is a module that enables us to compare the model-simulated clouds with observed cloud data from satellites (CloudSat/CALIPSO). This simulator can be adapted to many types of GCMs. The proper use of isotope data and other observation datasets might offer a unique opportunity to model development in a way that leads to more reliable future climate projections.

In this study, all analyses have been carried out using monthly average satellite data. Next year, the new TROPOspheric Monitoring Instrument (TROPOMI) will be launched on the ESA/GMES (European Space Agency/Global Monitoring for Environment and Security) Sentinel 5 Precursor mission. TROPOMI will be able to measure total column HHO and HDO at greatly improved precision and temporal and spatial resolution compared to SCIAMACHY. The spatial resolution is 7 by 7 km, far better than SCIAMACHY, which has spatial resolution of 120 by 30 km. TROPOMI will measure the water isotopologues in every second as the satellite moves. These configurations allow TROPOMI sampling the water isotopologues in high resolutions and also offer an opportunity to study the hydrologic cycle in high spatial and temporal resolution.

References

Abramowitz, M. and I. A. Stegun (1965), Handbook of Mathematical Functions, with Formulas, Graphs, and Mathematical Tables. Dover Publications.

Adidarma, W. K., E. A. Djajadiredja and W. M. Putuhena (2006), Agricultural drought indicators for the Pemali-Comal river basin. In: International Workshop on Client Oriented Agrometeorological Services to Support Agriculture Development.

Aggarwal, P. K., J. R. Gat and K. F. O. Froehlich (2007), Isotopes in the water cycle: Past, present and future of a developing science. IAEA: Springer.

Allen, R. G., L. S. Pereira, D. Raes and M. Smith (1998), Crop evapotranspiration-Guidelines for computing crop water requirements-FAO Irrigation and drainage paper 56. Rome: FAO - Food and Agriculture Organization of the United Nations.

Allen, R. G., L. S. Pereira, T. A. Howell and M. E. Jensen (2011), Evapotranspiration information reporting: I. factors governing measurement accuracy. Agr. Water Manage. 98, 899–920.

Alley, W. M. (1984), The Palmer Drought Severity Index: Limitation and assumptions. J. Clim. And Applied Meteorol. 23, 1100–1109.

Andrews, T., J. M. Gregory, M. J. Webb and K. E. Taylor (2012), Forcing, feedbacks and climate sensitivity in CMIP5 coupled atmosphere-ocean climate models. Geophys. Res. Let. 39.

Araguás-Araguás, L., K. Rozanski and K. Froehlich (1998), Stable isotope composition of precipitation over southeast Asia. J. Geophys. Res. 103, 28,721–28,742.

Arnold, J. G., P. M. Allen, R. Muttiah and G. Bernhardt (1995), Automated base flow separation and recession analysis techniques. groundwater 33.

Back, L. E. and C. S. Bretherton (2005), The relationship between wind speed and precipitation in the Pacific ITCZ. J. Clim. 18, 4317–4328.

Barnes, C. J. and G. B. Allison (1983), The distribution of deuterium and ^{18}O in dry soils, 1. theory. J. Hydrol. 60, 141–156.

Bechtold, P., J.-P. Chaboureau, A. Beljaars, A. K. Betts, M. Köhler, M. Miller and J.-L. Redelsperger (2004), The simulation of the diurnal cycle of convective precipitation over land in a global model. Q. J. R. Meteorol. Soc. 130, 3119–3137.

Becker, B., B. Kromer and P. Trimborn (1991), A stable-isotope tree-ring timescale of the late glacial/Holocene boundary. Nature 353, 647–649.

Betts, A. K. and C. Jakob (2002), Evaluation of the diurnal cycle of precipitation, surface thermodynamics, and surface fluxes in the ECMWF model using LBA data. J. Geophys. Res. 107.

BILLESBACH, D. P. (2011), Estimating uncertainty in individual eddy covariance flux measurements: a comparison of methods and a proposed new method. Agr. Forest Meteorol. 151, 394–405.

BLYTH, E. M. and R. J. HARDING (2011), Methods to separate observed global evapotranspiration into the interception, transpiration and soil surface evaporation components. Hydrol. Process. 25, 4063–4068.

BODAS-SALCEDO, A., M. J. WEBB, S. BONY, H. CHEPFER, J.-L. DUFRESNE, S. A. KLEIN, Y. ZHANG, R. MARCHAND, J. M. HAYNES, R. PINCUS and V. O. JOHN (2011), COSP: Satellite simulation software for model assessment. Bull. Amer. Meteor. Soc. 92, 1023–1043.

BOESCH, H., N. M. DEUTSCHER, T. WARNEKE, K. BYCKLING, A. J. COGAN, D. W. T. GRIFFITH, J. NOTHOLT, R. J. PARKER and Z. WANG (2013), HDO/H_2O ratio retrievals from GOSAT. Atmos. Meas. Tech. 6, 599–612.

BONY, S. and J.-L. DUFRESNE (2005), Marine boundary layer clouds at the heart of tropical cloud feedback uncertainties in climate models. Geophys. Res. Let. 32.

BONY, S., J.-L. DUFRESNE and H. LE TREUT (2004), On dynamic and thermodynamic components of cloud changes. Clim. Dyn. 22, 71–86.

BONY, S., C. RISI and F. VIMEUX (2008), Influence of convective process on the isotopic composition (δ^{18}O and δD) of precipitation and water vapor in the tropics: 1. radiative-convective equilibrium and Tropical Ocean-Global Atmosphere-Coupled Ocean-Atmosphere Response Experiment (TOGA-COARE) simulations. J. Geophys. Res. 113.

BORDI, I., S. FRIGIO, P. PARENTI, A. SPERANZA and A. SUTERA (2001), The analysis of the standardized precipitation index in the Mediterranean area: large-scale patterns. Annali di Geofisica 44.

BOWEN, G. J. and B. WILKINSON (2002), Spatial distribution of δ^{18}O in meteoric precipitation. Geology 30, 315–318.

BOWEN, I. S. (1926), The ratio of heat looses by conduction and by evaporation from any water surface. Phys. Rev. 27, 779–787.

BOWMAN, K. W., C. D. RODGERS, S. S. KULAWIK, J. WORDEN, E. SARKISSIAN, G. OSTERMAN, T. STECK, M. LOU, A. ELDERING, M. SHEPHARD, H. WORDEN, M. LAMPEL, S. CLOUGH, P. BROWN, C. RINSLAND, M. GUNSON and R. BEER (2006), Tropospheric Emission Spectrometer: Retrieval method and error analysis. IEEE Trans. Geosci. Remote Sensing 44, 1297–1307.

BROOKS, J. R., H. R. BARNARD, R. COULOMBE and J. J. MCDONNELL (2010), Eco-hydrologic separation of water between trees and streams in a mediterranean climate. Nat. Geosci. 3, 100–104.

BROWN, D., I. SIMMONDS and D. NOONE (2006), Modeling δ^{18}O in tropical precipitation and the surface ocean for present day climate. J. Geophys. Res. 111.

Brown, D., J. Worden and D. Noone (2008), Comparison of atmospheric hydrology over convective continental regions using water vapor isotope measurements from space. J. Geophys. Res. 113.

Brown, D., J. Worden and D. Noone (2013), Characteristics of tropical and subtropical atmospheric moistening derived from lagrangian mass balance constrained by measurements of HDO and H_2O. J. Geophys. Res. 118.

Brutsaert, W. (1982), Evaporation into the atmosphere: theory, history, and applications. Dordrecht: Reidel.

Burba, G. G. and D. J. Anderson (2007), Introduction to The Eddy Covariance Method: General 20 Guidelines and Conventional Work-flow. Lincoln: LI-COR Biosciences.

Calder, I. R. (1992), Deuterium tracing for the estimation of transpiration from trees part 2. estimation of transpiration rates and transpiration parameters using a time-averaged deuterium tracing method. J. Hydrol. 130, 27–35.

Calder, I. R., M. N. Narayanswamy, N. V. Srinivasalu, W. G. Darling and A. J. Lardner (1986), Investigation into the use of deuterium as a tracer for measuring transpiration from eucalypts. J. Hydrol. 84, 345–351.

Calder, I. R., G. S. Kariyappa, N. V. Srinivasalu and K. V. S. Murty (1992), Deuterium tracing for the estimation of transpiration from trees part 1. field calibration. J. Hydrol. 130, 17–25.

Cavanaugh, M. L., S. A. Kurc and R. L. Scott (2011), Evapotranspiration partitioning in semiarid shrubland ecosystem: a two-site evaluation of soil moisture control on transpiration. Ecohydrology 4, 671–681.

Cess, R. D., G. L. Potter, J. P. Blanchet, G. J. Boer, A. D. Del Genio, M. Déqué and Co-authors (1990), Intercomparison and interpretation of climate feedback processes in 19 Atmospheric General Circulation Models. J. Geophys. Res. 95, 16601–16615.

Choudhury, B. and N. DiGirolamo (1998), A biophysical process-based estimate of global land surface evaporation using satellite and ancillary data I. model description and comparison with observations. J. Hydrol. 205, 164–185.

Clark, I. and P. Fritz (1997), Environmental isotopes in hydrogeology. Boca Raton, Florida: CRC Press.

Clement, A. C., R. Burgman and J. R. Norris (2009), Observational and model evidence for positive low-level cloud feedback. Science 325, 460–464.

Coenders-Gerrits, A. M. J., R. J. van der Ent, T. A. Bogaard, L. Wang-Erlandsson, M. Hrachowitz and H. H. G. Savenije (2014), Uncertainties in transpiration estimates, brief communications arising. Nature 506, E1–E2.

Collins, W. D., P. J. Rasch, B. A. Boville, J. J. Hack, J. R. McCaa, D. L. Williamson and B. P. Briegleb (2006), The formulation and atmospheric simulation of the Community Atmosphere Model version 3 (CAM3). J. Clim. 19, 2144–2161.

CONROY, J. L., K. M. COBB and D. NOONE (2013), Comparison of precipitation isotope variability across the tropical Pacific in observations and SWING2 model simulations. J. Geophys. Res.-Atmos. 118, 5867–5892.

COVEY, C., K. M. AchutaRao, U. CUBASCH, P. JONES, S. J. LAMBERT, M. E. MANN, T. J. PHILIPS and K. E. TAYLOR (2003), An overview of results from Coupled Model Intercomparison Project. Glob. Plan. Chang. 37, 103–133.

CRAIG, H. (1961), Isotopic variations in meteoric waters. Science 133, 1702–1703.

CRAIG, H. and L. I. GORDON (1965), Deuterium and oxygen-18 variations in the ocean and the marine atmosphere. In: T. E, ed., Proceedings of the conference on stable isotopes in oceanographic studies and paleotemperatures, Laboratory of Geology and Nuclear Science Pisa, 9–130.

CUNTZ, M., J. OGÉE, G. D. FARQUHAR, P. PEYLIN and L. A. CERNUSAK (2007), Modelling advection and diffusion of water isotopologues in leaves. Plant Cell Environ. 30, 829–909.

CURTIS, S. and R. ADLER (2000), ENSO indices based on pattern of satellite-derived precipitation. J. Clim. 13, 2786–2793.

DAI, A. (2006), Precipitation characteristics in eighteen coupled climate models. J. Clim. 19, 4605–4630.

DAI, A. and T. M. L. WIGLEY (2000), Global patterns of ENSO-induced precipitation. Geophys. Res. Let. 27, 1283–1286.

DANSGAARD, W. (1964), Stable isotopes in precipitation. Tellus 16, 436–468.

DAWSON, T. E. and R. EHLERINGER (1998), Plants, isotopes and water use: A catchment-scale perspective. In: C. Kendall and J. J. McDonnell, eds., Isotope tracers in catchment hydrology, Amsterdam: Elsevier.

DEE, D. P., S. M. UPPALA, A. J. SIMMONS, P. BERRISFORD, P. POLI and CO-AUTHORS (2011), The ERA-interim reanalysis: configuration and performance of the data assimilation system. Q. J. R. Meteorol. Soc. 137, 553–597.

DIRMEYER, P. A. and K. L. BRUBAKER (2007), Characterization of the global hydrologic cycle from a back-trajectory analysis of atmospheric water vapor. J. Hydrometeorol. 8, 20–37.

DIRMEYER, P. A., X. GAO, M. ZHA, Z. GUO, T. OKI and N. HANASAKI (2006), GSWP-2: Multimodel analysis and implications for our perception of the land surface. B. Am. Meteorol. Soc. 87, 1381–1397.

DONGMANN, G., H. W. NURNBERG, H. FORSTEL and K. WAGENER (1974), On the enrichment of $H_2^{18}O$ in leaves of transpiring plants. Radiat. Environ. Bioph. 11, 41–52.

DUFRESNE, J.-L. and S. BONY (2008), An assessment of the primary sources of spread of global warming estimates from coupled atmosphere-ocean models. J. Clim. 21, 5135–5144.

EHHALT, D. H., U. SCHMIDT and L. E. HEIDT (1977), Vertical profiles of molecular hydrogen in the troposphere and stratosphere. J. Geophys. Res. 82.

EHHALT, D. H., J. A. DAVIDSON, C. A. CANTRELL, I. FRIEDMAN and S. TYLER (1989), The kinetic isotope effect in the reaction of H_2 with OH. J. Geophys. Res. 94, 9831–9836.

EHLERINGER, J. R. and T. E. DAWSON (1992), Water uptake by plants: perspectives from stable isotope composition. Plant Cell Environ. 15, 1073–1082.

FARQUHAR, G. D. and L. A. CERNUSAK (2005), On the isotopic composition of leaf water in the non-steady state. Funct. Plant Biol. 32, 293–303.

FASULLO, J. T. and K. E. TRENBERTH (2012), A less cloudy future: The role of subtropical subsidence in climate sensitivity. Science 338, 792–794.

FERRETTI, D. F., E. PENDALL, J. A. MORGAN, J. A. NELSON, D. LECAIN and A. R. MOSIER (2003), Partitioning evapotranspiration fluxes from a Colorado grassland using stable isotopes: Seasonal variations and ecosystem implications of elevated atmospheric CO_2. Plant Soil 254, 291–303.

FIELD, R. D. (2010), Observed and modeled controls on precipitation $\delta^{18}O$ over Europe: from local temperature to the Northern Annular Mode. J. Geophys. Res. 115.

FISCHER, M. J. and K. STURM (2006), Remoiso forcing for the iPILPS phase 1 experiments and the performance of REMOiso in three domains. Global Planet. Change 51, 73–89.

FLANAGAN, L. B., J. P. COMSTOCK and J. R. EHLINGER (1991), Comparison of modeled and observed environmental influences of the stable oxygen and hydrogen isotope composition of leaf water in phaseolus vulgaris l. Plant Physiol. 96, 588–596.

FRANKENBERG, C., K. YOSHIMURA, T. WARNEKE, I. ABEN, A. BUTZ, N. DEUTSCHER, D. GRIFFITH, F. HASE, J. NOTHOLT, M. SCHNEIDER, H. SCHRIJVER and T. RÖCKMANN (2009), Dynamic processes governing the isotopic composition of water vapor as observed from space and ground. Science 325, 1374–1377.

FRANKENBERG, C., D. WUNCH, G. TOON, C. RISI, R. SCHEEPMAKER, J.-E. LEE, P. WENNBERG and J. WORDEN (2013), Water vapor isotopologue retrievals from high-resolution GOSAT shortwave infrared spectra. Atmos. Meas. Tech. 6, 263–274.

FRANZ, P. and T. RÖCKMANN (2005), High-precision isotope measurements of $H_2^{16}O$, $H_2^{17}O$, $H_2^{18}O$, and the $\delta^{17}O$-anomaly of water vapor in the southern lowermost stratosphere. Atmos. Chem. Phys. 5, 2949–2959.

GALEWSKY, J., M. STRONG and Z. D. SHARP (2007), Measurements of water vapor D/H ratios from Mauna Kea, Hawaii, and implications for subtropical humidity dynamics. Geophys. Res. Let. 34.

GAT, J. R. (1996), Oxygen and hydrogen isotopes in the hydrologic cycle. Annu. Rev. Earth Planet. Sci. 24, 225–262.

GAT, J. R. and E. MATSUI (1991), Atmospheric water balance in the Amazon basin: An isotopic evapotranspiration model. J. Geophys. Res. 96, 13179–13188.

GAT, J. R., W. G. MOOK and H. A. J. MEIJER (2001), Environmental isotopes in the hydrological cycle principles and applications. In: IHP V, technical documents in hydrology, vol. 2, UNESCO-IAEA.

GEDZELMAN, S., J. LAWRENCE, J. GAMACHE, M. BLACK, E. HINDMAN, R. BLACK, J. DUNION, H. WILLOUGHBY and X. ZHANG (2003), Probing Hurricanes with stable isotopes of rain and water vapor. Mon. Weather Rev. 131, 1112–1127.

GEDZELMAN, S. D. (1988), Deuterium in water vapor above the atmospheric boundary layer. Tellus B 40, 134–147.

GEDZELMAN, S. D. and R. ARNOLD (1994), Modeling the isotopic composition of precipitation. J. Geophys. Res. 99, 10455–10471.

GEHRELS, J. C., J. E. M. PEETERS, J. J. D. VRIES and M. DEKKERS (1998), The mechanism of soil water movement as inferred from ^{18}O stable isotope studies. Hydrolog. Sci. J. 43, 579–594.

GERSHUNOV, A. and T. P. BARNETT (1998), Interdecadal modulation of ENSO teleconnections. Bull. Am. Meteorol. Soc. 79, 2715–2725.

GRANIER, A. (1985), Une nouvelle method pour la mesure du flux de sève brute dans le tronc des arbres (in French). Ann. Sci. Forest 42, 193–200.

GRIFFITH, D. W., T, I. JAMIE, M. ESLER, S. R. WILSON, S. D. PARKES, C. WARING and G. W. BRYANT (2006), Real-time measurements of stable isotopes in water and CO_2 by fourier transform infrared spectrometry. Isot. Environ. Healt. S. 42, 9–20.

GUPTA, P., D. NOONE, J. GALEWSKY, C. SWEENEY and B. H. VAUGHN (2009), Demonstration of high-precision continuous measurements of water vapor isotopologues in laboratory and remote field deployments using wavelength-scanned cavity ring-down spectroscopy (WS-CRDS) technology. Mass Spectrom. 23, 2534–2542.

GUTTMAN, N. B. (1994), On the sensitivity of sample L moments to sample size. J. Clim. 7, 1026–1029.

HAVERD, V., M. CUNTZ, D. GRIFFITH, C. KEITEL, C. TADROS and J. TWINING (2011), Measured deuterium in water vapour concentration does not improve the constraint on the partitioning of evapotranspiration in a tall forest canopy, as estimated using a soil vegetation atmosphere transfer model. Agr. Forest Meteorol. 151, 645–654.

HAVERD, V., M. R. RAUPACH, P. R. BRIGGS, J. G. CANADELL, P. ISAAC, C. PICKETT-HEAPS, S. H. ROXBURGH, E. VAN GORSEL, R. A. VISCARRA ROSSEL and Z. WANG (2013), Multiple observation types reduce uncertainty in Australias terrestrial carbon and water cycles. Biogeosciences 10, 2011–2040.

HENDERSON-SELLERS, A., M. FISCHER, I. ALEINOV, K. MCGUFFIE, W. J. RILEY, G. A. SCHMIDT, K. STURM, K. YOSHIMURA and P. IRANNEJAD (2006), Stable water isotope simulation by current land-surface schemes: Results of iPILPS phase 1. Global Planet. Change 51, 34–58.

HERBIN, H., D. HURTMANS, S. TURQUETY, C. WESPES, B. BARRET, J. HADJI-LAZARO, C. CLERBAUX and P.-F. COHEUR (2007), Global distributions of water vapour isotopologues retrieved from IMG/ADEOS data. Atmos. Chem. Phys. 7, 3957–3968.

HERBST, M., L. KAPPEN, F. THAMM and R. VANSELOW (1996), Simultaneous measurements of transpiration, soil evaporation and total evaporation in a maize field in northern Germany. J. Exp. Bot. 47, 1957–1962.

HERMAN, R. L., J. E. CHERRY, J. YOUNG, J. M. WELKER, D. NOONE, S. S. KULAWIK and J. WORDEN (2014), Aircraft validation of Aura Tropospheric Emission Spectrometer retrieval of HDO/H_2O. Atmos. Meas. tech. 7, 3127–3138.

HOFFMANN, G. and M. HEIMANN (1997), Water isotope modeling in the Asian monsoon region. Quaternary International 37, 115–128.

HOFFMANN, G., M. WERNER and M. HEIMANN (1998), Water isotope module of the ECHAM atmospheric general circulation model: A study on timescales from days to several years. J. Geophys. Res. 103, 16871–16896.

HORTON, R. E. (1919), Rainfall interception. Mon. Weather Rev. 47, 603–623.

HOSKING, J. R. M. (1990), Analysis and estimation of distribution using linear combinations of order statistic. J. Roy. Stat. Soc. 52B, 105–124.

HUFFMAN, G. J., R. F. ADLER, D. T. BOLVIN, G. GU, E. J. NELKIN, K. P. BOWMAN, Y. HONG, E. F. STOCKER and D. B. WOLF (2007), The TRMM multisatellite precipitation analysis (TMPA): Quasi-global, multiyear, combined-sensor precipitation estimates at fine scales. J. Hydromet. 8, 38–55.

ICHIYANAGI, K. and M. D. YAMANAKA (2005), Interannual variation of stable isotopes in precipitation at Bangkok in response to El Niño Southern Oscillation. Hydrol. Process. 19, 3413–3423.

IPCC (2007), Climate change 2007: The physical science basis. contribution of working group 1 to the fourth assessment report of the Intergovernmental Panel on Climate Change. In: S. Solomon, D. Qin, M. Manning, Z. Chen, M. M, K. B. Averyt, M. Tignor and H. L. Miller, eds., APCC Report, Cambridge University Press, 996 pp.

JASECHKO, S., Z. D. SHARP, J. J. GIBSON, S. J. BIRKS, Y. YI and P. J. FAWCETT (2013), Terrestrial water fluxes dominated by transpiration. Nature 496, 347–350.

JO, K.-N., K. S. WOO, S. YI, D. Y. YANG, H. S. LIM, Y. WANG, H. CHENG and R. L. EDWARDS (2014), Mid-latitude interhemispheric hydrologic seesaw over the past 550,000yr. Nature 508, 378–382.

John, V. O. and B. J. Soden (2007), Temperature and humidity biases in global climate models and their impact on climate feedbacks. Geophys. Res. Let. 34.

Johnson, D. G., K. W. Jucks, W. A. Traub and K. V. Chance (2001), Isotopic composition of stratospheric water vapor: Implications for transport. J. Geophys. Res. 106, 12219–12226.

Jouzel, J., R. D. Koster, R. J. Suozzo, G. L. Russell, J. W. C. White and W. S. Broecker (1991), Simulations of the HDO and $H_2^{18}O$ atmospheric cycles using the NASA GISS general circulation model: sensitivity experiments for present-day conditions. J. Geophys. Res. 96, 7495–7507.

Jouzel, J., R. B. Alley, K. M. Cuffey, W. Dansgaard, P. Grrotes, G. Hoffmann, S. J. Johnsen, R. D. Koster, D. Peel, C. A. Shuman, M. Stievenard, M. Stuiver and J. White (1997), Validity of the temperature reconstruction from water isotopes in ice cores. J. Geophys. Res. 102, 26471–26487.

Jouzel, J., V. Masson-Delmotte, O. Cattani, G. Dreyfus, S. Falourd and Co-authors (2007), Orbital and millennial Antarctic climate variability over the past 800,000 years. Science 317.

Keeling, C. D. (1958), The concentration and isotopic abundances of atmospheric carbon dioxide in rural areas. Geochim. Cosmochim. Acta 13, 322–334.

Keith, D. W. (2000), Stratosphere-troposphere exchange: Inferences from the isotopic composition of water vapor. J. Geophys. Res. 105, 15167–15173.

Kelliher, F. M., B. M. M. Köstner, D. Y. Hollinger, J. N. Byers, J. E. Hunt, T. M. McSeveny, R. Meserth, P. L. Weir and E.-D. Schulze (1992), Evaporation, xylem sap flow, and tree transpiration in a New Zealand broad-leaved forest. Agr. Forest Meteorol. 62, 53–73.

Kendall, C. and A. Caldwell (1998), Fundamentals of isotope geochemistry. In: C. Kendall and J. J. McDonnell, eds., Isotope tracers in catchment hydrology, Amsterdam: Elsevier.

Kendall, C. and T. B. Coplen (2001), Distribution of oxygen-18 and deuterium in river waters across the United States. Hydrol. Process. 15, 1363–1393.

Kool, D., N. Agam, N. Lazarovitch, J. L. Heitman, T. J. Sauer and A. Ben-Gal (2014), A review of approaches for evapotranspiration partitioning. Agr. Forest Meteorol. 184, 56–70.

Kuang, Z., G. C. Toon, P. O. Wennberg, and Y. L. Yung (2003), Measured HDO/H_2O ratios across the tropical tropopause. Geophys. Res. Let. 30.

Kummerow, C., W. Barnes, T. Kozu, J. Shiue and J. Simpson (1998), The Tropical Rainfall Measuring Mission (TRMM) sensor package. J. Atmos. Oceanic Technol. 15, 809–817.

Kurita, N. (2013), Water isotopic variability in response to mesoscale convective system over the tropical ocean. J. Geophys. Res. Atmos. 118, 10376–10390.

Kurita, N., D. Noone, C. Risi, G. A. Schmidt, H. Yamada and K. Yoneyama (2011), Intraseasonal isotopic variation associated with the Madden-Julian Oscillation. J. Geophys. Res. 116.

Lacour, J.-L., C. Risi, L. Clarisse, S. Bony, D. Hurtmans, C. Clerbaux and P.-F. Coheur (2012), Mid-tropospheric δD observations from IASI/MetOp at high spatial and temporal resolution. Atmos. Chem. Phys. 12, 10817–10832.

Lai, C.-T., J. R. Ehleringer, B. J. Bond and K. T. Paw U (2006), Contributions of evaporation, isotopic non-steady state transpiration and atmospheric mixing on the δ^{18}O of water vapour in Pacific Northwest coniferous forests. Plant Cell Environ. 29, 77–94.

Landais, A., C. Risi, S. Bony, F. Vimeux, L. Descroix, S. Falourd and A. Bouygues (2010), Combined measurements of ^{17}Oexcess and d-excess in African monsoon precipitation: Implications for evaluating convective parameterizations. Earth and Planet. Sci. Let. 298, 104–112.

Latif, M., D. Anderson, T. Barnett, M. Cane, R. Kleeman, A. Leetmaa, J. OBrien, A. Rosati and E. Schneider (1998), A review of the predictability and prediction of ENSO. J. Geophys. Res. 103, 14375–14393.

Lawrence, D. M. and J. M. Slingo (2004), An annual cycle of vegetation in a GCM, part I: implementation and impact on evaporation. Clim. Dynam. 22, 87–105.

Lawrence, D. M., P. E. Thornton, K. W. Oleson, and G. B. Bonan (2007), The partitioning of evapotranspiration into transpiration, soil evaporation, and canopy interception in a GCM: Impacts on land-atmosphere interaction. J. Hydrometeorol. 8, 862–880.

Lawrence, J. R., S. D. Gedzelman, J. Gamache and M. Black (2002), Stable isotopologue ratios: Hurricane Olivia. J. Atmos. Chem. 41, 67–82.

Lawrence, J. R., S. D. Gedzelman, D. Dexheimer, H. K. Cho, G. D. Carrie, R. Gasparini, C. R. Anderson, K. P. Bowman and M. I. Biggerstaff (2004), Stable isotopic composition of water vapor in the tropics. J. Geophys. Res. 109.

Lee, D., J. Kim, K.-S. Lee and S. Kim (2010), Partitioning of catchment water budget and its implications for ecosystem carbon exchange. Biogeosciences 7, 1903–1914.

Lee, J., J. Worden, D. Noone, K. Bowman, A. Eldering, A. LeGrande, J.-L. F. Li, G. Schmidt and H. Sodemann (2011), Relating tropical ocean clouds to moist processes using water vapor isotope measurements. Atmos. Chem. Phys. 11, 741–752.

Lee, J.-E. and I. Fung (2007), "amount-effect" of water isotopes and quantitative analysis of post-condensation processes. Hydrol. Process. 22, 1–8.

Lee, J.-E., I. Fung, D. J. DePaolo and C. C. Henning (2007a), Analysis of the global distribution of water isotopes using the NCAR atmospheric general circulation model. J. Geophys. Res. 112, 1–14.

LEE, J.-E., C. RISI, I. FUNG, J. WORDEN, R. SCHEEPMAKER, B. LINTNER and C. FRANKENBERG (2012), Asian monsoon hydrometeorology from TES and SCIA-MACHY water vapor isotope measurements and LMDZ simulations: Implications for speleothem climate record interpretation. J. Geophys. Res. 117.

LEE, X., S. SARGENT, R. SMITH and B. TANNER (2005), In situ measurement of the water vapor $^{18}O/^{16}O$ isotope ratio for atmospheric and ecological applications. Am. Meteorolog. Soc. 22, 555–565.

LEE, X., K. KIM and R. SMITH (2007b), Temporal variations of the $^{18}O/^{16}O$ signal of the whole-canopy transpiration in a temperate forest. Global Biogeochem. Cy. 21.

LEGRANDE, A. N. and G. A. SCHMIDT (2011), Water isotopologues as a quantitative paleosalinity proxy. Paleocenogra. 26.

LEKSHMY, P. R., M. MIDHUN, R. RAMESH and R. A. JANI (2014), ^{18}O depletion in monsoon rain relates to large scale organized convection rather than the amount of rainfall. Sci. Rep. 4.

LOSSOW, S., J. STEINWAGNER, J. URBAN, E. DUPUY, C. D. BOONE, S. KELLMANN and CO-AUTHORS (2011), Comparison of HDO measurements from Envisat/MIPAS with observations by Odin/SMR and SCISAT/ACE-FTS. Atmos. Meas. Tech. 4, 1855–1874.

MAJOUBE, M. (1971a), Oxygen-18 and deuterium fractionation between water and steam (in French). J. Chim. Phys. 68, 1423–1436.

MAJOUBE, M. (1971b), Fractionation in O-18 between ice and water vapor (in French). J. Chim. Phys. 68, 625–636.

MARTINELLI, L. A., R. L. VICTORIA, L. S. L. STERNBERG, A. RIBEIRO and M. Z. MOREIRA (1996), Using stable isotopes to determine sources of evaporated water to the atmosphere in the Amazon basin. J. Hydrol. 183, 191–204.

MCKEE, T. B., N. DOESKEN and J. KLEIST (1993), The relationship of drought frequency and duration to time scales, preprints, eighth conf. on applied climatology. anaheim, ca. Am.Meteorol. Soc. , 179–184.

MERLIVAT, L. (1978), Molecular diffusivities of $H_2^{16}O$, $HD^{16}O$, and $H_2^{18}O$ in gases. J. Chem. Phys. 69, 2864–2871.

MIGUEZ-MACHO, G. and Y. FAN (2012), The role of groundwater in the Amazon water cycle: 2. influence on seasonal soil moisture and evapotranspiration. J. Geophys. Res. 117.

MIRALLES, D. G., R. A. M. DE JEU, J. H. GASH, T. R. H. HOLMES and A. J. DOLMAN (2011), Magnitude and variability of land evaporation and its components at the global scale. Hydrol. Earth Syst. Sci. 15, 967–981.

MITCHELL, P. J., E. VENEKLAAS, H. LAMBERS and S. S. O. BURGESS (2009), Partitioning of evapotranspiration in a semi-arid eucalypt woodland in south-western Australia. Agr. Forest Meteorol. 149, 25–37.

MOERMAN, J. W., K. M. COBB, J. F. ADKINS, H. SODEMANN, B. CLARK and A. A. TUEN (2013), Diurnal to interannual rainfall δ^{18}O variations in northern Borneo driven by regional hydrology. Earth Plan. Sci. Let. 369-370, 108–119.

MONTEITH, J. L. (1981), Evaporation and surface temperature. Q. J. Roy. Meteorol. Soc. 107, 1–27.

MOOK, W. G. (2001), Environmental isotopes in the hydrological cycle - principles and applications. In: IHP V, technical documents in hydrology, vol. 1, UNESCO-IAEA.

MOORE, M., Z. KUANG and P. N. BLOSSEY (2014), A moisture budget perspective of the amount effect. Geophys. Res. Lett. 41, 1329–1335.

MOREIRA, M. Z., L. D. S. L. STERNBERG, L. A. MARTINELLI, R. L. VICTORIA, E. M. BARBOSA, L. C. M. BONATES and D. C. NEPSTAD (1997), Contribution of transpiration to forest ambient vapour based on isotopic measurements. Global Change Biol. 3, 439–450.

MOYER, E. J., F. W. IRION, Y. L. YUNG and M. R. GUNSON (1996), ATMOS stratospheric deuterated water and implications for troposphere-stratosphere transport. Geophys. Res. Let. 23, 2385–2388.

NAGLER, P. L., R. L. SCOTT, C. WESTENBURG, J. R. CLEVERLY, E. P. GLENN and A. R. HUETE (2005), Evapotranspiration on western U.S. river estimated using the enhanced vegetation index from modis and data from eddy covariance and bowen ratio flux towers. Remote Sens. Environ. 97, 337–351.

NOONE, D. (2007), Assessing global model hydrology with simulations from the Stable Water-isotope INtercomparison Group. In: J. Cote, ed., Research Activities in Atmospheric and Oceanic Modeling Report No. 36, Switzerland: World Meteorological Organization, 4–21.

NOONE, D. (2012), Pairing measurements of the water vapor isotope ratio with humidity to deduce atmospheric moistening and dehydration in the tropical midtroposphere. J. Clim. 25, 4476–4494.

NOONE, D. and I. SIMMONDS (2002), Associations between δ^{18}O of water and climate parameters in a simulation of atmospheric circulation for 1979-95. J. Clim. 15, 3150–3169.

NOURI, H., S. BEECHAM, F. KAZEMI and A. M. HASSANLI (2013), A review of ET measurement techniques for estimating the water requirements of urban landscape vegetation. Urban Water J. 10:4, 247–259.

OGÉE, J., M. CUNTZ, P. PEYLIN and T. BARIAC (2007), Non-steady-state, non-uniform transpiration rate and leaf anatomy effects on the progressive stable isotope enrichment of leaf water along monocot leaves. Plant Cell Environ. 30, 367–387.

OKI, T. and S. KANAE (2006), Global hydrological cycles and world water resources. Science 313, 1068–1072.

OLESON, K. W., Y. DAI, G. BONAN, R. E. DICKINSON, P. A. DIRMEYER, F. HOFFMAN and CO-AUTHORS (2004), Technical description of the community land model (CLM). NCAR Tech. Note NCAR/TN-461+STR, NCAR, Boulder, Colorado.

Oort, A. H. and J. J. Yienger (1996), Observed interannual variability in the Hadley circulation and its connection to ENSO. Am. Meteorolog. Soc. 9, 2751–2767.

Palmer, W. C. (1965), Meteorological droughts. Weather Bureau Research Paper 45 58.

Payne, V. H., D. Noone, A. Dudhia, C. Piccolo and R. G. Grainger (2007), Global satellite measurements of HDO and implications for understanding the transport of water vapor into the stratosphere. Q. J. R. Meteorol. Soc. 133, 1459–1471.

Petit, J. R., J. Jouzel, D. Raynaud, N. I. Barkov, J.-M. Barnola, I. Basile and Co-authors (1999), Climate and atmospheric history of the past 420,000 years from the Vostok ice core, Antarctica. Nature 399, 429–436.

Pierce, D. W., T. P. Barnett, E. J. Fetzer and J. Gleckler (2006), Three-dimensional tropospheric water vapor in coupled climate models compared with observations from the AIRS satellite system. Geophys. Res. Let. 33.

Pommier, M., J.-L. Lacour, C. Risi, F. M. Bréon, C. Clerbaux, P.-F. Coheur, K. Gribanov, D. Hurtmans, J. Jouzel and V. Zakharov (2014), Observation of tropospheric δD by IASI over western Siberia: comparison with a general circulation model. Atmos. Meas. Tech. 7, 1581–1595.

Power, S., T. Casey, C. Folland, A. Colman and V. Mehta (1999), Inter-decadal modulation of the impact of ENSO on Australia. Clim. Dynamic 15, 319–324.

Priestly, C. H. B. and R. J. Taylor (1972), On the assessment of surface heat flux and evaporation using large-scale parameters. Mon. Weather Rev. 100, 81–92.

Reeburgh, W. S. (1997), Figures summarizing the global cycles of biogeochemically important elements. Bull. Ecologic. Soc. Amer. 78, 260–267.

Rieck, M., L. Nuijens and B. Stevens (2012), Marine boundary layer cloud feedbacks in a constant relative humidity atmosphere. J. Atmos. Sci. 69, 2538–2550.

Risi, C., S. Bony and F. Vimeux (2008), Influence of convective processes on the isotopic composition (δ^{18}O and δD) of precipitation and water vapor in the tropics: 2. physical interpretation of the amount effect. J. Geophys. Res. 113.

Risi, C., S. Bony, F. Vimeux and J. Jouzel (2010), Water-stable isotopes in the LMDZ4 general circulation model: Model evaluation for present-day and past climates and application to climatic interpretation of tropical isotopic records. J. Geophys. Res. 115.

Risi, C., D. Noone, J. Worden, C. Frankenberg, G. Stiller, M. Kiefer, B. Funke, K. Walker and Co-authors (2012a), Process-evaluation of tropospheric humidity simulated by general circulation models using water vapor isotoplogues: 1. comparison between models and observations. J. Geophys. Res. 117.

Risi, C., D. Noone, J. Worden, C. Frankenberg, G. Stiller, M. Kiefer, B. Funke and Co-authors (2012b), Process-evaluation of tropospheric humidity simulated by general circulation models using water vapor isotopic observations: 2. using isotopic diagnostics to understand the mid and upper tropospheric moist bias in the tropics and subtropics. J. Geophys. Res. 117.

RISI, C., D. NOONE, C. FRANKENBERG and J. WORDEN (2013), Role of continental recycling in intraseasonal variations of continental moisture as deduced from model simulations and water vapor isotopic measurements. Water Resour. Res. 49, 4136–4156.

ROBERTSON, J. A. and C. A. GAZIS (2006), An oxygen isotope study of seasonal trends in soil water fluxes at two sites along a climate gradient in Washington state (USA). J. Hydrol. 328, 375–387.

RÖCKNER, E., K. ARPE, L. BENGTSSON, M. CHRISTOPH, M. CLAUSSEN and COAUTHORS (1996), The atmospheric general circulation model ECHAM-4: Model description and simulation of present-day climate. Max Planck Institute for Meteorology Rep. 218, MPI, Germany.

RODGERS, C. D. (2000), Inverse Methods for Atmospheric Sounding: Theory and Practice. N. J.: World Sci., River Edge.

ROEDEL, W. (2000), Physik unserer umwelt die atmosphäre (in German). Berlin: Springer.

ROPELEWSKI, C. and M. S. HALPERT (1987), Global and regional scale precipitation patterns associated with the El Niño/Southern Oscillation. Month. Weather Rev. 115, 1606–1626.

ROUPSARD, O., J.-M. BONNEFOND, M. IRVINE, P. BERBIGIER, Y. NOUVELLON, J. DAUZAT and CO-AUTHORS (2006), Partitioning energy and evapo-transpiration above and below a tropical palm canopy. Agr. Forest Meteorol. 139, 252–268.

ROZANSKI, K. (1985), Deuterium and oxygen-18 in european groundwater-links to atmospheric circulation in the past. Chem. Geol. 52, 349–363.

ROZANSKI, K., C. SONNTAG and K. O. MÜNNICH (1982), Factors controlling stable isotope composition of European precipitation. Tellus 34, 142–150.

ROZANSKI, K., L. ARAGUÁS-ARAGUÁS and R. GONFIANTINI (1993), Isotopic pattern in modern global precipitation. Geophys. Monograph 78, 1–36.

SAMUELS-CROW, K. E., J. GALEWSKY, D. R. HARDY, Z. D. SHARP, J. WORDEN and C. BRAUN (2014), Upwind convective influences on the isotopic composition of atmospheric water vapor over the tropical Andes. J. Geophys. Res. Atmos. 119.

SAVENIJE, H. H. G. (2004), The importance of interception and why we should delete the term evapotranspiration from our vocabulary. Hydrol. Process. 18, 1507–1511.

SCHEEPMAKER, R. A., C. FRANKENBERG, A. GALI, A. BUTZ, H. SCHRIJVER, N. M. DEUTSCHER, D. WUNCH, T. WARNEKE, S. FALLY and I. ABEN (2013), Improved water vapour spectroscopy in the 4174-4300 cm^{-1} region and its impact on SCIAMACHY HDO/H$_2$O measurements. Atmos. Meas. Tech. 6, 879–894.

SCHEEPMAKER, R. A., C. FRANKENBERG, N. M. DEUTSCHER, M. SCHNEIDER, S. BARTHLOTT and CO-AUTHORS (2015), Validation of SCIAMACHY HDO/H$_2$O measurements using the TCCON and NDACC-MUSICA networks. Atmos. Meas. Tech. 8, 1799–1818.

132

SCHLESINGER, W. H. and S. JASECHKO (2014), Transpiration in the global water cycle. Agr. Forest Meteorol. 189–190, 115–117.

SCHMIDT, G. A., G. HOFFMANN, D. T. SHINDELL and Y. HU (2005), Modeling atmospheric stable water isotopes and the potential for constraining cloud processes and stratosphere-troposphere water exchange. J. Geophys. Res. 110.

SCHMIDT, G. A., A. N. LEGRANDE and G. HOFFMANN (2007), Water isotope expressions of intrinsic and forced variability in a coupled ocean-atmosphere model. J. Geophys. Res. 112.

SCHNEIDER, M. and F. HASE (2011), Optimal estimation of tropospheric H_2O and δD with IASI/METOP. Atmos. Chem. Phys. 11, 11207–11220.

SCHNEIDER, M., F. HASE and T. BLUMENSTOCK (2006), Ground-based remote sensing of HDO/H_2O ratio profiles: Introduction and validation of an innovative retrieval approach. Atmos. Chem. Phys. 6, 4705–4722.

SCHNEIDER, M., K. YOSHIMURA, F. HASE and T. BLUMENSTOCK (2010), The ground-based FTIR networks potential for investigating the atmospheric water cycle. Atmos. Chem. Phys. 10, 3427–3442.

SCHNEIDER, M., S. BARTHLOTT, F. HASE, Y. GONZÁLEZ, K. YOSHIMURA, O. E. GARCÍA, E. SEPÚLVEDA and CO-AUTHORS (2012), Ground-based remote sensing of tropospheric water vapour isotopologues within the project MUSICA. Atmos. Meas. Tech. 5, 3007–3027.

SCHOTTERER, U., F. OLDFIELD and K. FROHLICH (1996), GNIP-Global network for isotopes in precipitation. Tech. Rep., International Atomic Energy Agency, Bern.

SCHUMACHER, C. and R. A. HOUZE JR (2003), Stratiform rain in the tropics as seen by the TRMM precipitation radar. J. Clim. , 1739–1756.

SCHUMACHER, C., R. A. HOUZE JR and I. KRAUCUNAS (2004), The tropical dynamical response to latent heating estimates derived from the TRMM precipitation radar. J. Clim. , 1341–1358.

SENEVIRATNE, S. I., T. CORTI, E. L. DAVIN, M. HIRSCHI, E. B. JAEGER, I. LEHNER, B. ORLOWSKY and A. J. TEULING (2010), Investigating soil moisture-climate interactions in a changing climate: A review. Earth-Sci. Rev. 99, 125–161.

SHEFFIELD, J., E. F. WOOD and M. L. RODERICK (2012), Little change in global drought over the past 60 years. Nature 491, 435–438.

SHERWOOD, S. C., S. BONY and J.-L. DUFRESNE (2014), Spread in model climate sensitivity traced to atmospheric convective mixing. Nature 505, 37–42.

SHUTTLEWORTH, W. J. (1993), Evaporation. In: D. R. Maidment, ed., Handbook of Hydrology, New York: McGraw-Hill, 4.1–4.53.

SIEGENTHALER, U. and H. OESCHGER (1980), Correlation of ^{18}O in precipitation with temperature and altitude. Nature 285, 314–317.

SMITH, J. A., A. S. ACKERMAN, E. J. JENSEN and O. B. TOON (2006), Role of deep convection in establishing the isotopic composition of water vapor in the tropical transition layer. Geophys. Res. Let. 33.

SMITH, R. B. (1992), Deuterium in North Atlantic storm tops,. J. Atmos. Sci. 49, 2041–2057.

SODEN, B. J. and I. M. HELD (2006), An assessment of climate feedbacks in coupled ocean-atmosphere models. J. Clim. 19, 3354–3360.

SOLOMON, S., K. H. ROSENLOF, R. W. PORTMANN, J. S. DANIEL, S. M. DAVIS, T. J. SANFORD and G.-K. PLATTNER (2010), Contributions of stratospheric water vapor to decadal changes in the rate of global warming. Science 327.

STEINWAGNER, J., M. MILZ, T. VON CLARMANN, N. GLATTHOR, U. GRABOWSKI, M. HÖPFNER, G. P. STILLER and T. RÖCKMANN (2007), HDO measurement with MI-PAS. Atmos. Chem. Phys. 7, 2601–2615.

STEINWAGNER, J., S. FUEGLISTALER, G. STILLER, T. VON CLARMANN, M. KIEFER, P. P. BORSBOOM, A. VAN DELDEN and T. RÖCKMANN (2010), Tropical dehydration processes constrained by the seasonality of stratospheric deuterated water. Nat. Geosci. 3, 262–266.

STEPPE, K., D. J. W. DE PAUW, T. M. DOODY and R. O. TESKEY (2010), A comparison of sap flux density using thermal dissipation, heat pulse velocity and heat field deformation methods. Agr. Forest Meteorol. 150, 1046–1056.

STEVENS, B. and S. BONY (2013), What are climate models missing? Science 340, 1053–1054.

STEWART, M. K. (1975), Stable isotope fractionation due to evaporation and isotopic exchange of falling waterdrops: application to atmospheric processes and evaporation of lakes. J. Geophys. Res. 80, 1133–1146.

STURM, P. and A. KNOHL (2010), Water vapor δ^2H and δ^{18}O measurements using off-axis integrated cavity output spectroscopy. Atmos. Meas. Tech. 3, 67–77.

SU, H., J. H. JIANG, C. ZHAI, T. J. SHEN, J. D. NEELIN, G. L. STEPHENS and Y. L. YUNG (2014), Weakening and strengthening structures in the hadley circulation change under global warming and implications for cloud response and climate sensitivity. J. Geophys. Res. Atmos. 119, 5787–5805.

SUD, Y. C. and G. K. WALKER (1993), A rain evaporation and downdraft parameterization to complement a cumulus updraft scheme and its evaluation using GATE data. Month. Weather. Rev. 121, 3019–3039.

SUTANTO, S. J. and W. K. ADIDARMA (2015), Analisis kekeringan di beberapa negara eropa dengan menggunakan data dari model iklim global dan di indonesia menggunakan data hujan (in Indonesian). Jurnal Sumber Daya Air 11.

SUTANTO, S. J., J. WENNINGER, A. M. J. COENDERS-GERRITS and S. UHLENBROOK (2012), Partitioning of evaporation into transpiration, soil evaporation and interception: a comparison between isotope measurements and a HYDRUS-1D model. Hydrol. Earth Syst. Sci. 16, 2605–2616.

Sutanto, S. J., G. Hoffmann, R. A. Scheepmaker, J. Worden, S. Houweling, K. Yoshimura, I. Aben and T. Röckmann (2015), Global-scale remote sensing of water isotopologues in the troposphere: representation of first-order isotope effects. Atmos. Meas. Tech. 8, 999–1019.

Tang, K. and X. Feng (2001), The effect of soil hydrology on the oxygen and hydrogen isotopic compositions of plants source water. Earth Planet. Sc. Let. 185, 355–367.

Thornthwaite, C. W. (1948), An approach toward a rational classification of climate. Geogr. Rev. 38, 55–94.

Tiedtke, M. (1989), A comprehensive mass flux scheme for cumulus parameterization in large-scale models. Month. Weather Rev. 117, 1779–1800.

Tindall, J. C., P. J. Valdes and L. C. Sime (2009), Stable water isotopes in HadCM3: Isotopic signature of El Niño-Southern Oscillation and the tropical amount effect. J. Geophys. Res. 114.

Todd, R. W., S. R. Evett and T. A. Howell (2000), The bowen ratio-energy balance method for estimating latent heat flux of irrigated alfalfa evaluated in a semi-arid, advective environment. Agr. Forest Meteorol. 103, 335–348.

Tremoy, G., F. Vimeux, S. Soumana, I. Souley, C. Risi, G. Favreau and M. Oï (2014), Clustering mesoscale convective systems with laser-based water vapor $\delta^{18}O$ monitoring in niamey (niger). J. Geophys. Res. Atmos. 119, 1–25.

Trenberth, K., J. Fasullo and J. Kiehl (2009), Earth's global energy budget. Bull. Amer. Meteor. Soc. 90, 311–323.

Trenberth, K. E. and J. M. Caron (2000), The Southern Oscillation revisited: Sea level pressures, surface temperatures, and precipitation. J. Clim. 13, 4358–4365.

Trenberth, K. E., G. W. Branstator, D. Karoly, A. Kumar, N.-G. Lau and C. Ropelewski (1998), Progress during TOGA in understanding and modeling global teleconnections associated with tropical seas surface temperatures. J. Geophys. Res. 103, 14291–14324.

Tsiko, C. T., H. Makurira, A. M. J. Gerrits and H. H. G. Savenije (2012), Measuring forest floor and canopy interception in a savannah ecosystem. Phys. Chem. Earth 47-48, 122–127.

Uemura, R., Y. Matsui, K. Yoshimura, H. Motoyama and N. Yoshida (2008), Evidence of deuterium excess in water vapor as an indicator of ocean surface conditions. J. Geophys. Res. 113.

Uppala, S. M., P. W. Kållberg, A. J. Simmons, U. Andrae, V. da costa Bechtold, M. Fiorino, K. Gibson and Co-authors (2005), The ERA-40 re-analysis. Q. J. R. Meteorol. Soc. 131, 2961–3012.

Vicente-Serrano, S. M., S. Begueria and J. I. Lopez-Moreno (2009), A multiscalar drought index sensitive to global warming: The Standardized Precipitation Evapotranspiration Index. J. Clim. 23, 1696–1718.

Vimeux, F., R. Gallaire, S. Bony, G. Hoffmann and J. C. H. Chiang (2005), What are the climate controls on δD in precipitation in the Zongo Valley (Bolivia)? implications for the Illimani ice core interpretation. Earth Plan. Sci. Let. 240, 205–220.

von Storch, H., H. Langenberg and F. Feser (2000), A spectral nudging technique for dynamical downscaling purpose. Month. Weather Rev. 128, 3664–3673.

Vuille, M. and M. Werner (2005), Stable isotopes in precipitation recording South American summer monsoon and ENSO variability: observations and model results. Clim. Dynamics 25, 401–413.

Waliser, D. E. and C. Gautier (1993), A satellite-derived climatology of the ITCZ. J. Clim. 6, 2162–2174.

Wang, L., K. K. Caylor and D. Dragoni (2009), On the calibration of continuous, high-precision δ^{18}O and δ^2H measurements using an off-axis integrated cavity output spectrometer. Rapid Commun. Mass Spectrom. 23, 530–536.

Wang, L., K. K. Caylor, J. C. Villegas, G. A. Barron-Gafford, D. D. Breshears and T. E. Huxman (2010), Partitioning evapotranspiration across gradients of woody plant cover: Assessment of a stable isotope technique. Geophys. Res. Let. 37.

Wang, L., S. P. Good, K. K. Caylor and L. A. Cernusak (2012a), Direct quantification of leaf transpiration isotopic composition. Agr. Forest Meteorol. 154–155, 127–135.

Wang, L., P. DOdorico, J. P. Evans, D. J. Eldridge, M. F. McCabe, K. K. Caylor and E. G. King (2012b), Dryland ecohydrology and climate change: critical issues and technical advances. Hydrol. Earth Syst. Sci. 16, 2585–2603.

Wang, X.-F. and D. Yakir (2000), Using stable isotopes of water in evapotranspiration studies. Hydrol. Process. 14, 1407–1421.

Webb, M. J., C. A. Senior, D. M. H. Sexton, W. J. Ingram, K. D. Williams and Co-authors (2006), On the contribution of local feedback mechanisms to the range of climate sensitivity in two GCM ensembles. Clim. Dyn. 27, 17–38.

Webster, C. R. and J. Heymsfield (2003), Water isotope ratios D/H, ^{18}O/^{16}O, ^{17}O/^{16}O in and out of clouds map dehydration pathways. Science 302, 1742–1745.

Wells, N., S. Goddard and M. J. Hayes (2004), A self-calibrating Palmer Drought Severity Index. Am. Meteorol. Soc. , 2335–2351.

Welp, L. R., X. Lee, K. Kim, T. J. Griffis, K. A. Billmark and J. M. Baker (2008), δ^{18}O of water vapour, evapotranspiration and the sites of leaf water evaporation in a soybean canopy. Plant Cell Environ. 31, 1214–1228.

WELS, C., R. J. CORNETT and B. D. LAZERTE (1990), Groundwater and wetland contributions to stream acidification: An isotopic analysis. Water Resour. Res. 26, 2993–3003.

WENNINGER, J., D. T. BEZA and S. UHLENBROOK (2010), Experimental investigations of water fluxes within the soil-vegetation-atmosphere system: stable isotope mass-balance approach to partition evaporation and transpiration. Phys. Chem. Earth 35, 565–570.

WENTZ, F. J., L. RICCIARDULLI, K. HILBURN and C. MEARS (2007), How much more rain will global warming bring? Science 317, 233–235.

WERNER, M., P. M. LANGEBROEK, T. CARLSEN, M. HEROLD and G. LOHMANN (2011), Stable water isotopes in the ECHAM5 general circulation model: Toward high-resolution isotope modeling on a global scale. J. Geophys. Res. 116.

WIEGELE, A., M. SCHNEIDER, F. HASE, S. BARTHLOTT, O. E. GARCÍA, E. SEPÚLVEDA, Y. GONZÁLEZ, T. BLUMENSTOCK, U. RAFFALSKI, M. GISI and R. KOHLHEPP (2014), The MUSICA MetOp/IASI H_2O and δD products: characterisation and long-term comparison to NDACC/FTIR data. Atmos. Meas. Tech. 7, 2719–2732.

WILLIAMS, D. G., W. CABLE, K. HULTINE, J. C. B. HOEDJES, E. A. YEPEZ, V. SIMONNEAUX, S. ER-RAKI, G. BOULET, H. A. R. DE BRUIN, A. CHEHBOUNI, O. K. HARTOGENSIS and F. TIMOUK (2004), Evapotranspiration components determined by stable isotope, sap flow and eddy covariance techniques. Agr. Forest Meteorol. 125, 241–258.

WILLIAMSON, D. L. and P. J. RASCH (1994), Water vapor transport in the NCAR CCM2. Tellus 46A, 34–51.

WORDEN, J., S. S. KULAWIK, M. W. SHEPHARD, S. A. CLOUGH, H. WORDEN, K. BOWMAN and A. GOLDMAN (2004), Predicted errors of tropospheric emission spectrometer nadir retrievals from spectral window selection. J. Geophys. Res. 109.

WORDEN, J., K. BOWMAN, D. NOONE, R. BEER, S. CLOUGH, A. ELDERING, B. FISHER and CO-AUTHORS (2006), Tropospheric emission spectrometer observation of the tropospheric HDO/H_2O ratio: estimation approach and characterization. J. Geophys. Res. 111.

WORDEN, J., D. NOONE and K. BOWMAN (2007), Importance of rain evaporation and continental convection in the tropical water cycle. Nature 445, 528–532.

WORDEN, J., D. NOONE, J. GALEWSKY, A. BAILEY, K. BOWMAN, D. BROWN, J. HURLEY, S. KULAWIK, J. LEE and M. STRONG (2011), Estimate of bias in Aura TES HDO/H_2O profiles from comparison of TES and in situ HDO/H_2O measurements at the Mauna Loa observatory. Atmos. Chem. Phys. 11, 4491–4503.

WORDEN, J., S. KULAWIK, C. FRANKENBERG, V. PAYNE, K. BOWMAN, K. CADY-PEIRARA, K. WECHT, J. LEE and D. NOONE (2012), Profiles of CH_4, HDO, H_2O, and N_2O with improved lower tropospheric vertical resolution from Aura TES radiances. Atmos. Meas. Tech. 5, 397–411.

WU, H., M. J. HAYES, D. A. WILHITE and M. D. SVOBODA (2005), The effect of the length of record on the standardized precipitation index calculation. Int. J. Climatol. 25, 505–520.

Wu, X., X.-Z. Liang and G. J. Zhang (2003), Seasonal migration of ITCZ precipitation across the equator: why cant GCMs simulate it? Geophys. Res. Let. 30, 1824.

Wunch, D., G. C. Toon, P. O. Wennberg, S. C. Wofsy, B. B. Stephens, M. L. Fischer and Co-authors (2010), Calibration of the total carbon column observing network using aircraft profile data. Atmos. Meas. Tech. 3, 1351–1362.

Xu, Z., H. Yang, F. Liu, S. An, J. Cui, Z. Wang and S. Liu (2008), Partitioning evapotranspiration flux components in a subalpine shrubland based on stable isotopic measurements. Bot. Stud. 49, 351–361.

Yepez, E. A., D. G. Williams, R. L. Scott and G. Lin (2003), Partitioning overstory and understory evapotranspiration in a semiarid savanna woodland from the isotopic composition of water vapor. Agr. Forest Meteorol. 119, 53–68.

Yepez, E. A., T. E. Huxman, D. D. Ignace, N. B. English, J. F. Weltzin, A. E. Castellanos and D. G. Williams (2005), Dynamic of transpiration and evaporation following a moisture pulse in semiarid grassland: A chamber-based isotope method for partitioning flux components. Agr. Forest Meteorol. 132, 359–376.

Yoshimura, K., M. Kanamitsu, D. Noone and T. Oki (2008), Historical isotope simulation using Re-analysis atmospheric data. J. Geophys. Res. 113.

Yoshimura, K., C. Frankenberg, J. Lee, M. Kanamitsu, J. Worden and T. Röckmann (2011), Comparison of an isotopic atmospheric general circulation model with new quasi-global satellite measurements of water vapor isotopologues. J. Geophys. Res. 116.

Yurtsever, Y. (1975), Worldwide survey of isotopes in precipitation. Vienna: IAEA report.

Zakharov, V. I., R. Imasu, K. G. Gribanov, G. Hoffmann and J. Jouzel (2004), Latitudinal distribution of the deuterium to hydrogen ratio in the atmosphere water vapor retrieved from IMG/ADEOS data. Geophys. Res. Let. 31.

Zelinka, M. D., S. A. Klein and D. L. Hartmann (2012), Computing and partitioning cloud feedbacks using cloud property histograms. part I: Cloud radiative kernels. J. Clim. 25, 3715–3735.

Zelinka, M. D., S. A. Klein, K. E. Taylor, T. Andrews, M. J. Webb, J. M. Gregory and P. M. Foster (2013), Contributions of different cloud types to feedbacks and rapid adjustments in CMIP5. J. Clim. 26, 5007–5027.

Zhang, L., D. J. Jacob, X. Liu, J. A. Logan, K. Chance, A. Eldering and B. R. Bojkov (2010a), Intercomparison methods for satellite measurements of atmospheric composition: application to tropospheric ozone from TES and OMI. Atmos, Chem, Phys. 10, 4725–4739.

Zhang, S., X. Wen, J. Wang, G. Yu and X. Sun (2010b), The use of stable isotopes to partition evapotranspiration fluxes into evaporation and transpiration. Acta Ecol. Sin. 30, 201–209.

Zhang, Y., Y. Shen, H. Sun and J. B. Gates (2011), Evapotranspiration and its partitioning in an irrigated winter wheat field: A combined isotopic and micrometeorologic approach. J. Hydrol. 408, 203–211.

Zhao, M. (2014), An investigation of the connections among convection, clouds, and climate sensitivity in a global climate model. J. Clim. 27, 1845–1862.

Acknowledgements

and letting me stayed at your place every time I was in Delft. Also thanks for being my travel buddy all the time, and a good friend. Anouk, thanks for our friendship. It is a great pleasure to know you and shares our time together with stories, food and movies. Last but the most important one, Iris, big thanks for everything that we do together. Your smile in the morning when I enter the office room really makes up my days. Also for the lunches that you buy when I play badminton, I would like to say thanks and "lekker".

Finally, I would like to say it again that I feel very blessed to be your friend guys. Saying thank you is not always enough to express my gratitude to you all. Thank you VERY much.

About the author

Samuel Jonson Sutanto was born on 20 July 1980 in Tegal, a small city in Central Java, Indonesia. He spent his childhood in Tegal and attended elementary and junior high school at "Santo Pius", school organized by the Catholic association. In 1995 he moved to a bigger city in order to get a better education. He attended the BOPKRI 1 high school, in Yogyakarta. Then in 1998, he moved to the city of Bandung and started his bachelor study at the Department of Civil Engineering, Parahyangan Catholic University.

In 2004, he obtained his bachelor degree, specializing in the field of hydraulic and water resources engineering. During his thesis period, he worked with the Research Center for Water Resources, Ministry of Public Works Indonesia as an intern. In 2005, he got a permanent position in the same office as a junior hydrology researcher. Here, Samuel has learnt how to be a good researcher from his colleagues and published papers both in Indonesian journals and conference proceedings, as an author and co-author. He also joined the national team to handle the hot mudflow disaster in Sidoarjo Indonesia, known as "LUmpur SIdoarjo" (LUSI) in year 2006. His works and contributions for Ministry led him to achieve "Sumaryanto Widayatin Young Scientist Award" from Ministry of Public Works, in 2013.

Samuel moved to the Netherlands in 2009 to start his master study at the Department of Water Science and Engineering, UNESCO-IHE, Delft. For his master study, he got a scholarship from Joint Japan World Bank Graduated Scholarship Program (JJ/WBGSP). In 2011, he was awarded a M.Sc. degree in Hydrology and Water Resources with the thesis entitled: "Partitioning of soil evaporation and transpiration fluxes using environmental isotopes and hydrometric measurement techniques". Study aboard allowed Samuel receiving another M.Sc. title, which is Master of Shopping and Cooking.

His special interests in stable water isotopologues brought him to Utrecht where he joined the Institute for Marine and Atmospheric research Utrecht (IMAU), Utrecht University to work on a Ph.D. research. While from the master study he learnt about the water isotopologues in the surface and ground water, for his Ph.D. he had to learn the water isotopologues in the atmospheric water vapor. During his research, he gained experiences not only in programming and writing papers, but also in presenting his results at international conferences. He was awarded the AGU young hydrology prize during the GEWEX conference for best poster presentation. Completing his degrees abroad gave Samuel the possibility to fulfill his passion, and to discover new places and countries. Samuel has visited 27 countries during his life so far.

Curriculum vitae

SAMUEL JONSON SUTANTO

Working experience

2011 - 2015   : IMAU, Utrecht University, the Netherlands.
2004 - present   : Research Center for Water Resources, Ministry of Public Works, Bandung Indonesia.

Education

2011 - 2015   : PhD in Atmospheric Physics and Chemistry, Utrecht University, the Netherlands.
2009 - 2011   : MSc in Hydrology and Water Resources, UNESCO-IHE, Delft, the Netherlands.
1998 - 2004   : BSc in Civil Engineering, Parahyangan Catholic University, Bandung, Indonesia.

Workshops and trainings

- GEWEX summer sessions, Delft University of Technology, 10-12 July 2014, Delft The Netherlands.

- River Basin Modeling Short Course, UNESCO-IHE, 6-24 April 2009, Delft The Netherlands.

- Legal Framework of Water Resources Management Asia Regional Course, IDLO, October 22 November 2, 2007, Sydney Australia.

Awards and Fellowships

- AGU young hydrology prize during GEWEX conference 2014 for poster presentation.

- Sumaryanto Widayatin Young Scientist Award 2013 from Ministry of Public Works, Indonesia.

- Joint Japan World Bank Graduated Scholarship Program (JJ/WBGSP) for master study in UNESCO-IHE, Delft, The Netherlands.

- STUNED fellowship for River Basin Modeling Short Course in UNESCO-IHE, Delft, The Netherlands.

- AUS AID in cooperation with Bill & Melinda Gates foundation fellowship for Legal Framework of Water Resources Management Asia Regional Course, Sydney, Australia.

Selected publications

Sutanto, S. J., Hoffmann, G., Worden, J., Scheepmaker, R. A., Aben, I., and Röckmann, T.: Atmospheric processes governing the changes in water isotopologues during ENSO events from model and satellite measurements, **submitted to J. Geophys., Res.**

Coenders-Gerrits, M., Bogaard, T., Wenninger, J., and **Sutanto, S. J**.: Synthesis on evaporation partitioning using stable isotopes, **submitted to Hydrol. Process.**

Sutanto, S. J., Hoffmann, G., Scheepmaker, R. A., Worden, J., Houweling, S., Yoshimura, K., Aben, I., and Röckmann, T.: Global scale remote sensing of water isotopologues in the troposphere: representation of first-order isotope effects, Atmos. Meas. Tech., 8, 999-1019, doi:10.5194/amt-8-999-2015, 2015.

Sutanto, S. J., van den Hurk, B., Dirmeyer, P. A., Seneviratne, S. I., Röckmann, T., Trenberth, K. E., Blyth, E. M., Wenninger, J., Hoffmann, G.: HESS Opinions A perspective on isotope versus non-isotope approaches to determine the contribution of transpiration to total evaporation, Hydrol. Earth Syst. Sci., 18, 2815-2827, doi:10.519/hess-18-2815-2014, 2014.

Sutanto, S. J., Hoffmann, G., Adidarma, W., and Röckmann, T.: Correlation of drought related to ENSO and water isotopes in Indonesia, conference proceeding, 4th International Seminar of HATHI, 6-8 September 2013, Yogyakarta, Indonesia, 2013.

Sutanto, S. J., Wenninger, J., Coenders-Gerrits, M., Uhlenbrook, S.: Partitioning of evaporation into transpiration, soil evaporation and interception: a comparison between isotope measurements and a HYDRUS-1D model, Hydrol. Earth Syst. Sci., 16, 2605-2616, doi: 10.5194/hess-16-2605-2012, 2012.

Sutanto, S. J., and Ginting, S.: Use of Proposed Reservoirs to Reduce Flood in Semarang City, conference proceeding, International Seminar of HATHI, 11-13 Mei 2009, Manado, Indonesia, 2009.

Selected conference presentations

Sutanto, S. J., Hoffmann, G., Worden, J., Scheepmaker, R. A., Aben I., and Röckmann, T.: Evaluation of water vapor isotopologues and humidity bias from ECHAM4 using TES and SCIAMACHY satellite observations, AGU fall meeting, San Francisco, USA, 2014 (poster presentation).

Sutanto, S. J., Hoffmann, G., Worden, J., Scheepmaker, R. A., and Röckmann, T.: The impact of ENSO on water vapor isotopologues in the tropical pacific: Evidence for changes in long-range transport and convective activity, 7th GEWEX conference, Den Haag, the Netherlands, 2014 (poster presentation).

Sutanto, S. J., Hoffmann, G., Worden, J., Scheepmaker, R. A., and Röckmann, T.: The impact of ENSO on water vapor isotopologues in the tropical pacific: Evidence for changes in long-range transport and convective activity, EGU conference, Vienna Austria, 2014 (oral presentation).

Sutanto, S. J., Hoffmann, G., Scheepmaker, R., and Röckmann, T.: Whats happening with the water isotoplogue during ENSO, 1st international workshop on advances in observations, models, and measurement techniques of atmospheric water vapor isotopes, CNRS Gif-Sur-Yvette, France, 2013 (oral presentation).

Sutanto, S. J., Hoffmann, G., Scheepmaker, R., and Röckmann, T.: The improvement of TES HDO/H_2O isotope effects in TES version 5 dataset, TES Scientific meeting, Harvard University, USA, 2013 (oral presentation).

Sutanto, S. J., Hoffmann, G., Scheepmaker, R., Röckmann, T., and Aben, I.: Application of TES HDO/H_2O averaging kernel to the ECHAM4 model using the improved and non-improved lower troposphere vertical resolution dataset, AGU fall meeting, San Francisco, USA, 2012 (poster presentation).

Sutanto, S. J., Mulyantari, F., and Asyantina, T.: Development of design flood formula in ungauged catchments using index flood and L-moment approach: study case West Java Province, Indonesia, IAHS-PUB symposium, Delft, the Netherlands, 2012 (oral presentation).

Sutanto, S. J., Wenninger, J., Coenders-Gerrits, M., and Uhlenbrook, S.: Quantifying water fluxes within soil-plant-atmosphere continuum system using hydrometric measurements and stable isotopes techniques, ERB Workshop, Luxembourg, 2011 (oral presentation).

Sutanto, S. J., Wenninger, J., Coenders-Gerrits, M., and Uhlenbrook, S.: Partitioning of Soil Evaporation and Transpiration for Plant Water Use Efficiency using Hydrometric Measurements and Environmental Isotopes Technique, 3rd International Water for Food Conference, Lincoln, Nebraska, USA, 2011 (Poster Presentation).

Ibrahim, A. B., Sutikno, D., **Sutanto, S. J**., and Lubis, R. S.: Revitalization of lake Pluit, 14th Regional Steering Committee Meeting for UNESO-IHP, Thailand, 2006 (Poster Presentation).